Improved Nickel-Catalyzed Catalyst-Transfer Polycondensation via Ligand Design

By

Se Ryeon Lee

A dissertation submitted in partial fulfillment
of the requirements for the degree of
Doctor of Philosophy
(Chemistry)
in The University of Michigan
2014

Doctoral Committee:

       Associate Professor Anne J. McNeil, Chair
       Professor Adam J. Matzger
       Professor Richard E. Robertson
       Professor John P. Wolfe

Dedication

To my loving parents and husband for believing in me.

Acknowledgments

I would like to express my special appreciation and thanks to my advisor, Professor Anne McNeil, for mentoring me for the past five years and encouraging my research in both good and bad times. Your advice on both research and my career has been priceless.

I would also like to thank all past and present McNeil group members who have shared with me the many crazy graduate school moments; Kelsey Carter, Danielle Zurcher, Zack Bryan, Ariana Hall, Pete Goldberg, Mitchell Smith, Dr. Ed Palermo, Dr. Jing Chen, Dr. Cheryl Moy, Yash Adhia, Dr. Erica Locke, and Dr. Jonas Locke. All of you have been there to support me intellectually and mentally helping me get through it all.

Many thanks are due to friends outside of the lab as well. I want to thank friends from college for checking to see if I'm still alive. I want to thank friends from Harvest Mission Community Church for their support, prayers, and a lot of good board game and dance nights. I would like to thank friends from book club for all the wine and good book discussion. I would like to thank Jamie Nieusma and Jeff Rupert for all their support and Disney movies to keep me sane.

A special thanks are due to my family. I would like to thank my in-laws, Jane and Chris Castello, for their support and encouragement. I want to thank my parents, Chong Dae and Mi Hwa, for their love and sacrifice all my life. I would not have been who I am now without your prayers day and night. 엄마아빠 고마워요. 사랑해요!

Last, but most, I want to thank my husband, Justin Nieusma, for his love and support since high school. Words cannot express how grateful I am to have you in my life. I love you!

Table of Contents

Chapter

List of Figures

ix

List of Tables

List of Schemes

List of Appendices

Abstract

Chapter 1 provides an introduction to π-conjugated polymers and their applications. Understanding the structure-property relationships is crucial in expanding the application scope for π-conjugated polymers. Currently, the catalyst transfer polycondensation is used to synthesize well-defined polymers. This thesis details our efforts to overcome limitations, chain transfer and slow initiation, to promote controlled chain-growth polymerization.

Chapter 2 demonstrates our efforts to minimize chain transfer in catalyst transfer polycondensation by modifying the electronics of ancillary ligands of Ni precatalysts. We showed that electron-rich ligands promote chain-growth behavior by stabilizing Ni-polymer π-complex and increasing the intramolecular oxidative addition rate. During this investigation, we found that the initiation is substantially slower than the propagation rate and that modification of ancillary ligands can not increase initiation rate selectively.

Chapter 3 describes the importance of fast initiation in controlled catalyst transfer polycondensation and our efforts to selectively increase the initiation rate without increasing the propagation rate. We found that modifying the reactive ligands leads to change in the initiation rate. Computational studies demonstrated that the delocalization of charges on Ni catalyst by reactive ligands during the initiation is the key to increasing the initiation rate.

Chapter 4 demonstrates our efforts to increase the initiation rate beyond the propagation rate by modifying Ni precatalysts. We selected a number of heteroaromatic and aromatic reactive ligands and calculated the activation barriers using the computational method developed in Chapter 3. The

computational study allowed us to narrow down the suitable targets, which we synthesized and tested experimentally. We found that a biphenyl-based reactive ligand leads to a faster initiation rate than propagation rate and promotes controlled chain-growth behavior.

Chapter 5 describes our findings, specifically the impact of ligand electronics on controlled catalyst trasfer polycondensation. Additionally, the future directions are presented, specifically implementing the computational method for other polymer syntheses, evaluating more electron-rich ancillary ligand for chain-growth, and exploring non-symmetric ancillary ligands to expand the ligand scope for current CTP method. The importance of thorough mechanistic studies and understanding of Ni precatalysts for expanding monomer scope and accessing copolymers are emphasized.

Chapter 1

Introduction

Organic π-conjugated polymers are macromolecules with conjugated backbones that result in π-electron delocalization and exhibit optical and electrical properties (*e.g.*, absorb/emit light and conduct charge), which are useful in various applications. To name a few, organic π-conjugated polymers are used in energy-related applications such as photovoltaics (PVs),[1] light-emitting diodes (LEDs),[2] and field-effect transistors (FETs)[3] and sensing applications[4] such as explosives detection.[5] Organic π-conjugated polymers are attractive materials compared to their inorganic counterparts because of their synthetically tunable properties, ability to be processed in solution for high speed production (*e.g.*, roll-to-roll processing[6]), flexibility, and low cost. To date, research has mainly focused on developing novel π-conjugated backbones by modifying monomer[7] or copolymer sequences (*e.g.*, block[8] and gradient[9]) to obtain desired optoelectronic and physical properties. For example, the polymer-fullerene macrophase separation in the active layer of bulk heterojunction solar cell is one of the biggest limitations as it results in decreased performance of the solar cell over time.[10] Recently, our group systematically studied the impact of random, block, and gradient copolymer as a compatilizing additive for phase-separated blends of two different homopolymers and found that the gradient copolymer exhibits the best performance in minimizing the phase separation.[9b] In a subsequent study, the novel gradient π-conjugated polymers composed of poly(3-hexylthiophene) (P3HT) and poly(thiophene) with phenyl-C61-butyric acid methyl ester (PCBM) side chain was synthesized using catalyst transfer polycondensation (CTP) and post-polymerization click chemistry (Scheme 1-1). By comparing P3HT/PCBM blend solar cell with and without the gradient

copolymer additive, we showed that the solar cell with gradient copolymer exhibited minimal changes in phase separation even after prolonged thermal annealing and concluded that it can be a promising material for stable solar cells.[9a] These findings suggest that systematic studies in understanding the structure-property relationships of the polymers are useful and important ways to expand the efficiency of known polymers, and ultimately, to increase the potential application scope.
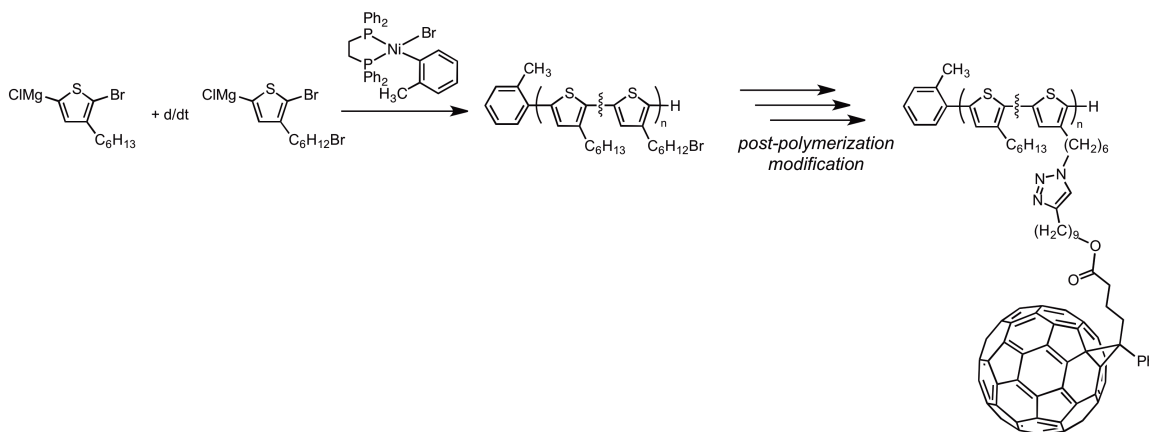
Scheme 1-1. Gradient π-conjugated copolymer.

In addition, efforts have been made to study the impact of polymer molecular weights and dispersity (Đ) on their properties but a clear correlation is hard to determine, mainly because of a lack of a synthetic method available to produce the polymers with precise weight and narrow dispersity. For example, Stingelin and coworkers have systematically studied the molecular weight (*i.e.*, number-averaged molecular weight, M_n) of P3HT at $4.0 \leq M_n \leq 130$ kDa and its impact on the microstructure of thin film and ultimately, charge transport ability (μ_{FET}) (*i.e.*, efficiency of FET). They demonstrated that high molecular weight P3HT has lamellar crystalline morphology whereas short-chain P3HT exhibits a chain-extended microstructure. In the chain-extended microstructure, polymers are randomly arranged to form amorphous morphology, which results in low μ_{FET}. The μ_{FET} is proportional to the increase in lamellar crystal thickness up to $M_n \leq 25$ kDa, at which point it becomes independent of chain length due to entangled

2

two-phase "fringed-micelle" architecture, which is mixture of well-packed lamellar structure (crystalline region) and random entanglements (amorphous region).[11] However, the polymers studied in this report have dispersity ranged from 1.3 to 3.7, which indicates that the correlation between molecular weight and properties are limited by the defects (*e.g.*, low MW polymers) in the polymer samples. Specifically, M_n = 25 kDa has shown to exhibit best performance, for which Đ = 1.8 and, could therefore contain low and high molecular weight polymer that influence the morphology. In another example, Galvin and coworkers studied the impact of dispersity on polymer properties, specifically LED efficiency using poly((2,5-bisoctyloxy)-1,4-phenylene vinylene)s (PPV). They showed that PPV with low molecular weight and narrow dispersity (*i.e.*, M_n= 4.2 kDa and Đ= 1.3) exhibits higher LED efficiency compared to the polymers with either lower M_n and narrow Đ or higher M_n and broad Đ.[12] Nevertheless, because two variables, M_n and Đ, are changing simultaneously, the conclusion about correlation between dispersity and efficiency cannot be drawn. These studies demonstrate not only the need for understanding the structure-property relationship of existing polymers to refine their usage in applications but also the need for synthetic methods to produce the polymers with narrow dispersity.

Until recently, the methods available to obtain the polymers with precise weight and narrow dispersity are post-polymerization purifications such as Soxhlet extraction and preparative gel permeation chromatography (prep GPC). However, these processes can be quite time-consuming, require high solvent usage, and lead to isolation of very little material at the end. Consequently, it is imperative to develop a synthetic method to control both molecular weight and dispersity of the final polymer to facilitate studies of the structure-property relationship and improve the efficiency of π-conjugated polymer based devices.

Polymerization method

π-Conjugated polymers are traditionally synthesized using transition metal-catalyzed cross coupling methods (*e.g.*, Suzuki,[13] Stille,[14] direct arylation,[15] oxidative coupling[16]) utilizing a step-growth polymerization mechanism. In step-

growth polymerizations, a catalyst randomly couples monomers and oligomers in solution to result in polymers (Scheme 1-2). Despite its advantage of having a large monomer scope, it is quite limited because it has very little control over molecular weight, dispersity, and copolymer sequence. Hence, the discovery of Ni-catalyzed Kumada catalyst-transfer polymerization (CTP), utilizing a chain-growth polymerization mechanism, has provided a great breakthrough to synthesize well-defined π-conjugated polymers. The ideal chain-growth method allows precise control over molecular weight with narrow dispersity (*i.e.*, Đ ≈ 1.0), and copolymer sequence to access novel structures such as gradient copolymers (Scheme 1-2).
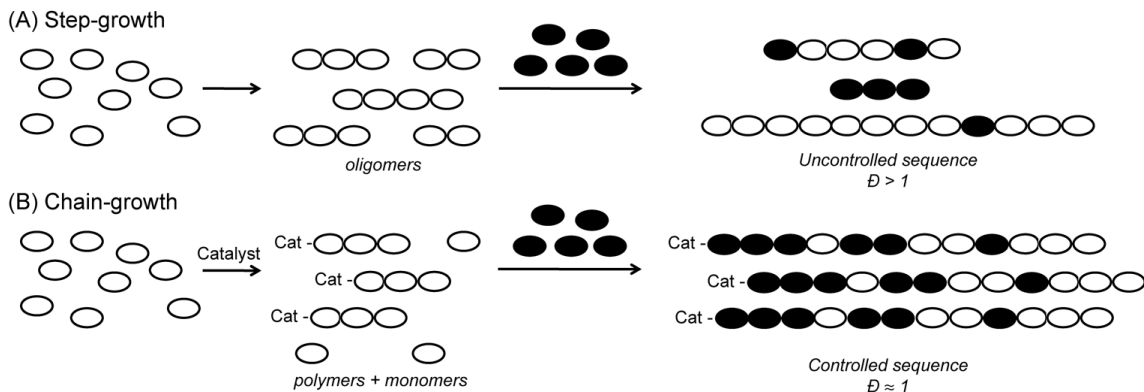
Scheme 1-2. Step-growth *versus* chain-growth methods.

Since its discovery in 2004 where Yokozawa[17] and McCullough[18] have independently demonstrated chain-growth polymerization of P3HT proceeds via linear growth of polymer molecular weight over the monomer conversion with relatively low Đ, many studies have been done to elucidate the mechanism of CTP (Scheme 1-3). It has been proposed that Ni stays associated to the polymer by forming a key intermediate, Ni-polymer π-complex (**I**), which undergoes intramolecular oxidative addition to result in a controlled polycondensation. Although there is no direct spectroscopic evidence of a Ni-polymer π-complex, many studies support this key intermediate, including previously known similar arene- and alkene-based π-complexes.[19] Also, recently our group reported compelling indirect evidence of a Ni-polymer π-complex. In this study, Ni catalyst

4

was reacted with Grignard reagent in the presence of more reactive competitive agent. The authors found that the major products were from the intramolecular pathway, indicating the presence of Ni-polymer π-complex.[20] The proposed mechanism has been further supported by rate and spectroscopic studies performed on the synthesis of poly(2,5-bis(hexyloxy)phenylene) (PP) and P3HT catalyzed by Ni(dppe)Cl$_2$ and Ni(dppp)Cl$_2$.[21] Although a Ni-polymer π-complex was not observed, the work provided evidence for the transmetalation and reductive elimination mechanistic steps. Furthermore, it revealed that the structure of ancillary ligand (*i.e.*, bite[21a] and cone angle[22]) influences the rate-limiting step of polymerization (*e.g.*, dppe = reductive elimination, dppp = transmetalation).
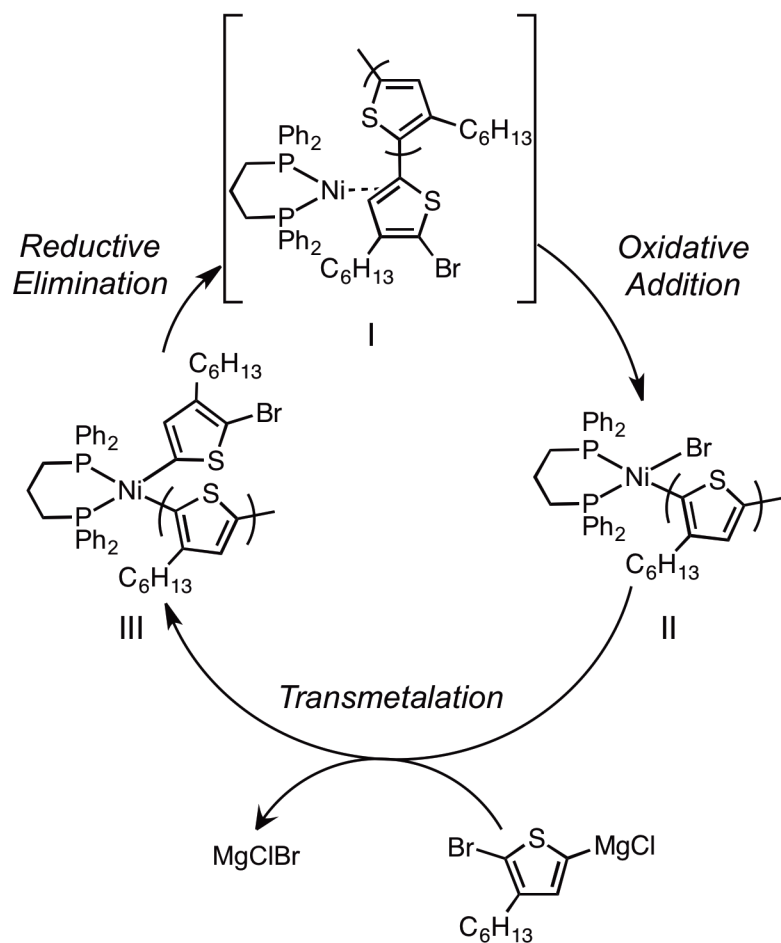
Scheme 1-3. Proposed mechanism for chain-growth.

Kumada CTP has shown to undergo a mostly living, chain-growth polymerization mechanism. A living polymerization is defined as chain polymerization that lacks the chain termination or chain transfer processes.[23] For CTP, the catalyst is shown to remain active at the polymer end even after the monomer is depleted and thus, the chain can be elongated by addition of more monomer. This chain extension allows the synthesis of copolymers such as block copolymers by adding two different batches of monomer (Scheme 1-4)[22,24] as well as the synthesis of polymers with specific end groups by adding chain-terminating molecules at the end of the reaction.[25] Similarly, the end group functionalization can be done at the beginning of the reaction by using a precatalyst with a reactive ligand, which has been utilized to graft polymers from surfaces for polymer brush architectures.[26] Overall, CTP provides a platform to synthesize the well-defined π-conjugated polymers, which can be utilized for methodical study of the structure-property relationship to improve device performances. Nevertheless, current CTP is limited due to side reactions and slow initiation, which are discussed in the next section.
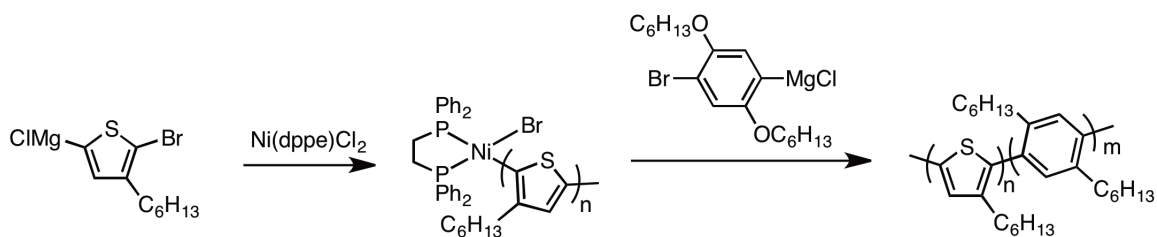
Scheme 1-4. Representative block copolymer synthesis.[22]

Limitation

Although CTP has been shown to be useful in controlling molecular weight and dispersity compared to the traditional step-growth mechanism, it is not without limitations. The difficulty in controlling the molecular weight and dispersity for high molecular weight polymer (*i.e.*, $M_n \geq 20$ kDa) indicates that the CTP is uncontrolled. In this thesis, we examined the two prevalent limitations of CTP and offer a solution to promote controlled chain-growth behavior.

(A) Disproportionation

Cat -OOO → Cat -OOOOOO

Cat -OOO → Cat -

(B) Chain Transfer

Cat -OOO → Cat -OOO

O Cat -OOO → Cat -O O

OOO

(C) Chain Termination

Cat -OOO → Cat -OOO

O Cat -OOO → Cat - O

O O OOO
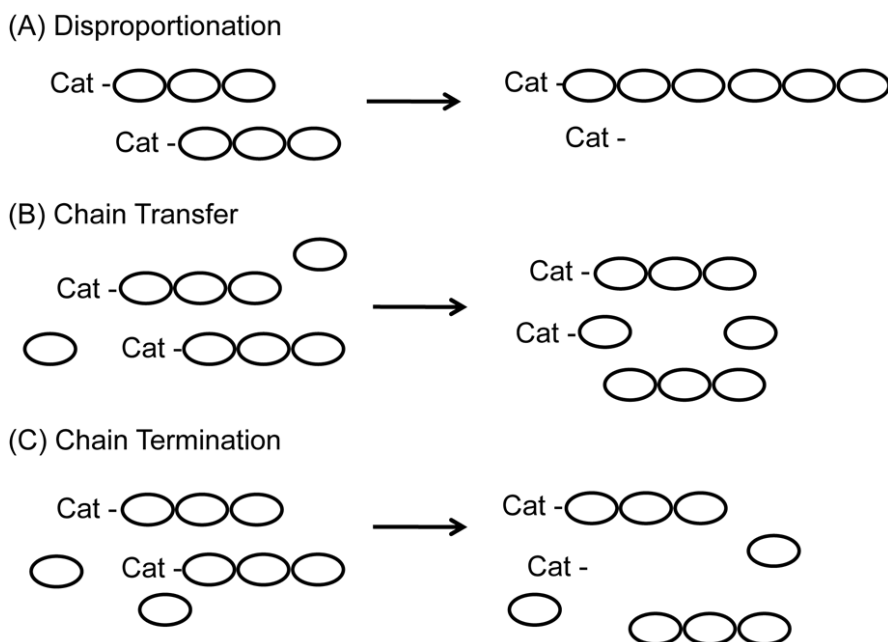
Scheme 1-5. Possible side reactions that lead to uncontrolled CTP.

One of the reasons for the uncontrolled polymerization is side reactions that cause deviation from the living, chain-growth mechanism. The main side reactions that are identified to date are disproportionation, chain transfer, and chain termination (Scheme 1-5). The disproportionation pathway is caused when two catalysts swap ligands and generate a polymer with twice the expected molecular weight after reductive elimination. Yokozawa and coworkers suggested the presence of a disproportionation pathway by using neutral H_2O as a quenching agent to terminate the polymerization and observing bimodal gel permeation chromatograms (GPC). The M_n of the first eluting peak was approximately twice that of the second peak, which indicates a competing disproportionation pathway that out-competes the proton termination pathway. This side-reaction can be overcome by using strong acid (*e.g.*, 5 M HCl) that increases the protonation rate over disproportionation, as demonstrated by an unimodal GPC observed in the same study.[27] Locklin and coworkers have also supported the disproportionation pathway with a simplified computational model. They computed the disproportionation energies of Ni-thienyl complexes differing

only in the structure of ancillary ligand (*i.e.*, bite and cone angle) and found that Ni catalysts with dppp and dppe ligands are less likely to undergo disproportionation in accordance with previously reported experimental study.[28]

Other side reactions, chain transfer and chain termination, also lead to uncontrolled CTP. For example, chain transfer is a result of displacement of polymer from the Ni(0) in Ni-polymer π-complex during propagation by competing molecules such as monomer, oligomers, and/or solvent (Scheme 1-5). To date, the chain transfer pathway has been considered insignificant because there is no evidence of Ni(0) reacting with 2,5-dibromo-3-hexylthiophene in the polymerization,[20,24a,29] which remains from Grignard monomer synthesis and can act as a competing reactive species. However, the presence of certain end groups such as Br/Br and H/Br in the resulting polymers synthesized with precatalyst $L_nNi(Ar)X$ suggest that chain transfer and/or chain termination is present because each polymer should only contain Ar/H end groups (Scheme 1-6). For example, H/H end groups can result from displacement of polymer from Ni-polymer π-complex with Grignard monomer (*i.e.*, chain transfer) and proton termination *via* acid quench. If the Ni(0) dissociates away from polymer after reductive elimination, the resulting polymer will have Ar/Br end groups. The combination of chain transfer and chain termination during polymerization can lead to any mixture of H, Br, and Ar end groups in the resulting polymers.

Controlled CTP   **Uncontrolled CTP**
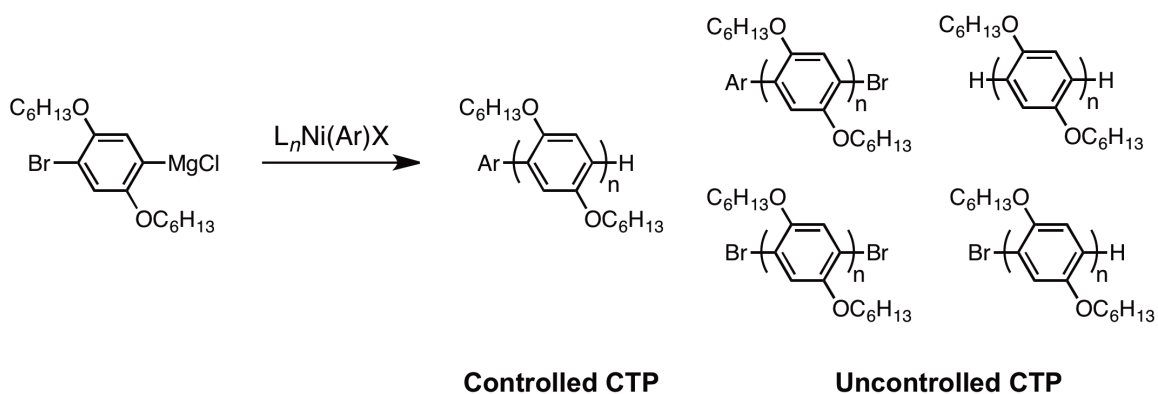
Scheme 1-6. Possible end groups resulting from controlled and uncontrolled CTP.

One way to overcome the possible side reaction caused by separation of Ni(0) and polymer is to modify the catalyst, specifically by using electron-rich ancillary ligand, to stabilize the Ni-polymer π-complex[30] and to increase the rate of intramolecular oxidative addition.[31] Indeed, we have shown that Ni precatalysts with electron-rich ancillary ligands exhibit better CTP with narrow Đ for the PP synthesis, whereas electron-poor precatalysts show uncontrolled CTP with broad Đ (Chapter 2 and Scheme 1-7).[32]
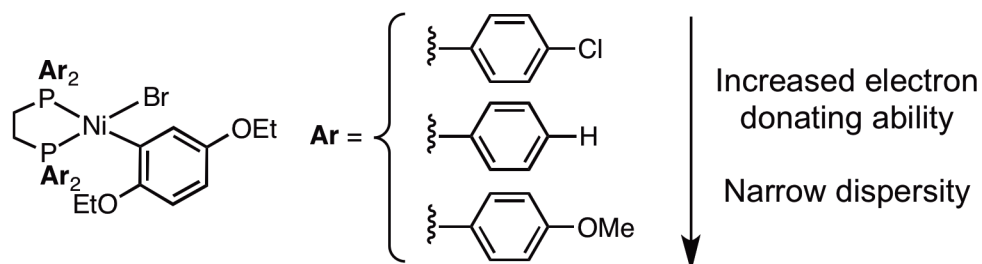
Scheme 1-7. Electron-rich ancillary ligands promote chain-growth as described in Chapter 2.

Another main limitation of current CTP is slow initiation relative to propagation. For precise control over molecular weight and dispersity of polymers, it is important for all the catalysts to react with monomer at the same time and consume the same amount of monomer in solution. CTP utilizes precatalysts such as partially heterogeneous L_nNiX_2 or homogeneous $L_nNi(Ar)X$ which inevitably undergoes initiation step before entering the propagation cycle (Scheme 1-8). Frequently, the partially heterogeneous $Ni(dppe)Cl_2$ and/or $Ni(dppp)Cl_2$ is used because it is commercially available. However, it is not possible for all the catalysts to undergo initiation at the same time because of the mostly insoluble L_nNiCl_2 salts at polymerization concentration. Luscombe and coworkers introduced functionalized precatalysts ($L_nNi(Ar)X$) with reactive ligands (Ar) that are homogeneous in solution to enable the equal interaction between all catalysts and monomer.[33] These soluble precatalysts have been utilized in many other studies since. However, the precatalysts are prepared *in situ*, which

9

contains impurities such as free PPh3, free chelating ligand, and/or bis-chelated Ni(II) complex, all of which can influence the polymerization.
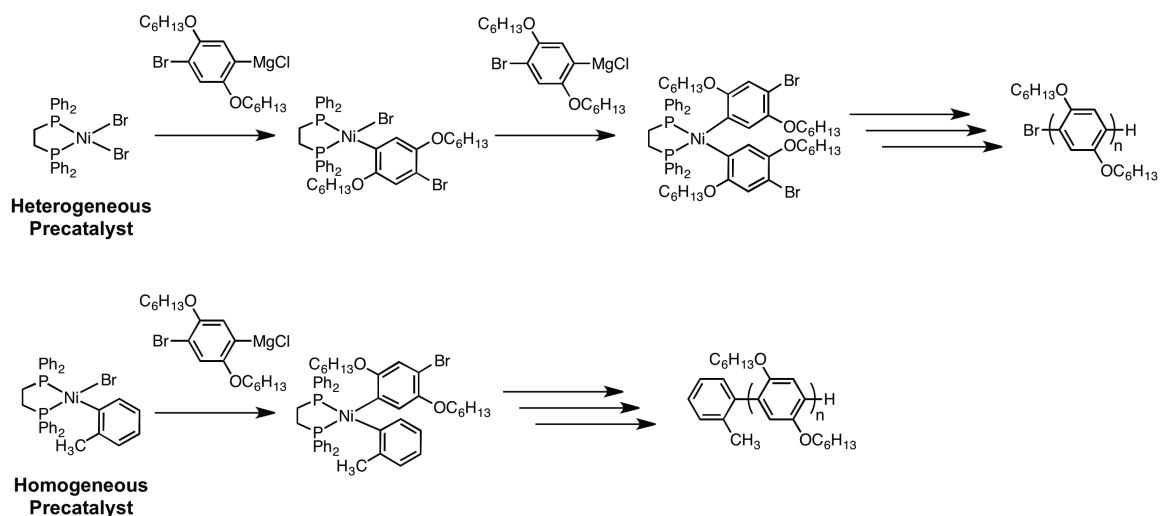
Scheme 1-8. Precatalysts used for CTP and initiation mechanism.

Recently, we have synthesized and isolated functionalized Ni precatalysts and studied their initiation rate. Surprisingly, we found that initiation of CTP is considerably slower than propagation (*e.g.*, 20 times) even with homogeneous precatalysts (Chapter 3 and Scheme 1-9). Furthermore, we observed an increase in Đ over monomer conversion, which explains the difficulty of controlling dispersity for high molecular weight polymers and demonstrates the importance of initiation in CTP. Further studies indicated that the initiation rate can be selectively increased compared to the propagation rate by modifying the reactive ligand (Chapter 3 and Scheme 1-10).[32] In combination with computational studies, we synthesized precatalysts with different reactive ligands and found a precatalyst that exhibits faster initiation than propagation (Chapter 4).
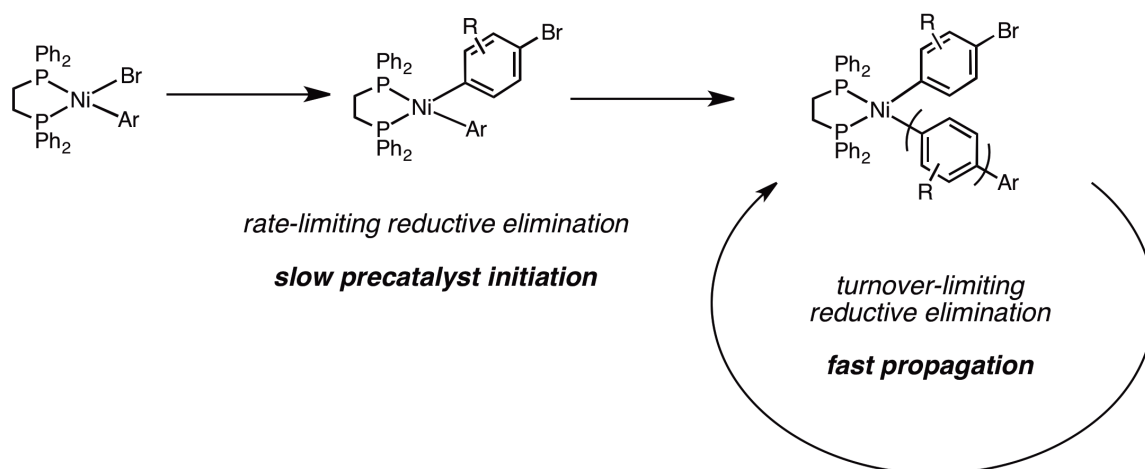
Scheme 1-9. Slow initiation and fast propagation.
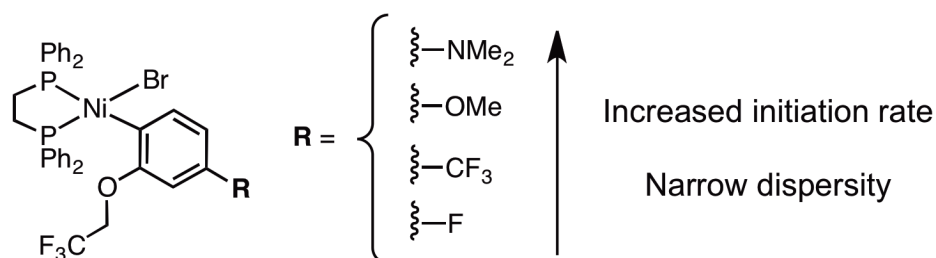
Scheme 1-10. Selectively increasing initiation rate via reactive ligand modification as demonstrated in Chapter 3.

Conclusion

This dissertation details my work in the McNeil group on the modification of Ni precatalysts, specifically ancillary and reactive ligands, to promote controlled CTP. We demonstrated that understanding the role of ligand in the mechanistic steps of polymerization allows us to enhance the chain-growth behavior of CTP by minimizing side reactions and increasing the initiation rate. This work provides a foundation for optimizing catalyst design to synthesize precisely controlled π-conjugated polymers, which will enable the study of structure-property relationships.

References Cited

(1)   For recent reviews, see: (a) Jhuo, H. J.; Yeh, P. N.; Liao, S. H.; Li, Y. L.; Cheng, Y. S.; Chen, S. A. *J. Chin. Chem. Soc.* **2014**, *61*, 115–126. (b) Scharber, M. C.; Sariciftci, N. S. *Prog. Polym. Sci.* **2013**, *38*, 1929–1940. (c) Darling, S. B.; You, F. Q. *R. Soc. Chem. Adv.* **2013**, *3*, 17633–17648. (d) Marrocchi, A.; Lanari, D.; Facchetti, A.; Vaccaro, L. *Energy Environ. Sci.* **2012**, *5*, 8457–8474. (e) Myers, J. D.; Xue, J. G. *Polym. Rev.* **2012**, *52*, 1–37.

(2)   For recent reviews, see: (a) Guo, X.; Baumgarten, M.; Mullen, K. *Prog. Polym. Sci.* **2013**, *38*, 1832–1908. (b) Wang, J.; Zhang, F. J.; Zhang, J.; Tang, W. H.; Tang, A. W.; Peng, H. S.; Xu, Z.; Teng, F.; Wang, Y. S. *J. Photochem. Photobiol.* **2013**, *17*, 69–104. (c) Deng, X. Y. *Int. J. Mol. Sci.* **2011**, *12*, 1575–1594. (d) Grimsdale, A. C.; Chan, K. L.; Martin, R. E.; Jokisz, P. G.; Holmes, A. B. *Chem. Rev.* **2009**, *109*, 897–1091.

(3)   For recent reviews, see: (a) Nielsen, C. B.; McCulloch, I. *Prog. Polym. Sci.* **2013**, *38*, 2053–2069. (b) Dong, H. L.; Fu, X. L.; Liu, J.; Wang, Z. R.; Hu, W. P. *Adv. Mater.* **2013**, *25*, 6158–6182. (c) Kola, S.; Sinha, J.; Katz, H. E. *J. Polym. Sci. Part B: Polym. Phys.* **2012**, *50*, 1090–1120.

(4)   For recent review, see: Rochat, S.; Swager, T. M. *ACS Appl. Mater. Interfaces* **2013**, *5*, 4488–4502.

(5)   (a) Yang, J. S.; Swager, T. M. *J. Am. Chem. Soc.* **1998**, *120*, 11864–11873. (b) Yang, J. S.; Swager, T. M. *J. Am. Chem. Soc.* **1998**, *120*, 5321–5322.

(6)   (a) Bottiger, A. P. L.; Jorgensen, M.; Menzel, A.; Krebs, F. C.; Andreasen, J. W. *J. Mater. Chem.* **2012**, *22*, 22501–22509. (b) Krebs, F. C.; Gevorgyan, S. A.; Alstrup, J. *J. Mater. Chem.* **2009**, *19*, 5442–5451.

(7)   Yokozawa, T. In *Conjugated Polymer Synthesis*; Wiley-VCH Verlag GmbH & Co. KGaA: 2010, p 35–58.

(8)   For recent examples, see: (a) Smith, K. A.; Pickel, D. L.; Yager, K.; Kisslinger, K.; Verduzco, R. *J. Polym. Sci. Part A: Polym. Chem.* **2014**, *52*, 154–163. (b) Li, F.; Yager, K. G.; Dawson, N. M.; Yang, J. H.; Malloy, K. J.; Qin, Y. *Macromolecules* **2013**, *46*, 9021–9031. (c) Wang, J.; Higashihara, T. *Polym. Chem.* **2013**, *4*, 5518–5526. (d) Robb, M. J.; Ku, S. Y.; Hawker, C. J. *Adv. Mater.* **2013**, *25*, 5686–5700.

(9)   (a) Palermo, E. F.; Darling, S. B.; McNeil, A. J. *J. Mater. Chem. C.* [online early access] DOI:10.1039/C3TC32512A. Published online February 25, 2014. http://pubs.rsc.org (accessed February 22, 2014) (b) Palermo, E. F.; van der Laan, H. L.; McNeil, A. J. *Polym. Chem.* **2013**, *4*, 4606–4611. (c) Locke, J. R.; McNeil, A. J. *Macromolecules* **2010**, *43*, 8709–8710.

(10)   Lee, J. U.; Jung, J. W.; Jo, J. W.; Jo, W. H. *J. Mater. Chem.* **2012**, *22*, 24265–24283.

(11)   Koch, F. P. V.; Rivnay, J.; Foster, S.; Muller, C.; Downing, J. M.; Buchaca-Domingo, E.; Westacott, P.; Yu, L. Y.; Yuan, M. J.; Baklar, M.; Fei, Z. P.; Luscombe, C.; McLachlan, M. A.; Heeney, M.; Rumbles, G.; Silva, C.; Salleo, A.; Nelson, J.; Smith, P.; Stingelin, N. *Prog. Polym. Sci.* **2013**, *38*, 1978–1989.

(12)   Menon, A.; Dong, H. P.; Niazimbetova, Z. I.; Rothberg, L. J.; Galvin, M. E. *Chem. Mater.* **2002**, *14*, 3668–3675.

(13)   For reviews, see: (a) Hoshi, Y.; Funyu, S. *J. Synth. Org. Chem. Jpn.* **2012**, *70*, 442–449. (b) Sakamoto, J.; Rehahn, M.; Wegner, G.; Schluter, A. D. *Macromol. Rapid Commun.* **2009**, *30*, 653–687.

(14)   For review, see: Carsten, B.; He, F.; Son, H. J.; Xu, T.; Yu, L. P. *Chem. Rev.* **2011**, *111*, 1493–1528.

(15)   For reviews, see: (a) Kowalski, S.; Allard, S.; Zilberberg, K.; Riedl, T.; Scherf, U. *Prog. Polym. Sci.* **2013**, *38*, 1805–1814. (b) Mercier, L. G.; Leclerc, M. *Acc. Chem. Res.* **2013**, *46*, 1597–1605.

(16)   For recent examples, see: (a) Fukumoto, H.; Omori, Y.; Yamamoto, T. *Polym. J.* **2013**, *45*, 462–465. (b) Torres, B. B. M.; Balogh, D. T. *J. Appl. Polym. Sci.* **2012**, *124*, 3222–3228. For review, see: (c) Sarhan, A. A. O.; Bolm, C. *Chem. Soc. Rev.* **2009**, *38*, 2730–2744.

(17)   Yokoyama, A.; Miyakoshi, R.; Yokozawa, T. *Macromolecules* **2004**, *37*, 1169–1171.

(18)   Sheina, E. E.; Liu, J. S.; Iovu, M. C.; Laird, D. W.; McCullough, R. D. *Macromolecules* **2004**, *37*, 3526–3528.

(19)   For recent examples, see: (a) Sylvester, K. T.; Wu, K.; Doyle, A. G. *J. Am. Chem. Soc.* **2012**, *134*, 16967–16970. (b) Ge, S. Z.; Hartwig, J. F. *J. Am. Chem. Soc.* **2011**, *133*, 16330–16333. (c) Johnson, S. A.; Huff, C. W.; Mustafa, F.; Saliba, M. *J. Am. Chem. Soc.* **2008**, *130*, 17278–17280. (d) Garcia, J. J.; Brunkan, N. M.; Jones, W. D. *J. Am. Chem. Soc.* **2002**, *124*, 9547–9555. (e) Braun, T.; Cronin, L.; Higgitt, C. L.; McGrady, J. E.; Perutz, R. N.; Reinhold, M. *New J. Chem.* **2001**, *25*, 19–21. (f) Boese, R.; Stanger, A.; Stellberg, P.; Shazar, A. *Angew. Chem. Int. Ed.* **1993**, *32*, 1475–1477. (g) Benn, R.; Mynott, R.; Topalovic, I.; Scott, F. *Organometallics* **1989**, *8*, 2299–2305.

(20)   Bryan, Z. J.; McNeil, A. J. *Chem. Sci.* **2013**, *4*, 1620–1624.

(21)   (a) Lanni, E. L.; McNeil, A. J. *Macromolecules* **2010**, *43*, 8039–8044. (b) Lanni, E. L.; McNeil, A. J. *J. Am. Chem. Soc.* **2009**, *131*, 16573–16579.

(22)   Lanni, E. L.; Locke, J. R.; Gleave, C. M.; McNeil, A. J. *Macromolecules* **2011**, *44*, 5136–5145.

(23)   Jenkins, A. D.; Kratochvil, P.; Stepto, R. F. T.; Suter, U. W. *Pure Appl. Chem.* **1996**, *68*, 2287–2311.

(24)   For recent examples, see: (a) Bryan, Z. J.; Smith, M. L.; McNeil, A. J. *Macromol. Rapid Commun.* **2012**, *33*, 842–847. (b) Ono, R. J.; Kang, S. S.; Bielawski, C. W. *Macromolecules* **2012**, *45*, 2321–2326. (c) Verswyvel, M.; Koeckelberghs, G. *Polym. Chem.* **2012**, *3*, 3203–3216. (d) Sui, A. G.; Shi, X. C.; Wu, S. P.; Tian, H. K.; Geng, Y. H.; Wang, F. S. *Macromolecules* **2012**, *45*, 5436–5443. (e) Smeets, A.; Willot, P.; De Winter, J.; Gerbaux, P.; Verbiest, T.; Koeckelberghs, G. *Macromolecules* **2011**, *44*, 6017–6025. (f) Li, L. S.; Hollinger, J.; Jahnke, A. A.; Petrov, S.; Seferos, D. S. *Chem. Sci.* **2011**, *2*, 2306–2310.

(25)   (a) Miyakoshi, R.; Yokoyama, A.; Yokozawa, T. *J. Am. Chem. Soc.* **2005**, *127*, 17542–17547. (b) Jeffries-El, M.; Sauve, G.; McCullough, R. D. *Macromolecules* **2005**, *38*, 10346–10352. (c) Jeffries-El, M.; Sauve, G.; McCullough, R. D. *Adv. Mater.* **2004**, *16*, 1017–1019.

(26)   For recent examples, see: (a) Tkachov, R.; Senkovskyy, V.; Oertel, U.; Synytska, A.; Horecha, M.; Kiriy, A. *Macromol. Rapid Commun.* **2010**, *31*, 2146–2150. (b) Tkachov, R.; Senkovskyy, V.; Horecha, M.; Oertel, U.; Stamm, M.; Kiriy, A. *Chem. Commun.* **2010**, *46*, 1425–1427. (c) Marshall, N.; Sontag, S. K.; Locklin, J. *Macromolecules* **2010**, *43*, 2137–2144. (d) Senkovskyy, V.; Tkachov, R.; Beryozkina, T.; Komber, H.; Oertel, U.; Horecha, M.; Bocharova,

V.; Stamm, M.; Gevorgyan, S. A.; Krebs, F. C.; Kiriy, A. *J. Am. Chem. Soc.* **2009**, *131*, 16445–16453. (e) Sontag, S. K.; Marshall, N.; Locklin, J. *Chem. Commun.* **2009**, 3354–3356. (f) Khanduyeva, N.; Senkovskyy, V.; Beryozkina, T.; Horecha, M.; Stamm, M.; Uhrich, C.; Riede, M.; Leo, K.; Kiriy, A. *J. Am. Chem. Soc.* **2009**, *131*, 153–161.

(27)   Miyakoshi, R.; Yokoyama, A.; Yokozawa, T. *Macromol. Rapid Commun.* **2004**, *25*, 1663–1666.

(28)   Bilbrey, J. A.; Sontag, S. K.; Huddleston, N. E.; Allen, W. D.; Locklin, J. *Acs Macro Letters* **2012**, *1*, 995–1000.

(29)   (a) Beryozkina, T.; Senkovskyy, V.; Kaul, E.; Kiriy, A. *Macromolecules* **2008**, *41*, 7817–7823. (b) Yokoyama, A.; Suzuki, H.; Kubota, Y.; Ohuchi, K.; Higashimura, H.; Yokozawa, T. *J. Am. Chem. Soc.* **2007**, *129*, 7236–7237.

(30)   Tolman, C. A.; Seidel, W. C.; Gosser, L. W. *Organometallics* **1983**, *2*, 1391–1396.

(31)   Slagt, V. F.; de Vries, A. H. M.; de Vries, J. G.; Kellogg, R. M. *Org. Process Res. Dev.* **2010**, *14*, 30–47.

(32)   Lee, S. R.; Bryan, Z. J.; Wagner, A. M.; McNeil, A. J. *Chem. Sci.* **2012**, *3*, 1562–1566.

(33)   (a) Bronstein, H. A.; Luscombe, C. K. *J. Am. Chem. Soc.* **2009**, *131*, 12894–12895. (b) Doubina, N.; Stoddard, M.; Bronstein, H. A.; Jen, A. K. Y.; Luscombe, C. K. *Macromol. Chem. Phys.* **2009**, *210*, 1966–1972.

Chapter 2[1,2]

Effect of Ligand Electronic Properties on Precatalyst Initiation and Propagation in Ni-Catalyzed Cross-Coupling Polymerizations

Introduction

Ni-catalyzed cross-coupling reactions to form sp^2–sp^2 carbon–carbon bonds are widely utilized in both small molecule[1] and polymer syntheses.[2] It was recently discovered that certain difunctionalized molecules undergo Ni-catalyzed polymerization in a chain-growth fashion.[3] These methods have gained attention because previously inaccessible materials, like all-conjugated block[4] and gradient[5] copolymers, could now be prepared.[6] A new mechanism was proposed to account for this unexpected chain-growth behavior, which involves an intermediate Ni^0-polymer π-complex.[7-9] We anticipated that these polymerizations could be improved by modifying the ligand electronic properties. Specifically, we hypothesized that electron-donating ligands would facilitate chain-growth because they should promote the formation[10] and reactivity[11] of Ni^0-polymer π-complexes. We demonstrate herein that an electron-rich ligand outperforms the other ligands in the chain-growth polymerizations by providing polymers with narrower molecular weight distributions.

During these studies we observed slow initiation of the Ni(II) precatalyst. Although this transformation is often assumed to be fast relative to the cross-coupling reaction, this is not always the case.[12] Slow precatalyst initiation can impact both the yield and substrate scope in small-molecule cross-coupling reactions. For example, the development of activated M(II) precatalysts has enabled thermally unstable boronic acids to be cross-coupled in high yields.[12b] Slow precatalyst initiation can also have a significant impact on polymerizations, influencing both the molecular weight and molecular weight distributions (Đ) of the resulting polymers.[13] Despite the importance of precatalyst initiation, its rate relative to the cross-coupling reaction is often unknown. Thus, we report herein on the relative rates of precatalyst initiation and polymerization. These studies led to the surprising conclusion that precatalyst initiation is approximately 20x slower than polymerization, despite the fact that they share similar catalyst resting states and rate-limiting steps. Overall, these mechanistic studies provide a comprehensive view of ligand electronic effects in Ni-catalyzed cross-coupling polymerizations and suggest how to improve the chain-growth polymerizations by modifying the catalyst structure.

Results and Discussion

Because most (L–L)NiX$_2$ precatalysts are insoluble in ethereal solvents, we prepared soluble precatalysts **1a**-**c** to avoid any complications from heterogeneous initiation. Key structural features of these catalysts include: (1) The *ortho*-substituted arene reactive ligand, which increases catalyst solubility and stability[14] and (2) bis(diarylphosphino)ethanes with electron-withdrawing (*p*-Cl, σ_{para} = 0.24) and electron-donating (*p*-OMe, σ_{para} = -0.12) substituents to tune reactivity.[15,16] The polymerization of monomer **2** was used to evaluate the influence of ligand electronic properties (eqn (1)).[8c,17,18]

Ar =
1a — Cl
1b
1c — OMe

$$2 \xrightarrow[\substack{THF \\ 0\,°C}]{Ni\ catalyst} P2 \quad (1)$$
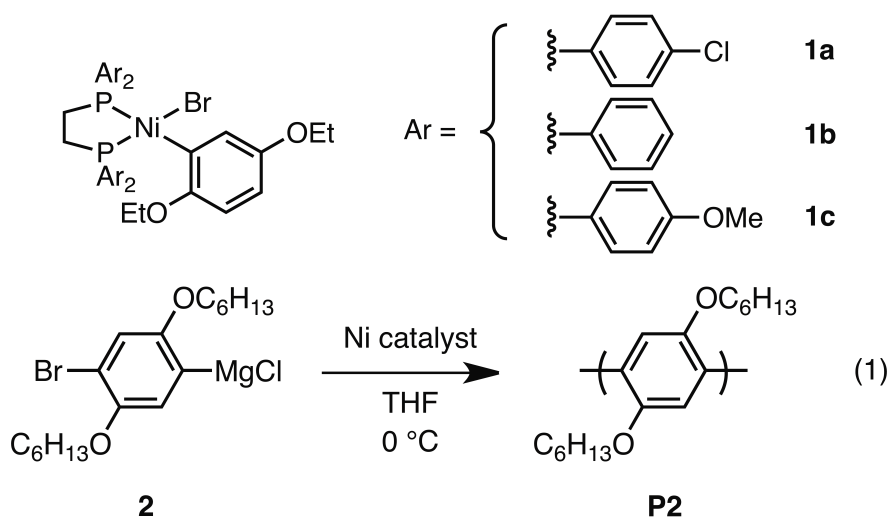
Initial rates (0-10% conversion) were monitored *via in situ* IR spectroscopy, following loss of monomer **2** as a function of time (Appendix 1). All three precatalysts (**1a-c**) exhibited polymerization rates with a zero-order dependence on [monomer] and approximately first-order dependence on [catalyst] (Figure 2-1A/B).[19] These rate data are consistent with either a turnover-limiting reductive elimination or intramolecular oxidative addition (*via* a Ni^0-polymer π-complex). To distinguish between these two scenarios, ^{31}P NMR spectroscopic studies were used to elucidate the catalyst resting state (Appendix 1). The observed pair of proximate doublets with narrow coupling constant was consistent with a (L–L)Ni(aryl)$_2$ species (**8**) as the resting-state (Appendix 1).[8c] Combined, these rate and spectroscopic results are consistent with a turnover-limiting reductive elimination for all three catalysts. The electron-poor ligand gave the fastest rates of reductive elimination (Hammett ρ value = +3.2 ± 0.4). This result is also consistent with a turnover-limiting reductive elimination because it involves a formal reduction of Ni(II) to Ni(0), which should be accelerated when the electron-density at the metal center is decreased.[20]
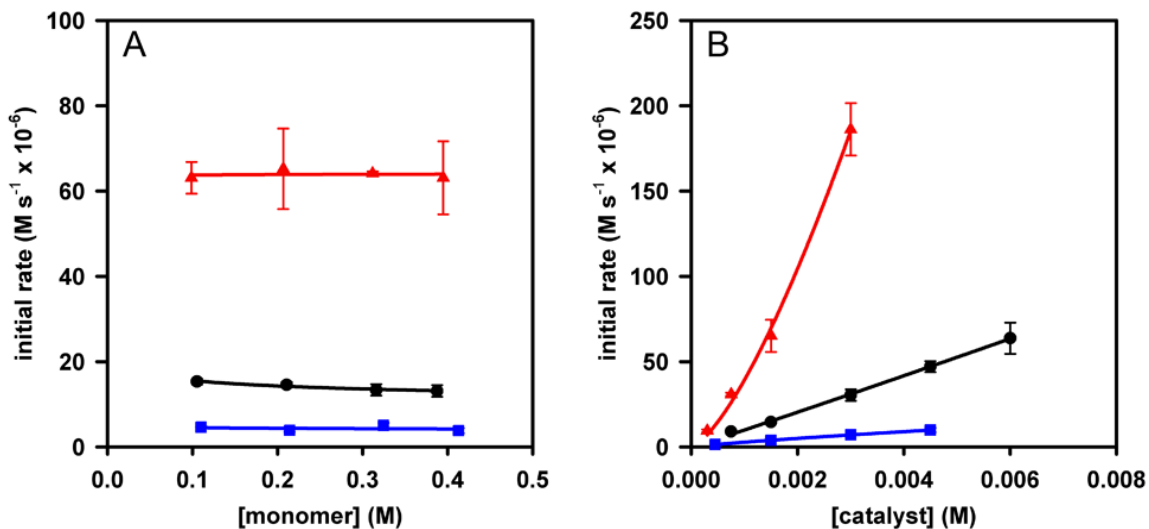
Figure 2-1. Plot of the initial rate *versus* (A) [monomer] and (B) [catalyst] for the polymerization of **2** in THF at 0 °C using catalysts **1a** (▲), **1b** (●) and **1c** (■).

During these studies, a significant induction period was observed, which varied based on both the catalyst and monomer concentrations. We suspected that this was due to slow precatalyst initiation because a similar slow initiation was observed for (L-L)NiCl$_2$ using bis(dialkylphosphino)ethane-based ligands.[8a,21] To measure the precatalyst initiation rates, model complexes **3a**-**c** were prepared. The key structural feature is a *para*-F substituent, which enabled *in situ* monitoring *via* ^{19}F NMR spectroscopy. To observe a single turnover, (2-methoxyphenyl)magnesium bromide (**4**) was used instead of monomer **2** (eqn (2)).[22]
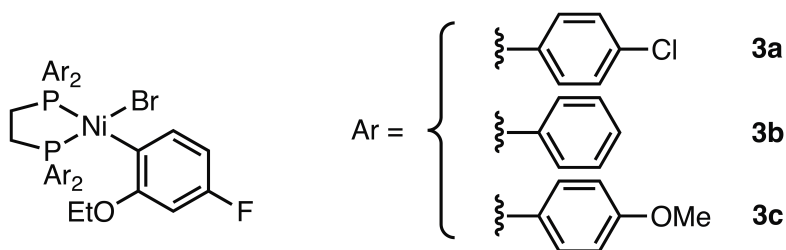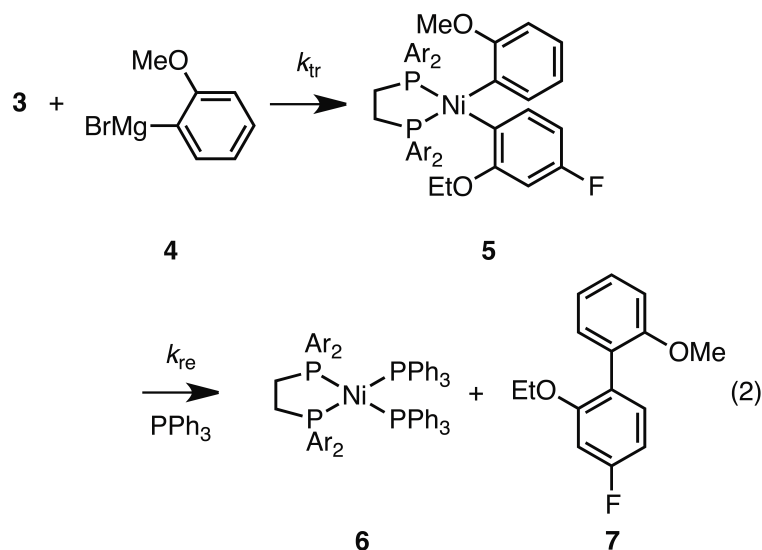
The loss of precatalyst **3**, formation and loss of intermediate **5**, and formation of product **7** were followed as a function of time (Figure 2-2A). The fact that all three species (**3**, **5** and **7**) were readily observed suggests that the relative rates of transmetalation and reductive elimination were similar. As a result, the effect of ligand electronic properties on both steps could be determined. By fitting the data for all three species to the rate equations (eqn (3)-(5)), the rate constants for both transmetalation (k_{tr}) and reductive elimination (k_{re}) were obtained (Appendix 1, Figure 2-2B and Table 2-1).[23]

$$\frac{d[\mathbf{3}]}{dt} = -k_{tr}[\mathbf{3}][\mathbf{4}] \qquad (3)$$

$$\frac{d[\mathbf{5}]}{dt} = k_{tr}[\mathbf{3}][\mathbf{4}] - k_{re}[\mathbf{5}] \qquad (4)$$

$$\frac{d[\mathbf{7}]}{dt} = k_{re}[\mathbf{5}] \qquad (5)$$
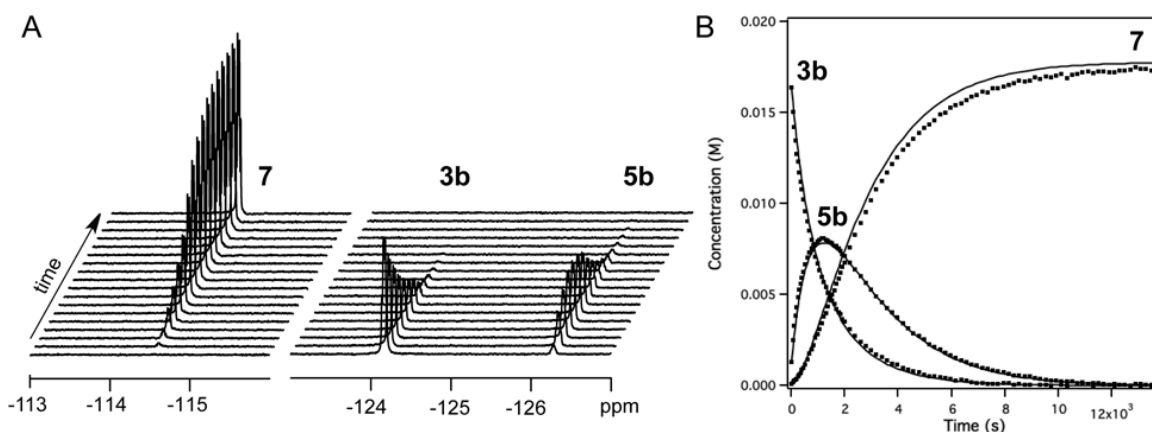
Figure 2-2. (A) Representative ^{19}F NMR spectroscopic data for the reaction depicted in eqn (2) using catalyst **3b**. (B) Representative fits of the data to eqn (3)-(5) to obtain the rate constants.

Table 2-1. Rate constants for precatalyst initiation and propagation.

	Precatalyst Initiation[a]		Propagation[b]	
catalyst	k_{tr} $(M^{-1} \cdot s^{-1} \times 10^{-3})$	k_{re} $(s^{-1} \times 10^{-3})$	catalyst	k_{re} $(s^{-1} \times 10^{-3})$
3a	140 ± 30	1.8 ± 0.2	**1a**	43 ± 6
3b	26 ± 3	0.43 ± 0.07	**1b**	9.7 ± 0.4
3c	12 ± 2	0.18 ± 0.01	**1c**	2.6 ± 0.2

[a]Reaction conditions: [**3**] = 0.02 M, [**4**] = 0.04 M, THF, -5 °C.
[b]Reaction conditions: [**1**] = 0.0015 M, [**2**] = 0.2 M, THF, 0 °C.

The electron-poor ligand led to the fastest rate constants for both transmetalation and reductive elimination. Because transmetalation (**3** → **5**) involves a formal nucleophilic substitution reaction at the metal center, it is reasonable that the electron-poor ligand, which enhances the electrophilicity of the catalyst, exhibits the highest reactivity.[24] As noted above, the electron-poor ligand is also expected to facilitate the reductive elimination.[20] Remarkably, the magnitude of the electronic effect is similar for both transmetalation (Hammett ρ value = +2.98 ± 0.06) and reductive elimination (Hammett ρ value = +2.8 ± 0.1).

Under these stoichiometric conditions, both transmetalation and reductive elimination contribute to the overall initiation rate. In contrast, under catalytic conditions the high monomer concentration increases the transmetalation rates and reductive elimination becomes the rate-limiting step of precatalyst initiation.

Thus, we can compare the rate constants for precatalyst initiation and polymerization.[25] The surprising conclusion is that propagation is significantly faster (~20x) than precatalyst initiation (Table 2-1). This result was unexpected because both rate-limiting steps involve the same fundamental transformation (reductive elimination) and the resting states (**5** and **8**) are similar in structure. The only difference is the substitution pattern of the reactive arenes. Previous work by Shekhar and Hartwig revealed that reductive elimination from biarylplatinum complexes is fastest when the two reactive arenes are electronically differentiated (*e.g.*, electron-rich and electron-poor).[26] Based on their results, we suspect that the difference in rates may arise from the electronic differences of the two reactive arenes in **8** (*i.e.*, polyaryl and aryl), which are more differentiated than in **5** (*i.e.*, H versus F). Importantly, these results are consistent with our previous work wherein the symmetric (depe)Ni(aryl)$_2$ complex, formed during precatalyst initiation of (depe)NiCl$_2$, exhibited slower rates of reductive elimination than the polymerization resting state – (depe)Ni(polyaryl)(aryl).[8a] This result demonstrates that the slow initiation observed herein is not simply a function of the model system, but is relevant to polymerizations initiated with (L-L)NiCl$_2$. Although LiCl has been reported to accelerate precatalyst initiation for thiophene-based monomers and Ni(dppp)Cl$_2$,[21] this additive effect is limited to cases where transmetalation is the rate-limiting step. When reductive elimination is rate-limiting, as it is herein, LiCl will have no effect on the initiation or propagation rates.[8c]
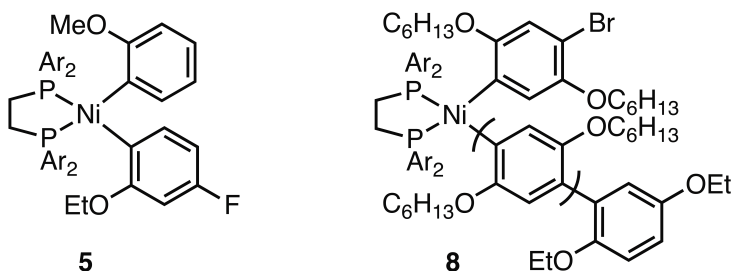
We concluded these studies by evaluating the chain-growth behavior of catalysts **1a-c** in the polymerization of monomer **2** (eqn (1)). As noted above, we

hypothesized that electron-donating ligands would improve the chain-growth polymerizations by both stabilizing the Ni^0-polymer π-complex and accelerating the subsequent oxidative addition reaction.[11] Both factors would minimize the opportunity for chain transfer and other competing reaction pathways to occur.

Indeed, the polymerizations with all three catalysts were consistent with a chain-growth mechanism, providing linear increases in molecular weight with conversion (Figure 2-3A). MALDI-TOF MS analysis of low molecular weight oligomers showed complete incorporation of Ar/H end-groups (where Ar = 2,5-diethoxybenzene, Appendix 1), consistent with each precatalyst initiating a single polymer chain.

Nevertheless, the dispersity (Đ) increased substantially with conversion for all three ligands, suggesting chain termination, chain transfer or other competing reaction pathways were occurring (Figure 2-3B). Notably, the electron-rich catalyst (**1c**) gave the narrowest Đ overall. The narrower Đ at the outset could be rationalized based on the relatively faster precatalyst initiation: propagation is merely 14x faster than initiation for **1c**. On the other hand, the increase in Đ with conversion is most readily explained by the intervention of competing reaction pathways. In principle, MALDI-TOF mass spectra acquired at later conversions would show evidence of these pathways (*i.e.*, an increase in polymers with H/H and H/Br end-groups). Unfortunately, we were unable to obtain high quality MALDI-TOF MS data for these higher molecular weight polymers. Nevertheless, the fact that the electron-donating ligand leads to the lowest dispersity suggests that it is effective in suppressing some of these competing reaction pathways, presumably via stabilization of the Ni(0)-polymer π-complex. The implication of these results is that further improvements in the chain-growth polymerizations may be achieved with ligands that are even more electron-donating than **1c**. Polymerizations performed at a higher monomer-to-catalyst ratio (100:1) gave high molecular weight polymers (29-41 kDa) in reasonable yields (54-67%) under these conditions.
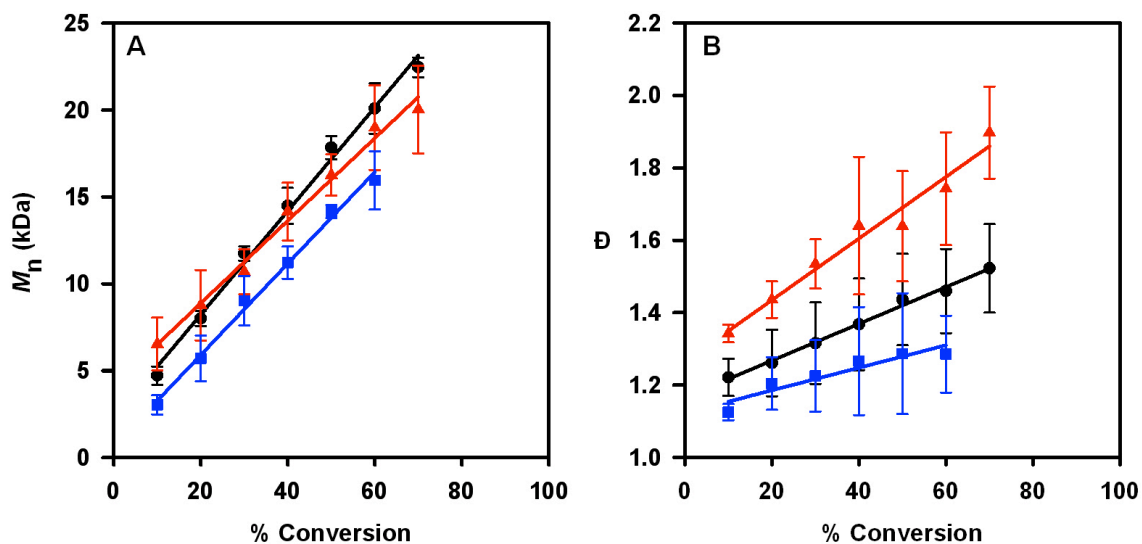
Figure 2-3. Plots of (A) number-average molecular weight (M_n) and (B) dispersity (Đ) *versus* conversion for the polymerization of **2** in THF at 0 °C using catalysts **1a** (▲), **1b** (●) and **1c** (■).

Conclusions

In summary, we demonstrated that ligand electronic properties have a significant impact on Ni-catalyzed chain-growth polymerizations. Specifically, the catalyst with the most electron-donating ligand gave improved chain-growth behavior compared to the conventional catalysts (Ni(dppe)Cl$_2$), due to both a suppression of chain-transfer and other competing pathways and a relative acceleration of precatalyst initiation over propagation. This new catalyst can provide access to polymers with better control over the molecular weight distribution and end-group functionality. By minimizing chain termination and transfer pathways, this catalyst will also lead to more homogeneous polymer samples in block and gradient copolymerizations.

These studies also revealed that precatalyst initiation is significantly slower than the cross-coupling polymerization. Similar results have been reported for Ni(II) and Pd(II) with boronic acids,[12b] suggesting that slow precatalyst initiation may be a more general phenomenon. Our studies revealed that, despite the different rates, both initiation and propagation proceed through the same rate-limiting step (reductive elimination) with structurally similar resting-states. As a consequence, changes to the ancillary ligand cannot be used to

overcome this limitation. Instead, the reactive ligand (*i.e.*, aryl in complexes such as (L–L)Ni(aryl)X) will need to be modified to accelerate precatalyst initiation selectively.[27]

References Cited

(1)	For recent reviews, see: (a) Magano, J.; Dunetz, J. R. *Chem. Rev.* **2011**, *111*, 2177–2250. (b) Hassan, J.; Sévignon, M.; Gozzi, C.; Schultz, E.; Lemaire, M. *Chem. Rev.* **2002**, *102*, 1359–1469.

(2)	For recent reviews, see: (a) Yamamoto, T. *Bull. Chem. Soc. Jpn.* **2010**, *83*, 431–455. (b) Geng, Y. H.; Huang, L.; Wu, S. P.; Wang, F. S. *Sci. Chin. Chem.* **2010**, *53*, 1620–1633. (c) Yokozawa, T.; Yokoyama, A. *Chem. Rev.* **2009**, *109*, 5595–5619. (d) Osaka, I.; McCullough, R. D. *Acc. Chem. Res.* **2008**, *41*, 1202–1214.

(3)	Ni-catalyzed chain-growth polymerizations were first reported in 2004. For reference, see: (a) Sheina, E. E.; Liu, J.; Iovu, M. C.; Laird, D. W.; McCullough, R. D. *Macromolecules* **2004**, *37*, 3526–3528. (b) Yokoyama, A.; Miyakoshi, R.; Yokozawa, T. *Macromolecules* **2004**, *37*, 1169–1171. (c) Miyakoshi, R.; Yokoyama, A.; Yokozawa, T. *Macromol. Rapid Commun.* **2004**, *25*, 1663–1666.

(4)	For recent examples of block copolymers prepared *via* this method, see: (a) Kim, J.; Siva, A.; Song, I. Y,; Park, T. *Polymer* **2011**, *52*, 3704–3709. (b) Higashihara, T.; Ohshimizu, K.; Ryo, Y.; Sakurai, T.; Takahashi, A.; Nojima, S.; Ree, M.; Ueda, M. *Polymer* **2011**, *52*, 3687–3695. (c) Ohshimizu, K.; Takahashi, A.; Higashihara, T.; Ueda, M. *J. Polym. Sci., Part A: Polym. Chem.* **2011**, *49*, 2709–2714. (d) Hollinger, J.; Jahnke, A. A.; Coombs, N.; Seferos, D. S. *J. Am. Chem. Soc.* **2010**, *132*, 8546–8547. (e) Van den Bergh, K.; Cosemans, I.; Verbiest, T.; Koeckelberghs, G. *Macromolecules* **2010**, *43*, 3794–3800. (f) Javier, A. E.; Varshney, S. R.; McCullough, R. D. *Macromolecules* **2010**, *43*, 3233–3237.

(5)	Locke, J. R.; McNeil, A. J. *Macromolecules* **2010**, *43*, 8709–8710.

(6)	For a comprehensive review, see: Kiriy, A.; Senkovskyy, V.; Sommer, M. *Macromol. Rapid Commun.* **2011**, *32*, 1503–1517.

(7)	(a) Tkachov, R.; Senkovskyy, V.; Komber, H.; Sommer, J. –U.; Kiriy, A. *J. Am. Chem. Soc.* **2010**, *132*, 7803–7810. (b) Achord, B. C.; Rawlins, J. W. *Macromolecules* **2009**, *42*, 8634–8639. (c) Beryozkina, T.; Senkovskyy, V.; Kaul, E.; Kiriy, A. *Macromolecules* **2008**, *41*, 7817–7823. (d) Miyakoshi, R.; Yokoyoma, A.; Yokozawa, T. *J. Am. Chem. Soc.* **2005**, *127*, 17542–17547. (e) Iovu, M. C.; Sheina, E. E.; Gil, R. R.; McCullough, R. D. *Macromolecules* **2005**, *38*, 8649–8656. See also, ref 21.

(8)	(a) Lanni, E. L.; Locke, J. R.; Gleave, C. M.; McNeil, A. J. *Macromolecules* **2011**, *44*, 5136–5145. (b) Lanni, E. L.; McNeil, A. J. *Macromolecules* **2010**, *43*, 8039–8044. (c) Lanni, E. L.; McNeil, A. J. *J. Am. Chem. Soc.* **2009**, *131*, 16573–16579.

(9)	Ni(0)-arene π-complexes have previously been implicated as intermediates in oxidative addition reactions. For a recent example, see: Li, T.; Garcia, J. J.; Brennessel, W. W.; Jones, W. D. *Organometallics* **2010**, *29*, 2430–2445.

(10)	Tolman, C. A.; Seidel, W. C.; Gosser, L. W. *Organometallics* **1983**, *2*, 1391–1396.

(11)   Electron-donating bidentate phosphines have been shown to accelerate Pd-catalyzed oxidative additions. For leading references, see: Slagt, V. F.; de Vries, A. H. M.; de Vries, J. G.; Kellogg, R. M. *Org. Process Res. Dev.* **2010**, *14*, 30–47. This result has theoretical support. For reference, see: Fazaeli, R.; Ariafard, A.; Jamshidi, S.; Tabatabaie, E. S.; Pishro, K. A. *J. Organomet. Chem.* **2007**, *692*, 3984–3993. See also, ref 24b.

(12)   For examples of slow precatalyst initiation: (a) *N*-heterocyclic carbene ligands: Nasielski, J.; Hadei, N.; Achonduh, G.; Kantchev, E. A. B.; O'Brien, C. J.; Lough, A.; Organ, M. G. *Chem. Eur. J.* **2010**, *16*, 10844-10853. (b) Phosphine ligands: Fan, X. –H.; Yang, L. –M. *Eur. J. Org. Chem.* **2011**, 1467–1471. Kinzel, T.; Zhang, Y.; Buchwald, S. L. *J. Am. Chem. Soc.* **2010**, *132*, 14073–14075. See also: Biscoe, M. R.; Fors, B. P.; Buchwald, S. L. *J. Am. Chem. Soc.* **2008**, *130*, 6686–6687.

(13)   For leading references, see: (a) Johnson, A. F.; Mohsin, M. A.; Meszena, Z. G.; Graves-Morris, P. *J. Macromol. Sci. Rev. Macromol. Chem. Phys.* **1999**, *C39*, 527–560. (b) Matyjaszewski, K. *J. Phys. Org. Chem.* **1995**, *8*, 197–207.

(14)   Nickel complexes containing *ortho*-substituted aryl groups have been reported to be more stable than other derivatives. For reference, see: (a) Hidai, M.; Kashiwagi, T.; Ikeuchi, T.; Uchida, Y. *J. Organomet. Chem.* **1971**, *30*, 279–282. (b) Chatt, J.; Shaw, B. L. *J. Chem. Soc.* **1960**, 1718–1729. The origin of this effect continues to be debated.

(15)   Both 1,2-bis(bis(4-(chlorophenyl)phosphino)ethane and 1,2-bis(bis(4-methoxyphenyl)phosphino)ethane were synthesized from 1,2-bis(dichlorophosphino)ethane and the corresponding Grignard reagent. For reference, see: Chatt, J.; Hussain, W.; Leigh, G. J.; Ali, H. M.; Pickett, C. J.; Rankin, D. A. *J. Chem. Soc., Dalton Trans* **1985**, 1131–1136.

(16)   Related complexes have been used in Ni-catalyzed polymerizations to generate end-labeled and surface-grafted conjugated polymers. For recent examples, see: (a) Marshall, N.; Sontag, S. K.; Locklin, J. *Chem. Commun.* **2011**, *47*, 5681–5689. (b) Sontag, S. K.; Sheppard, G. R.; Usselman, N. M.; Marshall, N.; Locklin, J. *Langmuir* **2011**, *27*, 12033–12041. (c) Doubina, N.; Paniagua, S. A.; Soldatova, A. V.; Jen, A. K. Y.; Marder, S. R.; Luscombe, C. K. *Macromolecules* **2011**, *44*, 512–520. (d) Smeets, A.; Wilot, P.; De Winter, J.; Gerbaux, P.; Verbiest, T.; Koeckelberghs, G. *Macromolecules* **2011**, *44*, 6017–6025. (e) Tkachov, R.; Senkovskyy, V.; Oertel, U.; Synytska, A.; Horecha, M.; Kiriy, A. *Macromol. Rapid Commun.* **2010**, *31*, 2146–2150.

(17)   Monomer **2** was prepared *in situ via* a Grignard metathesis reaction with *i*-PrMgCl. For reference, see: Shi, L.; Chu, Y.; Knochel, P.; Mayr, H. *J. Org. Chem.* **2009**, *74*, 2760–2764.

(18)   Miyakoshi, R.; Shimono, K.; Yokoyama, A.; Yokozawa, T. *J. Am. Chem. Soc.* **2006**, *128*, 16012–16013.

(19)   The rate dependence on [catalyst] for **1a** is 1.41 ± 0.08 (Figure 2-1B). The reaction order becomes 1.13 ± 0.06 when only the lowest three [catalyst] are fitted, suggesting that the non-linearity stems from the challenges associated with measuring extremely fast reaction rates.

(20)   For leading references on electronic effects of ligands in reductive eliminations, see: Hartwig, J. F. *Inorg. Chem.* **2007**, *46*, 1936–1947. For a recent example, see: Korenaga, T.; Abe, K.; Ko, A.; Maenishi, R.; Sakai, T. *Organometallics* **2010**, *29*, 4025–4035.

(21)   Slow initiation was also observed in the polymerization of hindered thiophenes with Ni(dppe)Cl$_2$ and Ni(dppp)Cl$_2$. For reference, see: (a) Wu, S.; Huang, L.; Tian, H.; Geng, Y.; Wang, F. *Macromolecules* **2011**, *44*, 7558–7567. (b) Lamps, J. –P.; Catala, J. –M. *Macromolecules*

2011, *44*, 7962–7968. (c) Tkachov, R.; Senkovskyy, V.; Komber, H.; Kiriy, A. *Macromolecules* **2011**, *44*, 2006–2015.

(22)   Note that 2 equiv of PPh$_3$ were needed to trap the Ni(0) generated during the reaction. Control experiments indicated that the excess PPh$_3$ does not affect the reaction rates, consistent with a post-rate-limiting ligand association (Appendix 1).

(23)   For leading references on the numerical integration procedure, see: (a) Hoepker, A. C.; Gupta, L.; Ma, Y.; Faggin, M. F.; Collum. D. B. *J. Am. Chem. Soc.* **2011**, *133*, 7135–7151. (b) Ma, Y.; Hoepker, A. C.; Gupta, L.; Faggin, M. F.; Collum. D. B. *J. Am. Chem. Soc.* **2010**, *132*, 15610–15623.

(24)   (a) In general, electron-donating ligands attenuate transmetalation reactions; however, most studies used monodentate ligands and these reactions often undergo ligand dissociation prior to transmetalation. For an example, see: Farina, V. *Pure Appl. Chem.* **1996**, *68*, 73–78. (b) For an excellent discussion, see: Jover, J.; Fey, N.; Purdie, M.; Lloyd-Jones, G. C.; Harvey, J. N. *J. Mol. Catal. A: Chem.* **2010**, *324*, 39–47.

(25)   Note that the reaction temperatures of the rate studies were different (initiation, -5 °C; propagation, 0 °C)

(26)   Shekhar, S.; Hartwig, J. F. *J. Am. Chem. Soc.* **2004**, *126*, 13016-13027.

(27)   To avoid the need for different precatalysts for each cross-coupling reaction, the desired precatalyst could be prepared *in situ* from (L–L)NiX$_2$ and one equivalent of a sterically hindered Grignard reagent to generate (L–L)Ni(aryl)X. For reference, see: Senkovskyy, V.; Sommer, M.; Tkachov, R.; Komber, H.; Huck, W. T. S.; Kiriy, A. *Macromolecules* **2010**, *43*, 10157–10161.

Chapter 3[1,2]

Accelerating Ni(II) Precatalyst Initiation using Reactive Ligands and Its Impact on Chain-Growth Polymerization

Introduction

Organic π-conjugated polymers are used in energy-related applications such as photovoltaics (PVs),[1] light-emitting diodes (LEDs)[2] and field effect transistors (FETs).[3] In all of these applications, the device performance can be substantially influenced by the polymer molecular weight and copolymer sequence, as well as the molecular weight distribution. For example, Kowalewski and coworkers observed improved charge carrier mobilities with higher molecular weight poly(3-hexylthiophene) in thin-film FETs.[4] In another example, Galvin and co-workers observed higher LED efficiencies when poly((2,5-bisoctyloxy)-1,4-phenylene vinylene)s with narrower molecular weight distributions were utilized.[5] Because device performance is dependent on molecular weight, copolymer sequence and polydispersity, synthesizing π-conjugated polymers with control over these variables is important. The recently developed Ni- and Pd-catalyzed chain-growth polymerization methods[6-8] have enabled unprecedented control over polymer molecular weight and copolymer sequence.[9-12] Nevertheless, the current methods exhibit sluggish precatalyst initiation (compared to propagation), as well as chain-transfer and chain-termination processes, all of which impact the polymer molecular weight, copolymer sequence and polydispersity. As a result, the continued development of new catalysts is needed.

We[13] and others[14] have investigated the impact of ancillary ligand structure on the Ni-catalyzed chain-growth polymerizations. We recently reported that catalysts ligated by electron-donating phosphines led to polymers with lower dispersities (Đ) than catalysts containing electron-withdrawing phosphines.[13a] These results were attributed to the impact of increased electron-density in promoting the formation and reactivity of a key intermediate (i.e., Ni(0)-polymer π-complex).[15] During these studies we observed a surprisingly slow precatalyst initiation relative to propagation (k_{rel} ~ 20), even for the conventional catalyst containing 1,2-bis(diphenylphosphino)ethane (dppe) as the ligand.[13a] Slow precatalyst initiation leads to broader sequence and molecular weight distributions in chain-growth polymerizations. Further studies revealed that the turnover-limiting step for both initiation and propagation is the same. As a consequence, the ancillary ligand cannot be used to selectively accelerate the initiation. An alternative is to use a reactive ligand (*e.g.*, a functionalized arene) to increase the precatalyst initiation rate without influencing the propagation rate.

We report herein the synthesis of four new Ni precatalysts with electronically varied reactive ligands and their impact on the initiation rate. Our precatalyst design was inspired by Shekhar and Hartwig's study of reductive elimination rates in (L-L)Pt(Ar)(Ar′) complexes.[16] The fastest rates were observed when the two reactive arenes were the most electronically differentiated. These rate differences were attributed to the increased electrophilicity and nucleophilicity of the two reacting arenes. We applied the same rationale to design a series of precatalysts with varying reactive ligands. Using this approach, we demonstrate herein that precatalyst initiation can be selectively accelerated over propagation, and that faster initiations produce polymer samples with narrower molecular weight distributions. Combined, these results highlight the important role of initiation in chain-growth polymerizations. Because the fastest rates were obtained when the reactive ligand was the most electronically differentiated from the monomer, we originally attributed this effect to the nucleophilicity/electrophilicity of the reacting arenes. However, computational studies revealed no correlation between the free energy barriers and atomic

charges at the reacting carbons. Instead, a strong correlation was observed between the free energy barriers and the change in charge delocalization onto the reactive ligands during the turnover-limiting step. As a consequence, the fastest rates are predicted to occur when the reactive ligand is substituted with resonance-based electron-withdrawing groups. Overall, these results demonstrate that a simple approach for improving chain-growth polymerizations of π-conjugated monomers is to modify the reactive ligand's electronic properties.

Results and discussion

To determine the reactive ligand influence on precatalyst initiation, Ni precatalysts **1a**–**d** were prepared (Appendix 2). The reactive ligand includes: (i) an *ortho*-trifluoroethoxy substituent for facile analysis via ^{19}F NMR spectroscopy and stabilization,[17] and (ii) *para*-substituents with varying electronic properties to tune the reductive elimination rate. Commercially available dppe was selected as the ancillary ligand because it mediates chain-growth polymerizations of several important π-conjugated monomers.[18]
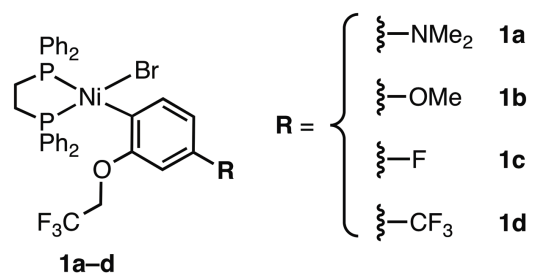
Initiation involves precatalyst **1** undergoing transmetalation with monomer (*i.e.*, aryl Grignard), followed by reductive elimination (eqn (1)). To prevent polymerization in our model system, Grignard **2** was used as a substitute for monomer **6**. The key difference is that the 4-Cl substituent (in **2**) minimizes the likelihood of further propagation due to its low reactivity in oxidative addition reactions.[19] Importantly, there should be minimal rate differences between the model system and the polymerization because Cl and Br have similar electronic

properties. Grignard **2** was prepared by Grignard metathesis with *i*-PrMgCl and 1-bromo-4-chloro-2,5-dimethoxybenzene (Appendix 2).[20] A quenched sample revealed exclusive formation of regioisomer **2**, indicating selective metathesis of the C-Br bond (Appendix 2).[21]

$$\frac{d[\mathbf{3}]}{dt} = -k_{re}[\mathbf{3}] \quad (2)$$
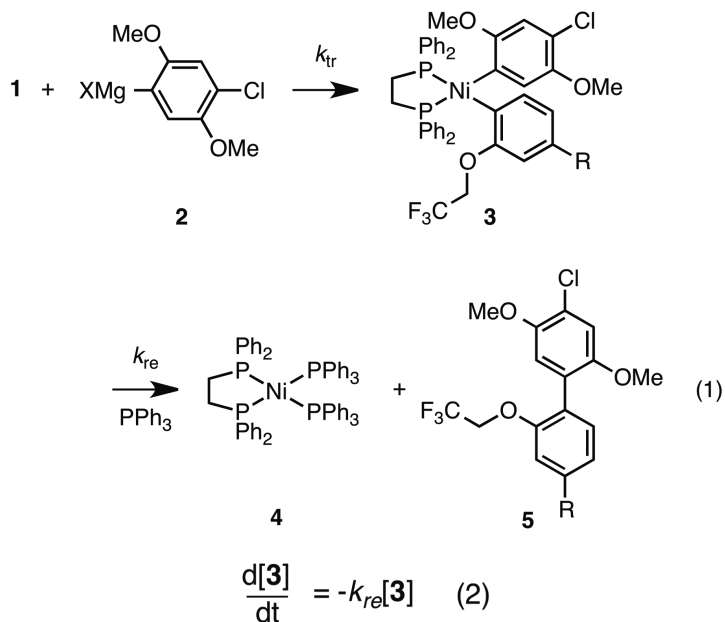
Initiation of precatalysts **1a–d** with stoichiometric amounts of Grignard **2** was monitored *via* ^{19}F NMR spectroscopy at 0 °C in THF (Figure 3-1A and Appendix 2). Triphenylphosphine (PPh_3) was used to trap the Ni(0) as complex **4** after reductive elimination. Control experiments revealed that excess PPh_3 has no effect on reaction rates (Appendix 2). Because transmetalation was too fast to monitor under these conditions, reductive elimination from intermediates **3a–d** was followed as a function of time (Figure 3-1A/B). The data were fit to corresponding rate equation (eqn (2)), providing the rate constants for reductive elimination (Table 3-1).[22] As anticipated, the reactive ligand had a dramatic impact on the reductive elimination rate constants. For example, intermediate **3c** (R = F) exhibited a reductive elimination rate constant that was two orders of magnitude slower than intermediate **3a** (R = NMe_2). Interestingly, reductive eliminations from both electron-poor intermediate **3d** (R = CF_3) and electron-rich

intermediate **3b** (R = OMe) were similar in magnitude, suggesting that the difference in reactive ligand electronic properties (compared to the monomer) is the predominant factor. The fastest rate constants were obtained when the reactive ligand contained a strongly resonance donating substituent, consistent with the notion that electrophilicity/nucleophilicity of the reactive ligands contributes to the rates. Significantly, the fastest precatalyst (**1a**) underwent initiation at a rate similar to propagation (k_{prop} = 9.7 x 10^{-3} s^{-1}).[13a,23] This result suggests that **1a** should produce polymer samples with the narrowest molecular weight distributions. Overall, these studies revealed that the reactive ligands dramatically influence the initiation rate.
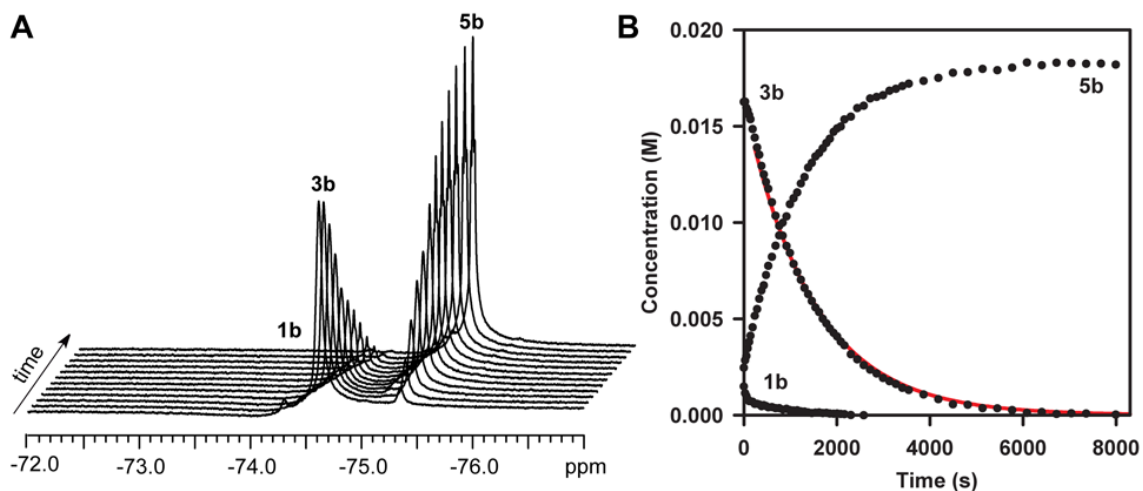
Figure 3-1. (A) Representative ^{19}F NMR spectroscopic data for the reaction depicted in eqn (1) using catalyst **1b**. (B) Representative fit of the data to eqn (2) to obtain the rate constant.

Table 3-1. Experimental rate constants (k_{re}) and free energy of activation ($\Delta G^{\ddagger}$) for precatalyst initiation.

Precatalyst	k_{re} (x 10^{-3} s^{-1})	$\Delta G^{\ddagger}$ (kcal/mol)
1a	6.88 ± 0.06	18.6
1b	0.671 ± 0.006	19.9
1c	0.0520 ± 0.0001	21.3
1d	0.222 ± 0.002	20.5

Monomer **6** was then polymerized with precatalysts **1a–d** to evaluate the impact of initiation rate on the resulting polymer samples. The polymerization was monitored via in situ IR spectroscopy and aliquots were periodically withdrawn and quenched to determine the number-average molecular weight (M_n) and Đ as a function of conversion by gel permeation chromatography (GPC). As evident in Figure 3-2A, the fastest initiating precatalyst (**1a**) yielded polymers with the lowest Đ whereas the slowest initiating precatalyst (**1c**) yielded polymers with the highest Đ. The GPC data reveals that the broadening of the Đ is due to low molecular weight oligomers (Figure 3-2B and Appendix 2). Because dispersities reflect slow initiations as well as chain-transfer and chain-termination events, MALDI-TOF MS analysis of the end-groups in low molecular weight oligomers was used to distinguish between these pathways. These studies revealed exclusively Ar/H end-groups for all four precatalysts, indicating that chain-transfer or chain-termination reactions are not occurring under these conditions (Appendix 2). Thus, the broadening of the Đ observed with these precatalysts can be largely attributed to the different relative rates of initiation versus propagation. To illustrate the magnitude of this effect, Figure 3-2C/D overlays the estimated concentration of unreacted precatalyst **1a/1c** with monomer **6** versus time for the polymerizations. These plots highlight the significance and underappreciated impact of a slow initiation on the chain-growth polymerizations. Overall, these studies reveal that selectively accelerating initiation using reactive ligands is a successful strategy for narrowing the molecular weight distributions in chain-growth polymerizations of π-conjugated monomers.
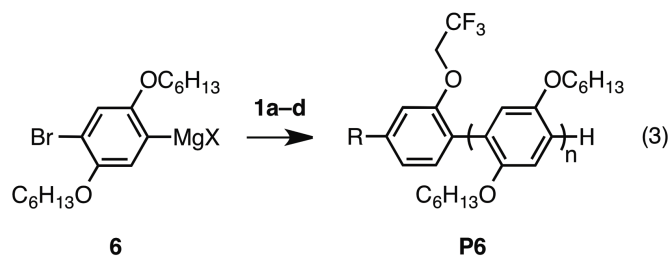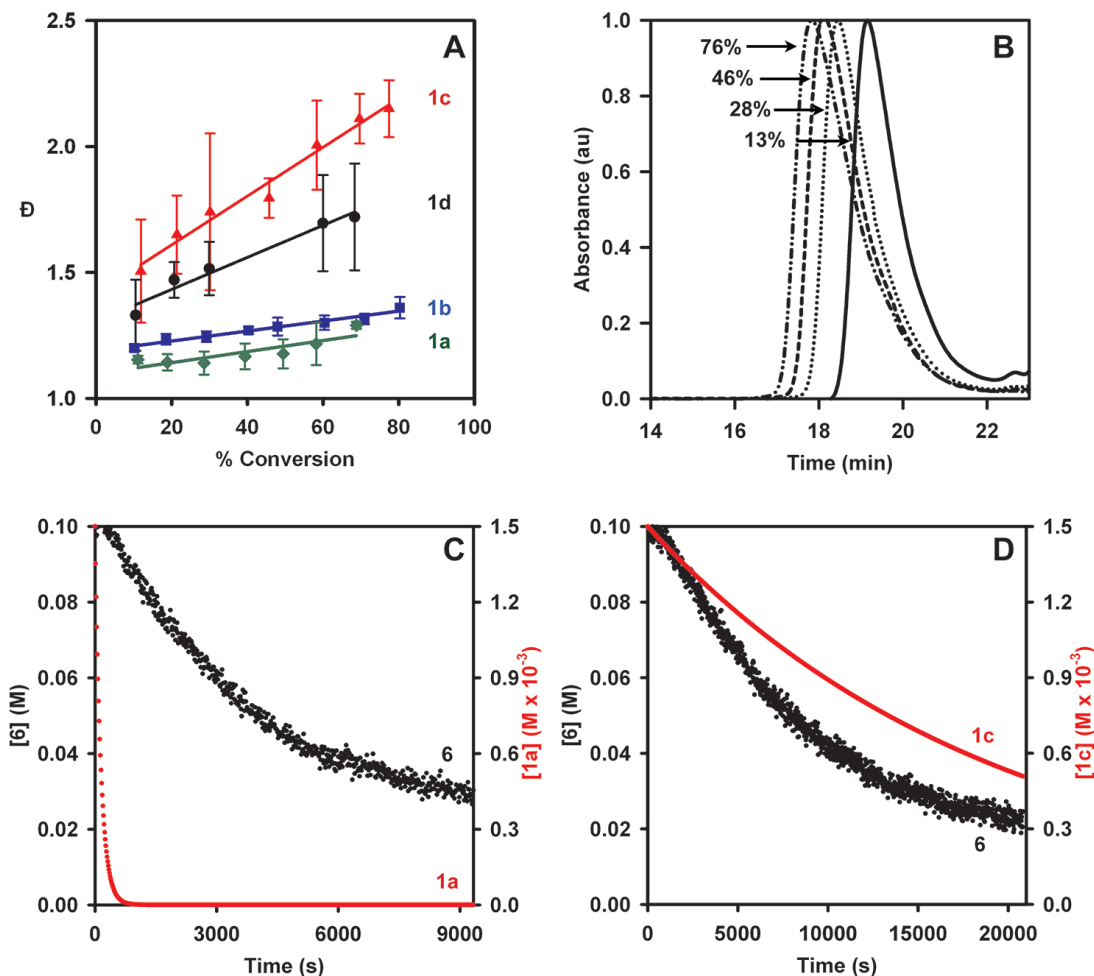
Figure 3-2. (A) Plot of dispersity (Đ) versus monomer conversion for the polymerization of **6** using precatalysts **1a–d**. (B) Representative gel permeation chromatograms at varying percent conversions for the polymerization of **6** with precatalyst **1c**. (C) and (D) Plot of [monomer] (black) and [precatalyst] (red) *versus* time for the polymerization of **6** with precatalysts **1a** (C) and **1c** (D).

To provide a framework for generalizing this approach, the free energy barriers for reductive elimination from **3** were computed for the four substituents examined experimentally, as well as R = H and 15 other *para*-substituents (see Appendix 2 for full list). Computations were performed using Guassian09, and employed the BP86 DFT functional[24] paired with the 6-311+G(d) basis set[25] for non-metal atoms and the SDB-cc-pVTZ basis set with the small core, fully relativistic effective core potential[26] for Ni. The predicted activation free energies (ΔG‡) for **3a–d** are in agreement with the experimental data.[27]

If the reductive elimination rates were purely determined by arene electrophilicity/nucleophilicity, as initially anticipated, the computed free energy barriers should correlate with the differences in atomic charges at the reacting carbons (as predicted by natural population analyses). Surprisingly, no such correlation was observed (Appendix 2). Instead, a modest correlation (r^2 = 0.65) was observed between the free energy barriers and the Hammett σ^- values,[28] which characterize the ability of a *para*-substituent to stabilize negative charge through direct resonance effects (Figure 3-3A). The importance of charge delocalization was further supported by a strong correlation (r^2 = 0.94) between the barrier heights and the *change* in the charge on the two arenes on going from **3** to the transition state (Figure 3-3B). This correlation indicates that the reductive elimination rates are largely modulated by the ability of the two arenes to stabilize the increasing electron density on the catalyst during reductive elimination. Importantly, the strong correlation is only observed when *both* rings are considered, indicating that there is some interplay between the delocalizing effect of the two arenes in the transition state. These results predict that the fastest initiation rates with monomer **2** (or **6**) will occur with strongly resonance-based electron-withdrawing substituents (e.g., R = NO_2) on precatalyst **1**. These and related reactive ligands will be the subject of future studies.
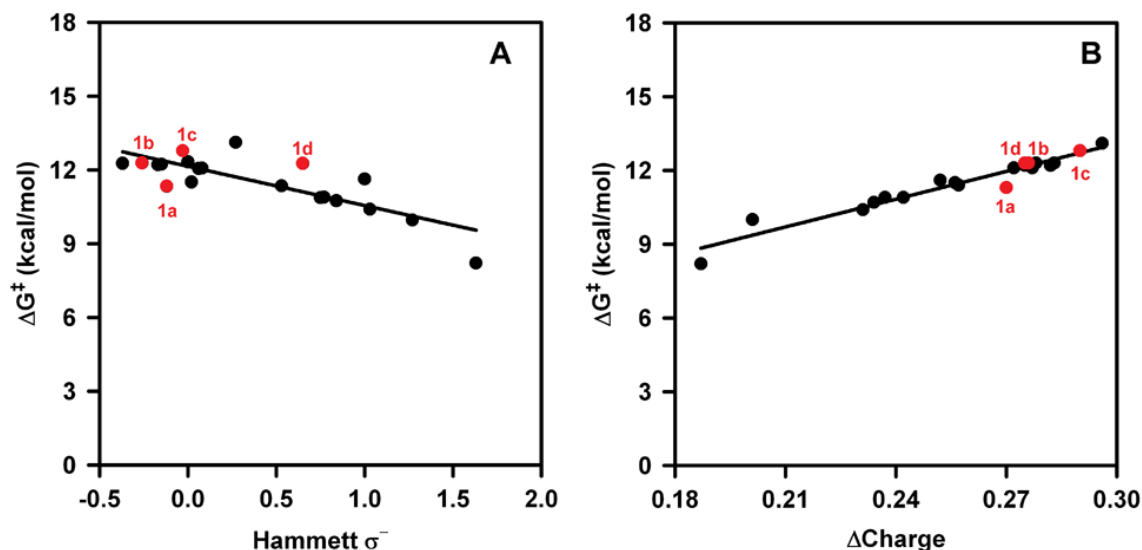
Figure 3-3. Plots of computed free energy barriers ($\Delta G^{\ddagger}$) for reductive elimination from **3** *versus* (A) Hammett σ^- values for substituent R and (B) the change in charge (ΔCharge) on the two reacting arenes going from **3** to the transition state, excluding the carbon atoms bound to Ni.

Conclusions

In summary, we have demonstrated that modifying the reactive ligand on the Ni precatalyst can be used to selectively accelerate initiation over propagation. We have shown that faster initiations lead to polymer samples with narrower molecular weight distributions, highlighting the importance of precatalyst initiation in these chain-growth polymerizations. Significantly, the PDIs obtained with precatalyst **1a** are the lowest reported for poly(2,5-bis(hexyloxy)phenylene) synthesis. Computational studies predict that the lowest activation free energies can be achieved with precatalysts containing resonance-based electron-withdrawing substituents, in contrast to our initial assumption about the nucleophilicity/electrophilicity of the reactive ligands. Although this work focuses on aryl cross-coupling reactions, the results are anticipated to be generalizable to heteroaryl cross-coupling reactions (*e.g.*, thiophenes) because the mechanism (including the turnover-limiting step) was previously shown to be similar.

References Cited

(1)   For recent reviews, see: (a) Li, G.; Zhu, R.; Yang, Y. *Nature Pho-ton.* **2012**, *6*, 153-161. (b) Boudreault, P. –L. T.; Najari, A.; Leclerc M. *Chem. Mater.* **2011**, *23*, 456–469. (c) Facchetti, A. *Chem. Mater.* **2011**, *23*, 733–758. (d) Beaujuge, P. M.; Fréchet, J. M. J. *J. Am. Chem. Soc.* **2011**, *133*, 20009–20029. (e) Brabec, C. J.; Gowrisanker, S.; Halls, J. J. M.; Laird, D.; Jia, S. J.; Williams, S. P. *Adv. Mater.* **2010**, *22*, 3839–3856.

(2)   For a recent review, see: Grimsdale, A. C.; Chan, K. L.; Martin, R. E.; Jokisz, P. G.; Holmes, A. B. *Chem. Rev.* **2009**, *109*, 897–1091.

(3)   For recent reviews, see: (a) Kola, S.; Sinha, J.; Katz, H. E. *J. Polym. Sci., Part B: Polym. Phys.* **2012**, *50*, 1090–1120. (b) Wang, C.; Dong, H.; Hu, W.; Liu, Y.; Zhu, E. *Chem. Rev.* **2012**, *112*, 2208–2267. (c) Virkar, A. A.; Mannsfield, S.; Bao, Z.; Stingelin, N. *Adv. Mater.* **2010**, *22*, 3857–3875.

(4)   Zhang, R.; Li, B.; Iovu, M. C.; Jeffries-EL, M.; Sauvé, G.; Cooper, J.; Jia, S.; Tristram-Nagle, S.; Smilgies, D. M.; Lambeth, D. N.; McCullough, R. D.; Kowalewski, T. *J. Am. Chem. Soc.* **2006**, *128*, 3480–3481.

(5)   Menon, A.; Dong, H.; Niazimbetova, Z. I.; Rothberg, L. J.; Galvin, M. E. *Chem. Mater.* **2002**, *14*, 3668–3675. Note that the opposite trend was observed for n-type conjugated polymers. For reference, see: Konezny, S. J.; Rothberg, L. J.; Galvin, M. E.; Smith, D. L. *Appl. Phys. Lett.* **2010**, *97*, 143305–143305–3.

(6)   Ni-catalyzed chain-growth polymerizations were first reported in 2004. For references, see: (a) Yokoyama, A.; Miyakoshi, R.; Yokozawa, T. *Macromolecules* **2004**, *37*, 1169–1171. (b) Miyakoshi, R.; Yokoyama, A.; Yokozawa, T. *Macromol. Rapid Commun.* **2004**, *25*, 1663–1666. (c) Sheina, E. E.; Liu, J. S.; Iovu, M. C.; Laird, D. W.; McCullough, R. D. *Macromolecules* **2004**, *37*, 3526–3528.

(7)   For recent reviews, see: (a) Yokozawa, T.; Nanashima, Y.; Ohta, Y. *ACS Macro Lett.* **2012**, *1*, 862–866. (b) McNeil, A. J.; Lanni E. L. New Conjugated Polymers and Synthetic Methods. In *Synthesis of Polymers*; Schlüter, D. A., Hawker, C. J., Sakamoto, J., Eds.; Wiley-VCH: Germany, 2012; Vol. 1, pp475–486. (c) Kiriy, A.; Senkovskyy, V.; Sommer, M. *Macromol. Rapid Commun.* **2011**, *32*, 1503–1517. (d) Okamoto, K.; Luscombe, C. K. *Polym. Chem.*, **2011**, *2*, 2424–2434. (e) Yokozawa, T.; Yokoyama, A. *Chem. Rev.* **2009**, *109*, 5595–5619.

(8)   (a) Zhang, H. –H.; Xing, C. –H.; Hu, Q. –S. *J. Am. Chem. Soc.* **2012**, *134*, 13156–13159. (b) Bryan, Z. J.; Smith, M. L.; McNeil, A. J. *Macromol. Rapid Commun.* **2012**, *33*, 842–847. (c) Yokozawa, T.; Suzuki, R.; Nojima, M.; Ohta, Y.; Yokoyama, A. *Macromol. Rapid Commun.* **2011**, *32*, 801–806. (d) Elmalem, E.; Kiriy, A.; Huck, W. T. S. *Macromolecules* **2011**, *44*, 9057–9061. (e) Verswyvel, M.; Verstappen, P.; De Cremer, L.; Verbiest, T.; Koeckelberghs, G. *J. Polym. Sci., Part A: Polym. Chem.* **2011**, *49*, 5339–5349. (f) Yokozawa, T.; Kohno, H.; Ohta, Y.; Yokoyama, A. *Macromolecules* **2010**, *43*, 7095–7100. (g) Grisorio, R.; Suranna, G. P. Mastrorilli, P. *Chem. Eur. J.* **2010**, *16*, 8054–8061. (h) Huang, W.; Su, L.; Bo, Z. *J. Am. Chem. Soc.* **2009**, *131*, 10348–10349. (i) Beryozkina, T.; Boyko, K.; Khanduyeva, N.; Senkovskyy, V.; Horecha, M.; Oertel, U.; Simon, F.; Stamm, M.; Kiriy, A. *Angew. Chem. Int. Ed.* **2009**, *48*, 2695–2698. (j) Yokoyama, A.; Suzuki, H.; Kubota, Y.; Ohuchi, K.; Higashimura, H.; Yokozawa, T. *J. Am. Chem. Soc.* **2007**, *129*, 7236–7237.

(9)   For recent examples of all-conjugated block copolymers, see: (a) Lin, Y.; Lim, J. A.; Wei, Q.; Mannsfeld, S. C. B.; Briseno, A. L.; Watkins, J. J. *Chem. Mater.* **2012**, *24*, 622–632. (b) Umezawa, K.; Oshima, T.; Yoshizawa-Fujita, M.; Takeoka, Y.; Rikukawa, M. *ACS Macro. Lett.*

2012, *1*, 969–972. (c) Bhatt, M. P.; Huynh, M. K.; Sista, P.; Nguyen, H. Q.; Stefan, M. C. *J. Polym. Sci., Part A: Polym. Chem.* **2012**, *50*, 3086–3094. (d) Sui, A. G.; Chi, X. C.; Wu, S. P.; Tian, H. K.; Geng, Y. H.; Wang, F. S. *Macromolecules* **2012**, *45*, 5436–5443. (e) Song, I. Y.; Kim, J.; Im, M. J.; Moon, M. J.; Park, T. *Macromolecules* **2012**, *45*, 5038–5068. (f) Hollinger, J.; DiCarmine, P. M.; Karl, D.; Seferos, D. S. *Macromolecules* **2012**, *45*, 3772–3778.

(10)   For examples of gradient copolymers, see: (a) Palermo, E. F.; McNeil, A. J. *Macromolecules* **2012**, *45*, 5948–5955. (b) Locke, J. R.; McNeil, A. J. *Macromolecules* **2010**, *43*, 8709–9710.

(11)   For recent examples of surface-grafted polymers, see: (a) Marshall, N.; Sontag, S. K.; Locklin, J. *Chem. Commun.* **2011**, *47*, 5681–5689. (b) Senkovskyy, V.; Senkovska, I.; Kiriy, A. *ACS Macro Lett.* **2012**, *1*, 494–498. (c) Doubina, N.; Jenkins, J. L.; Paniagua, S. A.; Mazzio, K. A.; MacDonald, G. A.; Jen, A. K. Y.; Armstrong, N. R.; Marder, S. R.; Luscombe, C. K. *Langmuir* **2012**, *28*, 1900–1908. (d) Sontag, S. K.; Sheppard, G. R.; Usselman, N. M.; Marshall, N.; Locklin, J. *Langmuir* **2011**, *27*, 12033–12041.

(12)   For recent examples of end-functionalized polymers, see: (a) Kochemba, W. M.; Kilbey, S. M.; Pickel, D. L. *J. Polym. Sci., Part A: Polym. Chem.* **2012**, *50*, 2762–2769. (b) Stefan, M. C.; Bhatt, M. P.; Sista, P.; Magurudeniya, H. D. *Polym. Chem.* **2012**, *3*, 1693–1701. (c) Yuan, M.; Okamoto, K.; Bronstein, H. A.; Luscombe, C. K. *ACS Macro Lett.* **2012**, *1*, 392–395. See also, ref 13a.

(13)   (a) Lee, S. R.; Bryan, Z. J.; Wagner, A. M.; McNeil, A. J. *Chem. Sci.* **2012**, *3*, 1562–1566. (b) Lanni, E. L.; Locke, J. R.; Gleave, C. M.; McNeil, A. J. *Macromolecules* **2011**, *44*, 5136–5145. (c) Lanni, E. L.; McNeil, A. J. *Macromolecules* **2010**, *43*, 8039-8044. (d) Lanni, E. L.; McNeil, A. J. *J. Am. Chem. Soc.* **2009**, *131*, 16573–16579.

(14)   Fpr recent examples, see: (a) Nanashima, Y.; Shibata, R.; Miyakoshi, R.; Yokoyama, A.; Yokozawa, T. *J. Polym. Sci., Part A: Polym. Chem.* **2012**, *50*, 3628–3640. (b) Sui, A.; Shi, X.; Wu, S.; Tian, H.; Geng, Y.; Wang, F. *Macromolecules* **2012**, *45*, 5436–5443. (c) Magurudeniya, H. D.; Sista, P.; Westbook, J. K.; Ourso, T. E.; Nguyen, K.; Maher, M. C.; Alemseghed, M. G.; Biewer, M. C.; Stefan, M. C. *Macromol. Rapid Commun.* **2011**, *32*, 1748–1752. (d) Doubina, N.; Stoddard, M.; Bronstein, H. A.; Jen, A. K. –Y.; Luscombe, C. K. *Macromol. Chem. Phys.* **2009**, *210*, 1966–1972.

(15)   Bryan, Z. J.; McNeil, A. J. *Chem. Sci.* **2013**, *4*, 1620–1624.

(16)   Shekhar, S.; Hartwig, J. F. *J. Am. Chem. Soc.* **2004**, *126*, 13016-13027.

(17)   Nickel complexes containing *ortho*-substituted aryl groups have been reported to be more stable than other derivatives. For references, see: (a) Hidai, M.; Kashiwagi, T.; Ikeuchi, T.; Uchida, Y. *J. Organomet. Chem.* **1971**, *30*, 279–282. (b) Chatt, J.; Shaw, B. L. *J. Chem. Soc.* **1960**, 1718–1729. The origin of this effect continues to be debated.

(18)   For examples, see: (a) Higashihara, T.; Goto, E.; Ueda, M. *ACS Maco. Lett.* **2012**, *1*, 167–170. (b) Wu, B.; Sun, Y.; Huang, L.; Wang, J.; Zhou, Y.; Geng, Y.; Wang, F. *Macromolecules* **2010**, *43*, 4438–4440. (c) Yokoyama, A.; Kato, A.; Miyakoshi, R.; Yokozawa, T. *Macromolecules* **2008**, *41*, 7271–7273. (d) Adachi, I.; Miyakoshi, R.; Yokoyama, A.; Yokozawa, T. *Macromolecules* **2006**, *39*, 7793–7795. (e) Miyakoshi, R.; Shimono, K.; Yokoyama, A.; Yokozawa, T. *J. Am. Chem. Soc.* **2006**, *128*, 16012–16013. See also, ref 10.

(19)   All four precatalysts showed a small amount of an unidentified product in the ^{19}F NMR spectrum, which may be attributable to either further propagation or poor shimming due to precipitation of **5** (Appendix 2).

(20)   Shi, L.; Chu, Y.; Knochel, P.; Mayr, H. *J. Org. Chem.* **2009**, *74*, 2760–2764.

(21)   Shi, L.; Chu, Y.; Knochel, P.; Mayr, H. *Org. Lett.* **2012**, *14*, 2602–2605.

(22)   The data for [**5**] *versus* time was not fit because of competing precipitation under these conditions.

(23)   Both initiation and propagation have the same turnover-limiting step (*i.e.*, reductive elimination) and, as a consequence, the rate constants can be directly compared.

(24)   (a) Becke, A. D. *Phys. Rev. A* **1988**, *38*, 3098–3100. (b) Perdew, J. P. *Phys. Rev. B* **1986**, *33*, 8822–8824.

(25)   (a) Clark, T.; Chandrasekhar, J.; Spitznagel, G. W.; Schleyer, P. V. R. *J. Comp. Chem.* **1983**, *4*, 294–301. (b) McLean, A. D.; Chandler, G. S. *J. Chem. Phys.* **1980**, *72*, 5639–5648. (c) Raghavachari, K.; Binkley, J. S.; Seeger, R.; Pople, J. A. *J. Chem. Phys.* **1980**, *72*, 650–654.

(26)   (a) Martin, J. M. L.; Sundermann, A. *J. Chem. Phys.* **2001**, *114*, 3408–3420. (b) Dolg, M.; Wedig, U.; Stoll, H.; Preuss, H. *J. Chem. Phys.* **1987**, *86*, 866–872.

(27)   BP86 paired with similar basis sets was previously shown to provide reliable barrier heights for a Ni-catalyzed carbon-bromine bond formation. For reference, see: Renz, A. L.; Pérez, L. M.; Hall, M. B. *Organometallics* **2011**, *30*, 6365–6371.

(28)   Hansch, C.; Leo, A.; Taft, R. W. *Chem. Rev.* **1991**, *91*, 165–195.

Chapter 4

Utilizing Heteroaromatic and Aromatic Reactive Ligands to Selectively Increase Initiation Rates

Introduction

Organic π-conjugated polymers have been studied extensively in recent years for a growing number of applications in energy-related fields such as photovoltaics (PVs),[1] light emitting diodes (LEDs),[2] and field effect transistors (FETs),[3] and biomedical fields[4] such as sensors for cancer cells.[5] The properties and performance of these devices are directly related to their structures, namely monomer (*i.e.*, repeat unit functionality),[6] molecular weight,[7] molecular weight distribution,[8] and/or copolymer sequences (*e.g.*, block,[9] alternating,[10] and gradient[11]). Precise control over the polymer structure allows for not only reliable and reproducible device performances, but also understanding of the structure-property relationship to enhance the properties and to expand the application scope.[12] Recent developments in Ni- and Pd-catalyzed catalyst-transfer polycondensation (CTP)[1d,13] have facilitated synthesis of π-conjugated polymers with unprecedented sequences such as gradient π-conjugated polymers[11] and high molecular weight polymers (*e.g.*, 130 kg/mol poly(3-hexylthiophene))[7b] that were not accessible by traditional step-growth polymerization. However, even though they are defined as living, chain-growth, the current methods are limited due to slow initiation[14] and side reactions such as chain-transfer, chain-termination,[14b,15] and disproportionation.[16] As a result, defects in polymer sequences and high molecular weight dispersities (Đ) are often observed. To overcome these limitations, a controlled CTP method, with fast initiation and minimized side reactions, is desired.
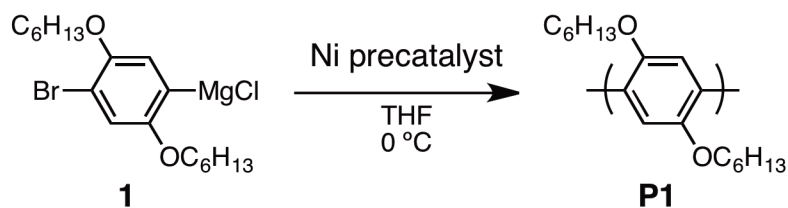
Scheme 4-1. Polymerization of **1** mediated by Ni precatalysts.
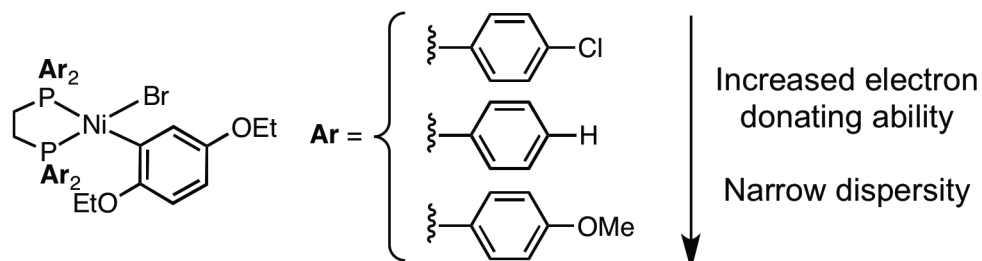
Scheme 4-2. Electron-rich ancillary ligands promote chain-growth as described in Chapter 2.

Recently, we have investigated and reported the impact of ancillary and reactive ligand structures on poly(2,5-bis(hexyloxy)phenylene) (**P1**) synthesis using Ni catalysts (Scheme 4-1). We found that catalysts with electron-donating phosphine ancillary ligands led to lower molecular weight dispersities (Đ), which were attributed to minimization of side reactions via stabilization of a key intermediate (*i.e.,* Ni(0)-polymer π-complex) and increased intramolecular oxidative addition rate (Scheme 4-2).[14b]

Additionally, we have shown that the initiation rate can be selectively increased relative to propagation by simply modifying the electronic properties of reactive ligand (Scheme 4-3).[14a] The importance of initiation rate on chain-growth polymerization was demonstrated as the slowest initiators gave a Đ = 2.13 whereas the fastest initiator gave a Đ = 1.12 at the same conversion, emphasizing the detrimental effect of slow initiation on CTP method. Nevertheless, the fastest initiator still showed a slower initiation than propagation (k_i = 6.88 x 10^{-3} s^{-1} vs k_p = 12.9 x 10^{-3} s^{-1}). Computational studies predicted a faster initiation rate can be obtained with resonance-based electron-withdrawing groups. However, the suggested substituents (*e.g.,* NO_2- or carbonyl-containing

group) were not compatible with the polymerization reaction conditions (*e.g.*, side reaction with the Grignard monomer).[14a]
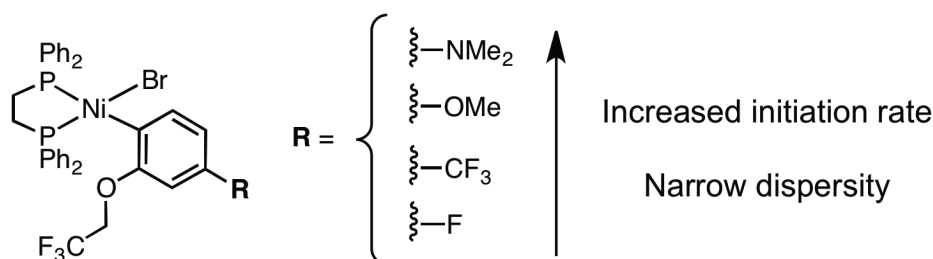
Scheme 4-3. Reactive ligands selectively increase initiation rate as demonstrated in Chapter 3.

In this chapter, we demonstrate the synthesis of new Ni precatalysts with electronically varied heteroaromatic and aromatic reactive ligands to selectively increase the initiation rate over the propagation rate. The computational method previously developed by Dr. Steven Wheeler and Jacob Bloom at Texas A&M University was a valuable resource to screen for suitable precatalysts by calculating the potential energy barrier for reductive elimination (*i.e.*, the rate-limiting step of initiation). Then, the precatalysts were synthesized and initiation rates were measured using *in situ* IR spectroscopy to compare with the computational results. Using this approach, we found a Ni precatalyst with an initiation rate faster than the propagation rate and thus, optimized catalyst design for controlled Ni-catalyzed CTP of π-conjugated monomers.

Results and discussion

To identify the suitable catalysts for fast initiation, computations were performed by Dr. Steven Wheeler and Jacob Bloom at Texas A&M University using the previously reported method.[14a] The method utilized Guassian09 and employed the BP86 DFT functional[17] paired with the 6-311 +G(d) basis set[18] for non-metal atoms and the SDB-cc-pVTZ basis set with the small core, fully relativistic effective core potential[19] for Ni. The reactive ligand was selected based on feasibility of synthesis and with an *ortho*-methyl substituent for

stabilization.[14a] Also, we selected the *sp²*-hybridized carbon as the coupling partner to monomer because *sp²*-*sp²* coupling reactions have been shown to be much faster than *sp³*-hybridized carbon[20] or *sp²*- hybridized heteroatoms for concerted reductive elimination.[21] 1,2-Bis(diphenylphosphino)ethane (dppe) was selected as the ancillary ligand because it is commercially available and is used in other π-conjugated polymer syntheses.[22] To be consistent with our previous method, Grignard **12** was used as a monomer for the initiation model system. During initiation, the Ni precatalyst undergoes transmetalation with monomer (**12**) followed by reductive elimination. With dppe as an ancillary ligand, we can assume that reductive elimination is the rate-limiting step and the resting state of Ni catalyst is complex **I** (Scheme 4-4)[23] because the rate-limiting step of polymerization has been reported to be influenced by the size of ancillary ligand (*i.e.*, bite[24] and cone angle[25]) but not by the reactive ligands. Using this method, we calculated the energy barrier of reductive elimination (*i.e.*, transformation from **I** to **II**) for various reactive ligands and compared them to the fastest initiator reported so far, precatalyst **9** (Table 4-1).

As anticipated, vinyl complex **2** exhibited the lowest potential energy for reductive elimination. It has been proposed that less steric hindrance and greater overlap of *sp²*-hybridized orbitals during the transition state decreases the transition state energy,[20] thus increasing the rate of reductive elimination. Interestingly, furan and benzofuran have lower energy barriers than structurally similar thiophene and benzothiophene. Based on the transition state and product conformers, we found that there is less steric hindranace from the methyl group in furan than thiophene, which we attributed to smaller atom size of oxygen compared to sulfur. Remarkably, biphenyl has also been shown to be a relatively fast initiator, which we hypothesized is due to extended resonance compared to substituted phenyl group such as precatalyst **9**.
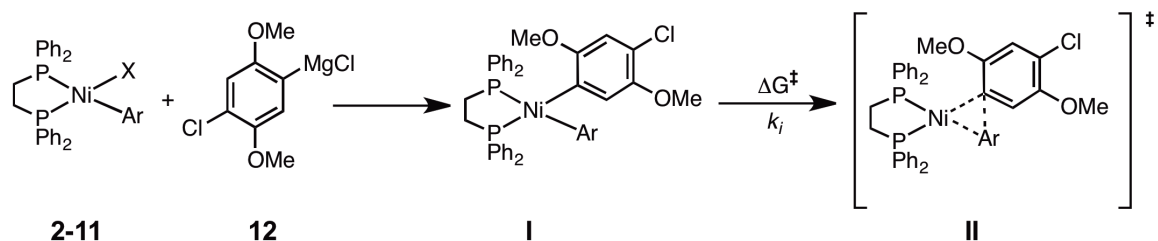
Scheme 4-4. Computational model for catalyst initiation.

Table 4-1. List of heteroaromatic and aromatic reactive ligands and their calculated potential energy barriers for the reductive elimination step of initiation.

Ar	Potential Energy (kcal/mol)	Ar	Potential Energy (kcal/mol)
2	6.9	**7**	10.6
3	7.8	**8**	11.6
4	8.0	**9**	12.0
5	8.9	**10**	12.3
6	9.6	**11**	12.3

Scheme 4-5. Representative synthesis of precatalyst **6**.

Scheme 4-6. Pre-initiation of Ni(dppe)Cl$_2$ with 10 equiv monomer **1** for propagation rate study.

Next, we synthesized Ni precatalysts and used them for the polymerization of monomer **1** to evaluate the results from the computational studies (Scheme 4-1). Previously, we synthesized the reactive ligands to include a ^{19}F-labeled substituent and analyzed initiation rates of precatalysts with stoichiometric amounts of Grignard **12** *via* ^{19}F NMR spectroscopy.[14] This method provided accurate initiation rate constants, however, the synthetic route can be arduous with the different heteroaromatic and aromatic groups included in the computational study. Therefore, the precatalysts were synthesized exactly as predicted by the computational method, using modified literature procedures for oxidative addition of ArX (*i.e.*, Cl or Br) to Ni(0) sources, Ni(cod)$_2$ or Ni(PPh$_3$)$_4$, followed by ligand exchange with dppe (Scheme 4-5).[14,24,26] The 10% monomer (**1**) conversion was monitored via *in situ* IR spectroscopy at 0 °C in THF (Appendix 3), which provided the combined initiation and propagation rate and allowed us to compare it to the propagation rate of pre-initiated Ni(dppe)Cl$_2$.[27] The initial rate of **P1** synthesis was measured with Ni(dppe)Cl$_2$, which was reacted with 10 equivalents of **1** prior to polymerization (**12**, Scheme 4-6 and Appendix 3). This pre-initiation allows us to measure the propagation rate over the 10% monomer conversion without the bias caused by the reactive ligand and

slow initiation. For ease of comparison, the rate of reaction over the first 10% monomer conversion was converted to observed rate constant (k_{obs}) based on the corresponding rate equation (eqn (1)), providing the rate constant of each precatalyst during the induction period of the polymerization (Table 2).

$$rate = -\frac{d[1]}{dt} = k_{obs}[Ni]_{total} \tag{1}$$

Because we assume that all Ni is undergoing initiation ($[Ni]_i$) or propagation ($[Ni]_p$), k_{obs} is a combination of initiation and propagation rates.

$$k_{obs} = k_i X + k_p Y \tag{2}$$

where $\quad X = \dfrac{[Ni]_i}{[Ni]_{total}}$ and $\quad Y = \dfrac{[Ni]_p}{[Ni]_{total}} \tag{3}$

Therefore the following equation can be derived.

$$k_{obs} = k_i \frac{[Ni]_i}{[Ni]_{total}} + k_p \frac{[Ni]_p}{[Ni]_{total}} \tag{4}$$

The initiation rate can also be described as equation (5) based on consumption of Ni species undergoing initiation. The initial Ni concentration is the total concentration of Ni species at all time (eqn (6)), thus equation (7) can be derived from following equations.

$$[Ni]_i = [Ni]_{i(0)} e^{-k_i t} \tag{5}$$

$$[Ni]_{total} = [Ni]_{i(0)} \tag{6}$$

$$\frac{[Ni]_i}{[Ni]_{total}} = e^{-k_i t} \tag{7}$$

Since the total concentration of Ni is a combination of Ni species during initiation and propagation, the equation can be further derived to equation (10) by combining equations (7) and (9).

$$[Ni]_{total} = [Ni]_i + [Ni]_p \tag{8}$$

$$\frac{[Ni]_{total}}{[Ni]_{total}} = \frac{[Ni]_i}{[Ni]_{total}} + \frac{[Ni]_p}{[Ni]_{total}} \tag{9}$$

$$\frac{[Ni]_p}{[Ni]_{total}} = 1 - \frac{[Ni]_i}{[Ni]_{total}} = 1 - e^{-k_i t}$$

(10)

Finally, the combination of equations (4), (7), and (10) results in an equation that describes the relationship between known values of k_{obs}, k_p, and t (*i.e.*, time for 10% conversion in seconds) and an unknown value of k_i. The solve function of Mathematica was utilized to calculate k_i for each catalyst using equation (11).

$$k_{obs} = k_i(e^{-k_i t}) + k_p(1 - e^{-k_i t})$$

(11)
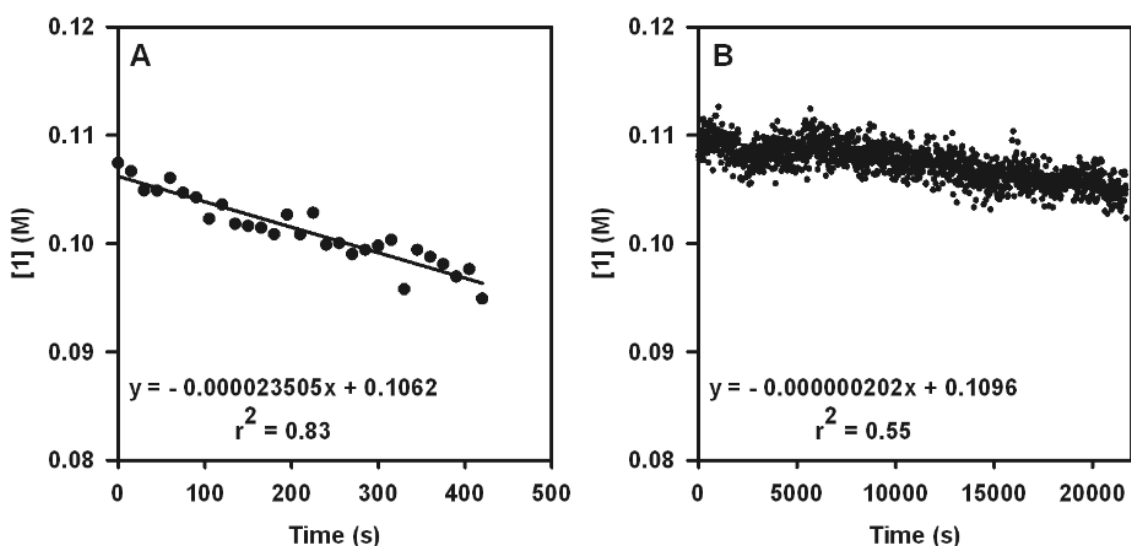
Figure 4-1. Representative *in situ* IR spectroscopy data for the reaction depicted in Scheme 4-1 using (A) precatalyst **6** and (B) precatalyst **7**

Table 4-2. Experimental rate constants (k_{obs}) for 10% monomer consumption. (temp = 0 °C in THF, [Ni] = 0.0015 M, [**1**] = 0.10 M)

Ni precatalyst	Rate (x10^{-6} M s^{-1})[a]	k_{obs} (x10^{-3} s^{-1})[a]	k_i (x10^{-3} s^{-1})
4	13.6 ± 0.8	9.1 ± 0.5	1.4 ± 0.2
6	20 ± 4	14 ± 3	-[b]
7	0.4 ± 0.2	0.3 ± 0.2	0.002 ± 0.002
8	15 ± 2	10 ± 1	1.9 ± 0.7
9[14a]	16 ± 3	11 ± 2	4 ± 3[c]
10	13.0 ± 0.2	8.7 ± 0.1	1.40 ± 0.02
12	19.3 ± 0.9	12.9 ± 0.6	-

[a]For the conversion of rate to k_{obs}, eqn (1) was used.
[a]Mathematica solve function does not work when k_{obs} is greater than the k_p (12.9 x 10^{-3} s^{-1}).
[b]The initiation rate was calculated from k_{obs} and eqn (11). The initiation rate measured via ^{19}F NMR spectroscopy is 6.88 ± 0.06 x 10^{-3} s^{-1}.

To date, precatalysts **4**, **6**, **7**, **8**, **9**, and **10** were successfully synthesized and investigated for polymerization of **1** (Appendix 3). Generally, the reactive ligands with low computational energy barriers exhibited relatively small k_{obs} similar to precatalyst **9**, which suggests fast initiation. Specifically, precatalyst **6** showed a faster initiation rate than precatalyst **9** (*i.e.*, the previously reported fastest initiator)[14a] and the propagation rate (k_p = 12.9 ± 0.6 x 10^{-3} s^{-1}), demonstrating that the computational study can aid in precatalyst design (Figure 4-1A). Unfortunately, most precatalysts with lower energy barriers than precatalyst **9** showed similar initiation rates, not better. In an extreme case, precatalyst **7** has shown a very sluggish induction period (*e.g.*, 5% monomer conversion at 6h) (Figure 4-1B). We attributed the slow initiation to other factors that were not accounted for in the computational studies. For example, the precatalyst **7** may undergo slow transmetalation due to steric hindrance caused by the bulky reactive group. The rate of nucleophilic attack of Grignard monomer at the metal center will be decreased due to the crowding by the *ortho*-phenyl substituent, and result in a change in the rate-limiting step to transmetalation. Understanding the role of reactive ligands in the transmetalation step is beyond the scope of this work, as it is a controversial field due to the less well-known role of the Grignard reagent during the transition state of transmetalation.[28] Furthermore, the Ni catalyst with a pyridinium reactive ligand, structurally similar to **4**, has been shown to exhibit M=C double-bond character (*i.e.*, carbenoid-bonding) due to a large M→L π-back-donation.[26] Cleavage of the stronger M-C bond is expected to reduce reductive elimination rates due to a high activation barrier. Overall, these studies suggest that the computational model can help narrow down the suitable targets for Ni precatalyst but cannot be used alone without experimental studies.
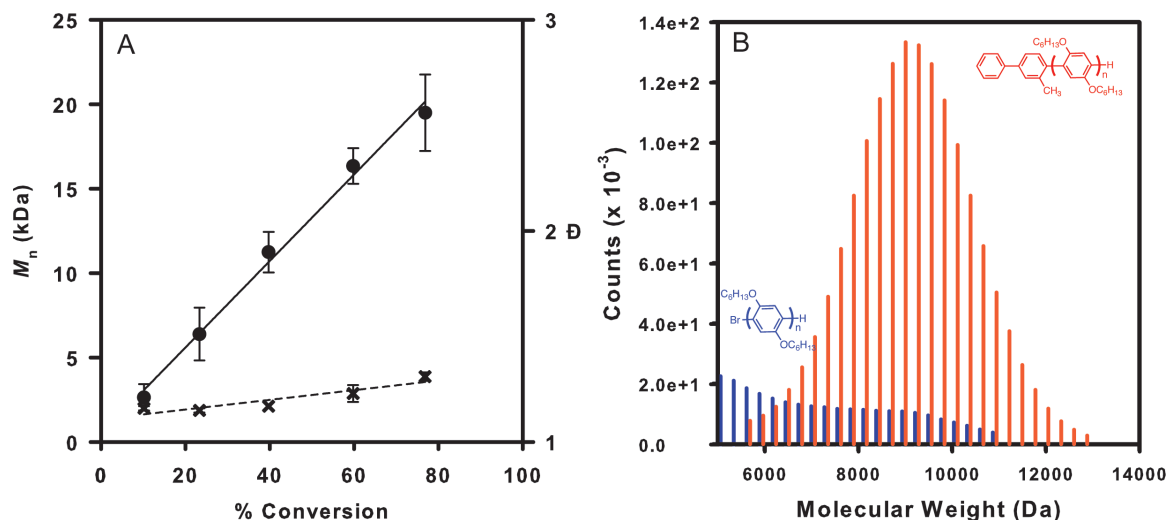
Figure 4-2. (A) Plot of average molecular weight (M_n) and dispersities (Ð) *versus* monomer conversion for the polymerization of **1** using precatalyst **6**. (B) Representative MALDI TOF-MS spectrum of polymer **P1** synthesized with precatalyst **6**.

Subsequently, monomer **1** was polymerized to study the impact of initiation rate on the resulting polymer. Aliquots were withdrawn from the polymerization up to 80% monomer conversion and quenched with acid to determine the number-average molecular weight (M_n) and dispersity (Ð) by gel permeation chromatography (GPC) as a function of conversion determined by *in situ* IR spectroscopy. Notably, most precatalysts, excluding precatalyst **6**, consistently showed low molecular weight dispersity (Ð~1.2-1.4) at very high conversion (Figure 4-2A and Appendix 3). Also, aliquots at 20-40% monomer conversion were analyzed by MALDI-TOF MS linear mode for end group analysis. The precatalyst **6** showed a high ratio of Ar/H end-groups compared to Br/H end-groups (Figure 4-2B), indicating that polymerization is mostly controlled CTP method. Nevertheless, we observed Br/H and/or H/H end-groups with some precatalysts, suggesting the presence of side reactions such as chain-transfer and/or chain-termination that have been previously reported with dppe as the ancillary ligand.[14b] Therefore, it is imperative to incorporate both the biphenyl reactive ligand and the electron-rich ancillary ligand for an optimized catalyst with

fast initiation and minimized side reactions (**13**), which is currently being pursued in our group.

13
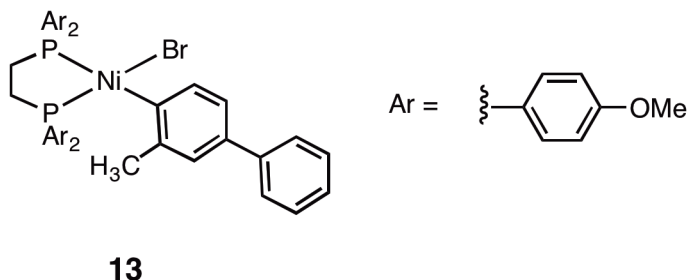
Conclusions

In summary, we have demonstrated that modifying the reactive ligand can selectively accelerate the initiation rate over the propagation rate to overcome the sluggish induction period. We have shown that the Ni precatalyst design can be optimized by utilizing a computational method to narrow down suitable reactive ligands. Most notably, precatalyst **6** is the fastest reported initiator for Ni-catalyzed CTP of monomer **1**. Combination of the reactive ligand (for fast initiation) and electron-rich ancillary ligand (for minimized side reactions) can result in an optimized Ni precatalyst for CTP (*i.e.*, living and controlled chain-growth polymerization). Although this report focuses on poly(2,5-bis(hexyloxy)phenylene) synthesis with new precatalysts, the results are anticipated to be generalizable to other polymerizations (*e.g.*, thiophenes) by modifying the computational method (Scheme 4-7), because they share a similar mechanism.[23]
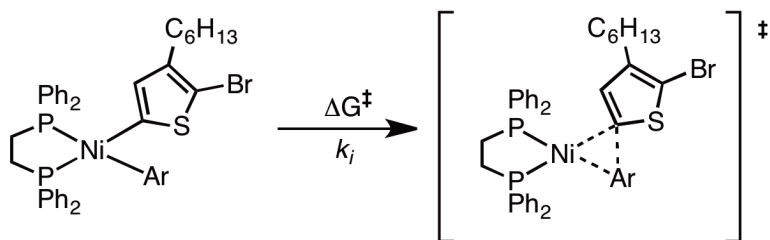
Scheme 4-7. Representative computational model for finding optimized Ni precatalysts for poly(3-hexylthiophene) synthesis

References Cited

(1)   For recent reviews, see: (a) Jhuo, H. J.; Yeh, P. N.; Liao, S. H.; Li, Y. L.; Cheng, Y. S.; Chen, S. A. *J. Chin. Chem. Soc.* **2014**, *61*, 115–126. (b) Scharber, M. C.; Sariciftci, N. S. *Prog. Polym. Sci.* **2013**, *38*, 1929–1940. (c) Darling, S. B.; You, F. Q. *R. Soc. Chem. Adv.* **2013**, *3*, 17633–17648. (d) Marrocchi, A.; Lanari, D.; Facchetti, A.; Vaccaro, L. *Energy Environ. Sci.* **2012**, *5*, 8457–8474. (e) Myers, J. D.; Xue, J. G. *Polym. Rev.* **2012**, *52*, 1–37.

(2)   For recent reviews, see: (a) Guo, X.; Baumgarten, M.; Mullen, K. *Prog. Polym. Sci.* **2013**, *38*, 1832–1908. (b) Wang, J.; Zhang, F. J.; Zhang, J.; Tang, W. H.; Tang, A. W.; Peng, H. S.; Xu, Z.; Teng, F.; Wang, Y. S. *J. Photochem. Photobiol.* **2013**, *17*, 69–104. (c) Deng, X. Y. *Int. J. Mol. Sci.* **2011**, *12*, 1575–1594. (d) Grimsdale, A. C.; Chan, K. L.; Martin, R. E.; Jokisz, P. G.; Holmes, A. B. *Chem. Rev.* **2009**, *109*, 897–1091.

(3)   For recent reviews, see: (a) Nielsen, C. B.; McCulloch, I. *Prog. Polym. Sci.* **2013**, *38*, 2053–2069. (b) Dong, H. L.; Fu, X. L.; Liu, J.; Wang, Z. R.; Hu, W. P. *Adv. Mater.* **2013**, *25*, 6158–6182. (c) Kola, S.; Sinha, J.; Katz, H. E. *J. Polym. Sci. Part B: Polym. Phys.* **2012**, *50*, 1090–1120.

(4)   For recent reviews, see: (a) Qu, Y.; Wu, Y.; Gao, Y.; Qu, S.; Yang, L.; Hua, J. *Sens. Actuators, B* **2014**, *197*, 13–19. (b) Li, J. W.; Liu, J.; Wei, C. W.; Liu, B.; O'Donnell, M.; Gao, X. H. *Phys. Chem. Chem. Phys.* **2013**, *15*, 17006–17015.

(5)   For a recent example, see: Ding, D.; Li, K.; Qin, W.; Zhan, R. Y.; Hu, Y.; Liu, J. Z.; Tang, B. Z.; Liu, B. *Advanced Healthcare Materials* **2013**, *2*, 500–507.

(6)   For a comprehensive list of conjugated polymers and their applications, see: Yamamoto, T. In *Conjugated Polymer Synthesis*; Wiley-VCH Verlag GmbH & Co. KGaA: 2010, p 1–33.

(7)   For recent examples, see: (a) Ma, Z. F.; Sun, W. J.; Himmelberger, S.; Vandewal, K.; Tang, Z.; Bergqvist, J.; Salleo, A.; Andreasen, J. W.; Inganas, O.; Andersson, M. R.; Muller, C.; Zhang, F. L.; Wang, E. R. *Energy Environ. Sci* **2014**, *7*, 361–369. (b) Koch, F. P. V.; Rivnay, J.; Foster, S.; Muller, C.; Downing, J. M.; Buchaca-Domingo, E.; Westacott, P.; Yu, L. Y.; Yuan, M. J.; Baklar, M.; Fei, Z. P.; Luscombe, C.; McLachlan, M. A.; Heeney, M.; Rumbles, G.; Silva, C.; Salleo, A.; Nelson, J.; Smith, P.; Stingelin, N. *Prog. Polym. Sci.* **2013**, *38*, 1978–1989.

(8)   (a) Kohn, P.; Huettner, S.; Komber, H.; Senkovskyy, V.; Tkachov, R.; Kiriy, A.; Friend, R. H.; Steiner, U.; Huck, W. T. S.; Sommer, J. U.; Sommer, M. *J. Am. Chem. Soc.* **2012**, *134*, 4790–4805. (b) Konezny, S. J.; Rothberg, L. J.; Galvin, M. E.; Smith, D. L. *Appl. Phys. Lett.* **2010**, *97*. 143305. (c) Menon, A.; Dong, H. P.; Niazimbetova, Z. I.; Rothberg, L. J.; Galvin, M. E. *Chem. Mater.* **2002**, *14*, 3668–3675.

(9)   For recent examples, see: (a) Smith, K. A.; Pickel, D. L.; Yager, K.; Kisslinger, K.; Verduzco, R. *J. Polym. Sci. Part A: Polym. Chem.* **2014**, *52*, 154–163. (b) Li, F.; Yager, K. G.; Dawson, N. M.; Yang, J. H.; Malloy, K. J.; Qin, Y. *Macromolecules* **2013**, *46*, 9021–9031. (c) Wang, J.; Higashihara, T. *Polym. Chem.* **2013**, *4*, 5518–5526. (d) Robb, M. J.; Ku, S. Y.; Hawker, C. J. *Adv. Mater.* **2013**, *25*, 5686–5700.

(10)   For recent examples, see: (a) Kato, S.; Shimizu, S.; Kobayashi, A.; Yoshihara, T.; Tobita, S.; Nakamura, Y. *J. Org. Chem.* **2014**, *79*, 618–629. (b) Griffin, G. B.; Lundin, P. M.; Rolczynski, B. S.; Linkin, A.; McGillicuddy, R. D.; Bao, Z. A.; Engel, G. S. *J. Chem. Phys.* **2014**, *140*, 034903. (c) Keshtov, M. L.; Marochkin, D. V.; Kochurov, V. S.; Khokhlov, A. R.; Koukaras, E. N.; Sharma,

G. D. *J. Mater. Chem. A.* **2014**, *2*, 155–171. (d) Zhuang, W. L.; Lundin, A.; Andersson, M. R. *J. Mater. Chem. A.* **2014**, *2*, 2202–2212.

(11)   (a) Palermo, E. F.; Darling, S. B.; McNeil, A. J. *J. Mater. Chem. C.* [online early access] DOI:10.1039/C3TC32512A. Published online February 25, 2014. http://pubs.rsc.org (accessed February 22, 2014) (b) Palermo, E. F.; van der Laan, H. L.; McNeil, A. J. *Polym. Chem.* **2013**, *4*, 4606–4611. (c) Locke, J. R.; McNeil, A. J. *Macromolecules* **2010**, *43*, 8709–8710.

(12)   For recent examples of thin-film morphology and property relationship, see: (a) Cataldo, S.; Pignataro, B. *Materials* **2013**, *6*, 1159–1190. (b) Yao, Y. F.; Dong, H. L.; Hu, W. P. *Polym. Chem.* **2013**, *4*, 5197–5205. (c) Wang, H. Y.; Xu, Y. Z.; Yu, X. H.; Xing, R. B.; Liu, J. G.; Han, Y. C. *Polymers* **2013**, *5*, 1272–1324.

(13)   For recent reviews, see: (a) Bryan, Z. J.; McNeil, A. J. *Macromolecules* **2013**, *46*, 8395–8405. (b) Yokozawa, T.; Nanashima, Y.; Ohta, Y. *ACS Macro Letters* **2012**, *1*, 862–866. (c) Stefan, M. C.; Bhatt, M. P.; Sista, P.; Magurudeniya, H. D. *Polym. Chem.* **2012**, *3*, 1693–1701. (d) Kiriy, A.; Senkovskyy, V.; Sommer, M. *Macromol. Rapid Commun.* **2011**, *32*, 1503–1517. (e) Okamoto, K.; Luscombe, C. K. *Polym. Chem.* **2011**, *2*, 2424–2434.

(14)   (a) Lee, S. R.; Bloom, J. W. G.; Wheeler, S. E.; McNeil, A. J. *Dalton Trans.* **2013**, *42*, 4218–4222. (b) Lee, S. R.; Bryan, Z. J.; Wagner, A. M.; McNeil, A. J. *Chem. Sci.* **2012**, *3*, 1562–1566.

(15)   The side reaction has been shown to be insignificant because other reactive species do not get consumed during CTP. For examples, see: (a) Bryan, Z. J.; McNeil, A. J. *Chem. Sci.* **2013**, *4*, 1620–1624. (b) Bryan, Z. J.; Smith, M. L.; McNeil, A. J. *Macromol. Rapid Commun.* **2012**, *33*, 842–847. (c) Beryozkina, T.; Senkovskyy, V.; Kaul, E.; Kiriy, A. *Macromolecules* **2008**, *41*, 7817–7823.   (d) Yokoyama, A.; Suzuki, H.; Kubota, Y.; Ohuchi, K.; Higashimura, H.; Yokozawa, T. *J. Am. Chem. Soc.* **2007**, *129*, 7236–7237. However, the dispersity of the polymer obtained using electron-poor Ni precatalysts is broader than those catalzed by electron-rich Ni precatalysts indicating instability of the NI-polymer π-complex, which results in chain-transfer and/or chain-termination. See ref 14b.

(16)   For computational study, see: (a) Bilbrey, J. A.; Sontag, S. K.; Huddleston, N. E.; Allen, W. D.; Locklin, J. *Acs Macro Letters* **2012**, *1*, 995–1000. For experimental study, see: (b) Lohwasser, R. H.; Thelakkat, M. *Macromolecules* **2011**, *44*, 3388–3397. (c) Miyakoshi, R.; Yokoyama, A.; Yokozawa, T. *Macromol. Rapid Commun.* **2004**, *25*, 1663–1666.

(17)   (a) Becke, A. D. *Phys. Rev. A* **1988**, *38*, 3098–3100. (b) Perdew, J. P. *Phys Rev B* **1986**, *33*, 8822–8824.

(18)   (a) Clark, T.; Chandrasekhar, J.; Spitznagel, G. W.; Schleyer, P. V. *J. Comput. Chem.* **1983**, *4*, 294–301. (b) Krishnan, R.; Binkley, J. S.; Seeger, R.; Pople, J. A. *J. Chem. Phys.* **1980**, *72*, 650–654. (c) Mclean, A. D.; Chandler, G. S. *J. Chem. Phys.* **1980**, *72*, 5639–5648.

(19)   (a) Martin, J. M. L.; Sundermann, A. *J. Chem. Phys.* **2001**, *114*, 3408–3420. (b) Dolg, M.; Wedig, U.; Stoll, H.; Preuss, H. *J. Chem. Phys.* **1987**, *86*, 866–872.

(20)   Low, J. J.; Goddard, W. A. *J. Am. Chem. Soc.* **1986**, *108*, 6115–6128.

(21)   Hartwig, J. F. In *Organotransition Metal Chemistry: From Bonding to Catalysis*; Murdzek, J., Ed.; University Science Books: Mill Valley, California, 2010, p 321–348.

(22)   For recent examples, see: (a) Wen, H. B.; Ge, Z. Y.; Liu, Y.; Yokozawa, T.; Lu, L.; Ouyang, X. H.; Tan, Z. *Eur. Polym. J.* **2013**, *49*, 3740–3743. (b) McDowell, J. J.; Schick, I.; Price, A.; Faulkner, D.; Ozin, G. *Macromolecules* **2013**, *46*, 6794–6805.

(23)   The rate-limiting step of Kumada CTP has shown to be reductive elimination with Ni(dppe)Cl$_2$ regardless of monomers. For reference, see: Lanni, E. L.; McNeil, A. J. *J. Am. Chem. Soc.* **2009**, *131*, 16573–16579.

(24)   Lanni, E. L.; McNeil, A. J. *Macromolecules* **2010**, *43*, 8039–8044.

(25)   Lanni, E. L.; Locke, J. R.; Gleave, C. M.; McNeil, A. J. *Macromolecules* **2011**, *44*, 5136–5145.

(26)   Stander-Grobler, E.; Schuster, O.; Heydenrych, G.; Cronje, S.; Tosh, E.; Albrecht, M.; Frenking, G.; Raubenheimer, H. G. *Organometallics* **2010**, *29*, 5821–5833.

(27)   The propagation rate has been previously reported using Ni(dppe)Cl$_2$ which was pre-initiated with 5 equiv monomer **1**. Rate = 20 ± 1 x 10^{-6} M s^{-1} and k_{obs} = 13.3 ± 0.7 x 10^{-3} s^{-1} For reference, see ref 23.

(28)   (a) Henriques, A. M.; Barbosa, A. G. H. *J. Phys. Chem. A* **2011**, *115*, 12259–12270. (b) Knochel, P.; Krasovskiy, A.; Sapountzis, I. In *Handbook of Functionalized Organometallics: Applications in Synthesis*; Knochel, P., Ed.; Blackwell Science Publ: Oxford, 2005, p 109–172. (c) Garst, J. E.; Soriaga, M. R. *Coord. Chem. Rev.* **2004**, *248*, 623–652.

Chapter 5

Conclusions and Future Directions

The market potential for organic π-conjugated polymers has increased significantly since their first discovery in 1970s[1] and is expected to reach 1.6 billion dollars in the US by 2017.[2] With such interest, the need for catalyst-transfer polycondensation (CTP) is great, as the method offers a platform to access precisely controlled π-conjugated polymers (*e.g.*, polymers with specific weight and narrow dispersity). The controlled π-conjugated polymer synthesis also allows us to obtain desired optoelectronic (*e.g.*, absorb/emit light and conduct charge) and physical (*e.g.*, solution processibility) properties for various applications by tuning their structures.[3] Nevertheless, challenges remain for studying structure-property relationships and expanding the application scope, primarily due to side reactions that compete with the CTP mechanistic pathway and the slow initiation rate.

We have demonstrated that controlled CTP of poly(2,5-bis(hexyloxy)phenylene) can be achieved via modification of Ni precatalysts. Side reactions, such as chain transfer, are hypothesized to occur due to an unstable Ni-polymer π-complex. By modifying the ancillary ligand of Ni precatalysts, we demonstrated that electron-rich catalysts exhibit better chain-growth behavior due to better stabilization of the Ni-polymer π-complex and increased intramolecular oxidative addition rate. Also, we showed that the initiation rate of Ni catalyzed CTP is considerably slower than the propagation rate (*e.g.*, 20 times), which has an immense impact on the dispersity of the resulting polymers.[4] We determined that the initiation rate can be selectively increased by modifying the reactive ligands of Ni precatalysts.[5] Through a combination of computational and experimental studies, we were able to

synthesize Ni precatalysts containing a *para*-biphenyl reactive ligand that showed a faster initiation rate than propagation rate and obtained controlled CTP evidenced by narrow dispersity.

In depth mechanistic studies *via* precatalyst modification have overcome some of the limitations for CTP. However, there are still more factors to be explored to utilize CTP for various conjugated polymer syntheses. For instance, current Ni precatalysts have been optimized for synthesis of poly(2,5-bis(hexyloxy)phenylene) (PP) and may have similar effects on other monomers such as thiophene. In our study, the computational method has been useful in finding a precatalyst with fast initiation by calculating the activation barrier of reductive elimination with 2,5-bis(methoxy)benzene monomer partner (Scheme 5-1). It is important to confirm if the computational method is generalizable by extending the study to other monomers and testing it experimentally. For example, the initiation activation barrier of poly(3-hexylthiophene) synthesis can be calculated using the same computational method with a thiophene monomer partner. The heteroaromatic reactive ligands will be selected based on different resonance and inductive contribution of substituents. The overall delocalization of charge has shown to be important on the initiation of PP synthesis and it will be necessary to repeat similar analysis for initiation of P3HT synthesis by comparing different substitution patterns (*e.g.*, 3-NMe$_2$ *versus* 4-NMe$_2$) (Scheme 5-2). The reproducibility of the method will allow us to generalize this computational approach to find catalysts for other polymer syntheses and ultimately, to obtain high molecular weight polymers with narrow dispersity and fewer defects.
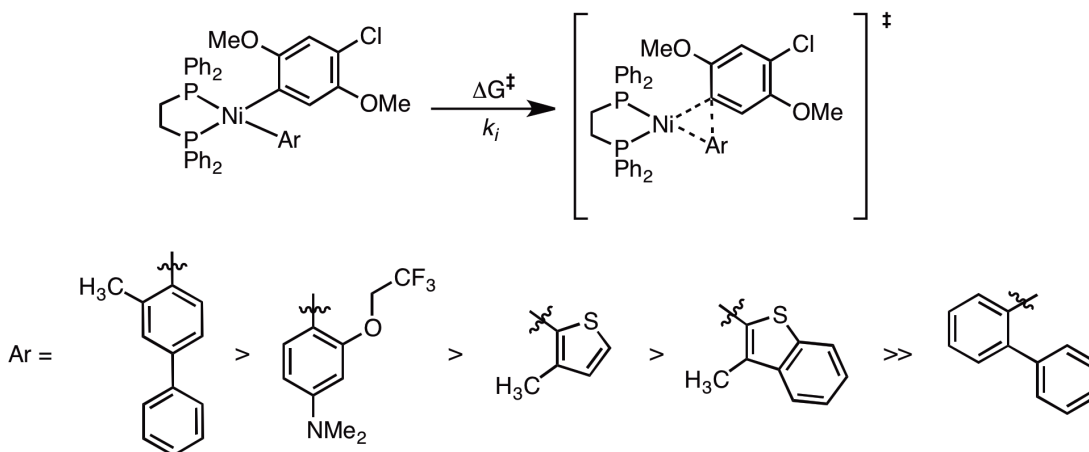
Scheme 5-1. Computational model for initiation of PP synthesis and order of initiation rate with varying aromatic and heteroaromatic reactive ligands.
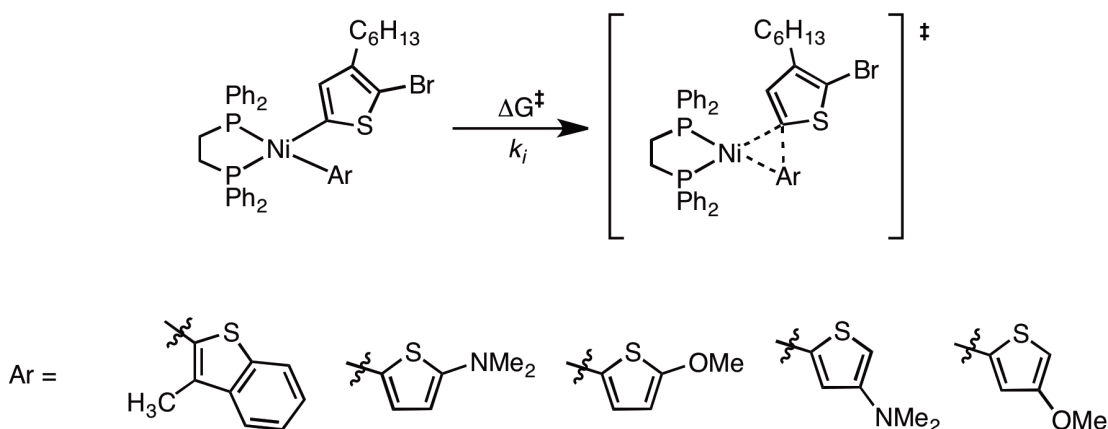
Scheme 5-2. Proposed computational model for initiation of P3HT synthesis and list of potential heteroaromatic reactive ligands.

Likewise, the impact of the ancillary ligand on the polymerization needs to be further explored. To date, the steric and electronic effects of chelated phosphine ligands have been extensively studied. However, exploring more electron-rich ancillary ligands and non-symmetric ligands may provide more insights into their impact on the mechanistic rates and expand the ligand scope for CTP. For example, an electron-rich ancillary ligand such as pyrrolidine-substituted phosphine **1** may further promote chain-growth behavior compared to **2** (*e.g.*, Đ = 1.27 for PP synthesis)[4] (Scheme 5-3).
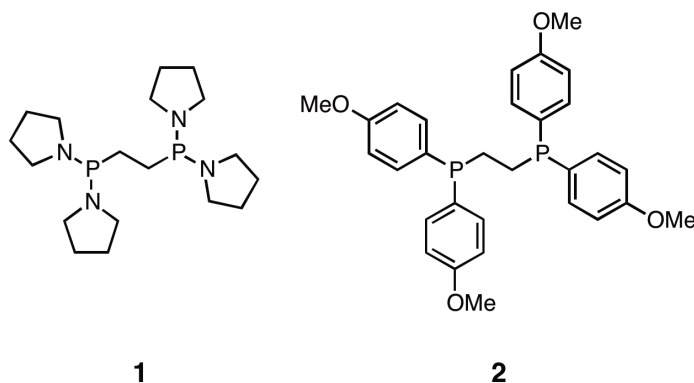
Scheme 5-3. Electron-rich ancillary ligand for controlled chain-growth.

Furthermore, non-symmetric ligands have not been explored for CTP but are promising alternatives because they have been used for Kumada cross-coupling with sterically hindered substrates at relatively low temperature and result in good yields (Scheme 5-4).[6] The current drawback with an electron-rich catalyst is that the reaction is very slow due to turnover-limiting reductive elimination. Excitingly, Hartwig and coworkers have shown that reductive elimination of aryl-amine coupling using non-symmetric ligand can be accelerated compared to electron-rich symmetric ligands.[7] Moreover, non-symmetric ancillary ligands have been shown to influence the catalyst geometry and mechanistic rates,[8-10] all of which can have impact on the chain-growth catalytic cycle. For instance, the copolymerization of two monomers can be aided by preferential geometry of Ni based on the trans influence and proceeds to C-C coupling *via* reductive elimination after fast equilibrium between two diastereomer species (Scheme 5-5). Thus, exploring non-symmetric ligands and their impact on the mechanistic steps of propagation may provide insights to expand the monomer scope for copolymer syntheses.
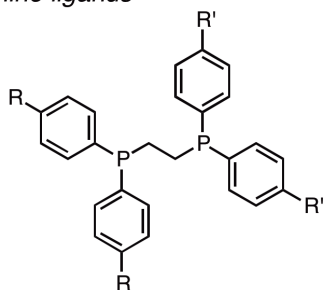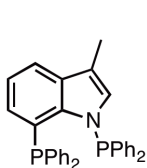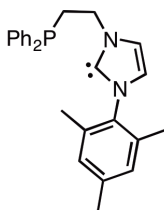
Scheme 5-4. Representative non-symmetric ligands for CTP.
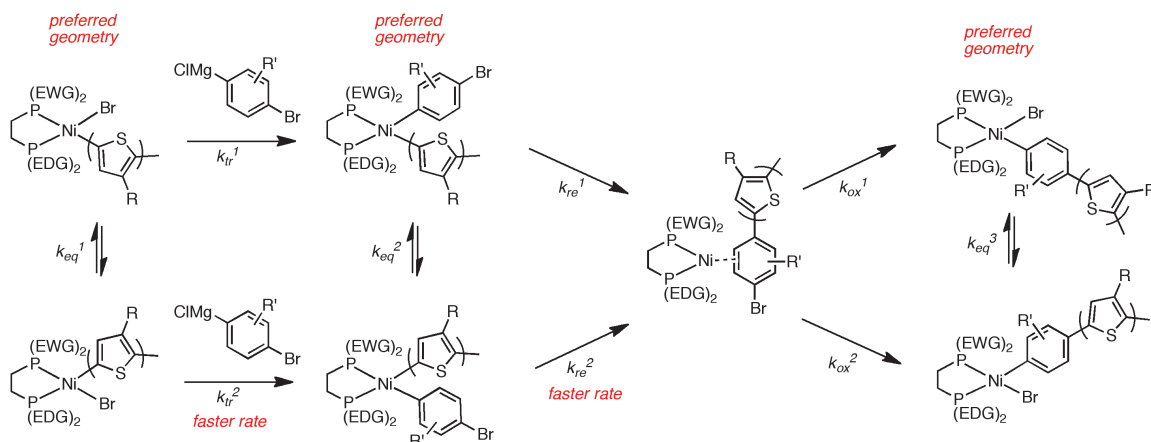
Scheme 5-5. Potential mechanism for CTP using non-symmetric ligands.

This thesis work suggests that simple modification of Ni precatalysts has a considerable influence on CTP and the resulting homopolymers. To synthesize new, well-defined materials with various copolymer sequences and architectures and to understand structure-property relationships, it is imperative to optimize the catalyst design for controlled CTP for a broad spectrum of monomers. To that end, the future work should continue to focus on gaining a mechanistic understanding and applying the chain-growth CTP method for more complex

monomers (Scheme 5-6) which will have a significant impact on future applications of π-conjugated polymers.
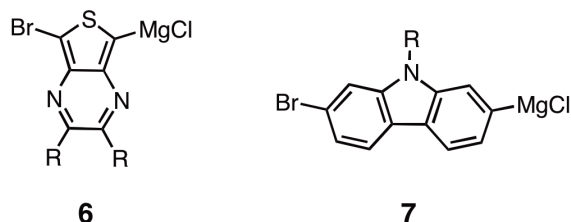
Scheme 5-6. Proposed monomers for CTP.

References Cited

(1)   (a) Chiang, C. K.; Druy, M. A.; Gau, S. C.; Heeger, A. J.; Louis, E. J.; MacDiarmid, A. G.; Park, Y. W.; Shirakawa, H. *J. Am. Chem. Soc.* **1978**, *100*, 1013–1015. (b) Chiang, C. K.; Fincher, C. R.; Park, Y. W.; Heeger, A. J.; Shirakawa, H.; Louis, E. J.; Gau, S. C.; MacDiarmid, A. G. *Phys. Rev. Lett.* **1977**, *39*, 1098–1101. (c) Shirakawa, H.; Louis, E. J.; MacDiarmid, A. G.; Chiang, C. K.; Heeger, A. J. *J Chem. Soc., Chem. Comm.* **1977**, 578–580.

 (2)   Polymer Solutions Newsblog, Demand Grows for Conductive Polymers. http://www.polymersolutions.com/blog/demand-grows-for-conductive-polymers/ Published online on April 16, 2012. (accessed March 28, 2014).

 (3)   For recent reviews, see: (a) Bryan, Z. J.; McNeil, A. J. *Macromolecules* **2013**, *46*, 8395–8405. (b) Marrocchi, A.; Lanari, D.; Facchetti, A.; Vaccaro, L. *Energy Environ. Sci.* **2012**, *5*, 8457–8474. (c) Stefan, M. C.; Bhatt, M. P.; Sista, P.; Magurudeniya, H. D. *Polym. Chem.* **2012**, *3*, 1693-1701. (d) Yokozawa, T.; Nanashima, Y.; Ohta, Y. *Acs Macro Letters* **2012**, *1*, 862–866. (e) Kiriy, A.; Senkovskyy, V.; Sommer, M. *Macromol. Rapid Commun.* **2011**, *32*, 1503–1517. (f) Okamoto, K.; Luscombe, C. K. *Polym. Chem.* **2011**, *2*, 2424–2434.

 (4)   Lee, S. R.; Bryan, Z. J.; Wagner, A. M.; McNeil, A. J. *Chem. Sci.* **2012**, *3*, 1562–1566.

 (5)   Lee, S. R.; Bloom, J. W. G.; Wheeler, S. E.; McNeil, A. J. *Dalton Trans.* **2013**, *42*, 4218–4222.

 (6)   (a) Ghosh, R.; Sarkar, A. *J. Org. Chem.* **2010**, *75*, 8283–8286. (b) Wolf, J.; Labande, A.; Natella, M.; Daran, J.-C.; Poli, R. *J. Mol. Catal. A: Chem.* **2006**, *259*, 205–212. (c) Wolf, J.; Labande, A.; Daran, J.-C.; Poli, R. *J. Organomet. Chem.* **2006**, *691*, 433–443.

 (7)   Yamashita, M.; Cuevas Vicario, J. V.; Hartwig, J. F. *J. Am. Chem. Soc.* **2003**, *125*, 16347–16360.

 (8)   For a discussion of reductive elimination geometry and rates, see: Hartwig, J. F. In *Organotransition Metal Chemistry: From Bonding to Catalysis*; Murdzek, J., Ed.; University Science Books: Mill Valley, California, 2010, p 321–348.

(9)   For a discussion of the trans effect, see: (a) Crabtree, R. H. *The Organometallic Chemistry of the Transition Metals*; John Wiley & Sons: New York, 2001. (b) Huheey, J. E.;

Keiter, E. A.; Keiter, R. L. *Inorganic Chemistry: Principles of Structure and Reactivity*, 4th ed.; HarperCollins College Publishers: New York, 1993.

(10)   For examples of preferred transmetallation geometry, see: (a) Faller, J. W.; Mazzieri, M. R.; Nguyen, J. T.; Parr, J.; Tokunaga, M. *Pure Appl. Chem.* **1994**, *66*, 1463–1469. (b) Faller, J. W.; Lambert, C.; Mazzieri, M. R. *J. Organomet. Chem.* **1990**, *383*, 161–177.

Appendix 1

Supporting Information for Chapter 2
Effect of Ligand Electronic Properties on Precatalyst Initiation and Propagation in
Ni-Catalyzed Cross-Coupling Polymerizations

I. Materials

Flash chromatography was performed on SiliCycle silica gel (40-63 μm) and thin layer chromatography was performed on Merck TLC plates pre-coated with silica gel 60 F254. *i*-PrMgCl (2 M in THF) was purchased in 100 mL quantities from Aldrich. Ni(cod)$_2$ and dppe were purchased from Strem. All other reagent grade materials and solvents were purchased from Aldrich, Acros, EMD, or Fisher and used without further purification unless otherwise noted. THF was dried and deoxygenated using an Innovative Technology (IT) solvent purification system composed of activated alumina, copper catalyst, and molecular sieves. *N*-Bromosuccinimide was recrystallized from hot water and dried over P$_2$O$_5$. Compounds **S1**,[1] **S2**,[1] **S3**,[2] **S4**,[3] **1a-c**,[2] **S5**,[2] **S6**,[3] and **3a-c**[2] were prepared from modified literature procedures.

II. General Experimental

NMR Spectroscopy: Unless otherwise noted, ^{1}H, ^{13}C, ^{19}F and ^{31}P NMR spectra for all compounds were acquired at rt in acetone-d_6 or CDCl$_3$ on a Varian vnmrs 700 operating at 700, 176, 660, and 283 MHz, Varian vnmrs 500 operating at 500, 126, 470, and 202 MHz or a Varian MR 400 operating at 400, 100, 376 and 162 MHz, respectively. For ^{1}H, ^{13}C, ^{19}F, and ^{31}P NMR spectra in deuterated solvents, the chemical shift data are reported in units of δ (ppm) relative to tetramethylsilane (TMS) and referenced with residual solvent. For ^{1}H, ^{19}F and ^{31}P NMR spectra in non-deuterated THF, the chemical shift data are reported in units of δ (ppm) and referenced with THF peak at 3.58 ppm in the ^{1}H NMR spectrum, which is then applied to all nuclei. Multiplicities are reported as follows: singlet (s), doublet (d), doublet of doublets (dd), triplet (t), quartet (q), quintet (quin), multiplet (m), broad resonance (br), and apparent triplet (at).

Mass Spectrometry: HRMS data were obtained on a Micromass AutoSpec Ultima Magnetic Sector mass spectrometer.

IR Spectroscopy: Samples were recorded using a Mettler Toledo ReactIR iC10 fitted with a Mercury Cadmium Telluride (MCT) detector, and AgX probe (9.5 mm x 1.5 mm) with a SiComp tip. The spectra were processed using icIR 4.0 software and raw absorbances were exported into Microsoft Excel or Sigma Plot 10 for analysis.

MALDI-TOF MS: MALDI-TOF mass spectra were recorded using Waters Tofspec-2E in reflectron mode at a unit mass resolution of 4000. The matrix, α-cyano-4-hydroxy-cinnamic acid (CHCA), was prepared at a concentration of 10 mg/mL in a solution of 50/50 (v/v) CH$_3$CN/EtOH. The instrument was mass calibrated with a mixture of peptides in the CHCA matrix. The polymer sample was dissolved in CH$_2$Cl$_2$ to obtain a ~1 mg/mL solution. A 3 µL aliquot of polymer solution was mixed with 3 µL of the matrix solution. 1 µL of this mixture was placed on the target plate and then air-dried.

Gel-Permeation Chromatography: Polymer molecular weights were determined by comparison with polystyrene standards (Varian, EasiCal PS-2 MW 580-377,400) on a Waters 1515 HPLC instrument equipped with Waters Styragel® (7.8 x 300 mm) THF HR 0.5, THF HR 1, and THF HR 4 type columns in sequence and analyzed with Waters 2487 dual absorbance detector (254 nm). Samples were dissolved in THF (with mild heating) and passed through a 0.2 µm PTFE filter prior to analysis.

Titrations of the Grignard Reagents: An accurately weighed sample of salicylaldehyde phenylhydrazone (typically between 290-310 mg) was dissolved in 5.00 mL of THF. A 0.50 mL aliquot of this solution was stirred at rt while ArMgCl was added dropwise using a 500 µL syringe. The initial solution is yellow and turns bright orange at the end-point.[4]

Statistical Analysis: Reported quantitative data represents the average of 2-3 experiments and the error bars represent the standard deviation in these measurements.

III. Synthetic Procedures
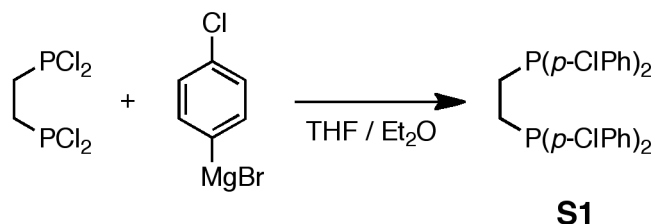
S1. An oven-dried Schlenk flask was brought into the glovebox and equipped with a stir bar,1,2-bis(dichlorophosphino)ethane (0.39 mL, 2.6 mmol, 1.0 equiv) and anhydrous THF (15 mL). The flask was then brought out of the glovebox and placed under N_2. After cooling to -40 °C, 4-chlorophenylmagnesium bromide (16.0 mL, 1 M in Et_2O, 6.0 equiv) was added dropwise over 15 min. The reaction mixture was stirred for 1 h at -40 °C and then warmed to rt. The clear yellow soln was quenched with an aq satd soln of NH_4Cl (50 mL). The mixture was extracted with Et_2O (3 x 30 mL) and the combined organic layers were dried over $MgSO_4$, filtered, and concentrated in vacuo until ~2 mL of soln was left. Methanol (200 mL) was added to give a white solid which was recrystallized in THF/MeOH to give 0.998 g of **S1** (73% yield). HRMS (EI): [M+] Calcd. for $C_{26}H_{20}P_2Cl_4$, 533.9794; found, 533.9793. ^{31}P NMR (162 MHz, $CDCl_3$) δ -14.9.
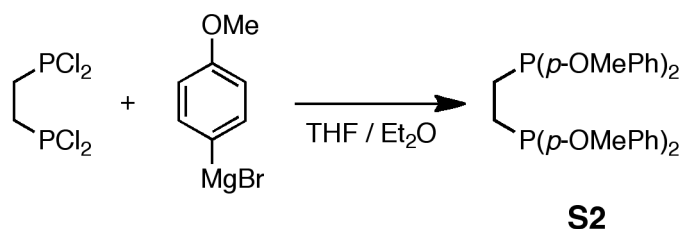

S2. An oven-dried Schlenk flask was brought into the glovebox and equipped with a stir bar, 1,2-bis(dichlorophosphino)ethane (0.39 mL, 2.6 mmol, 1.0 equiv) and anhydrous Et_2O (15 mL). The flask was then brought out of the glovebox and placed under N_2. After cooling to -40 °C, 4-methoxyphenylmagnesium bromide (30.0 mL, 0.5 M in THF, 6.0 equiv) was added dropwise over 15 min. The reaction mixture was stirred for 1 h at -40 °C and warmed to rt. Additional 4-methoxyphenylmagnesium bromide (10.0 mL, 0.5 M in THF, 2.0 equiv) was added dropwise and the mixture was stirred at 45 °C for 3 h. After cooling to rt, the clear yellow soln was quenched with an aq satd soln of NH_4Cl (50 mL). The mixture was extracted with Et_2O (3 x 30 mL) and the combined organic layers were dried over $MgSO_4$, filtered, and concentrated in vacuo until ~2 mL of soln was left. Methanol (200 mL) was added to give a white solid which was recrystallized in THF/MeOH to give 0.550 g of **S2** (42% yield). HRMS (EI): [M+] Calcd. for $C_{30}H_{32}O_4P_2$, 518.1776; found, 518.1787. ^{31}P NMR (162 MHz, $CDCl_3$) δ -16.1.

S3.
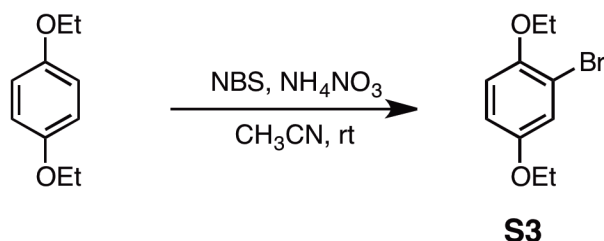
S3. A 25 mL round bottom flask was equipped with a stir bar. Sequentially, 1,4 diethoxybenzene (2.490 g, 15.00 mmol, 1.0 equiv), acetonitrile (7.5 mL), *N*-bromosuccinimide (2.670 g, 15.00 mmol, 1.0 equiv), and NH_4NO_3 (240.0 mg, 3.000 mmol, 0.2 equiv) were added. The solution was stirred at rt under N_2. After 30 min, the dark red solution was quenched with water (40 mL) and the mixture was extracted with Et_2O (3 x 50 mL). The combined organic layers were washed with water (2 x 150 mL), dried over $MgSO_4$, filtered, and concentrated in vacuo. The resulting oil was purified with silica gel chromatography, using 80/20 (v/v) hexanes/toluene as the eluent to give 1.980 g of **S3** as a clear colorless oil (54% yield). HRMS (EI): [M+] Calcd. for $C_{10}H_{13}BrO_2$, 244.0099; found, 244.0091.


S4.
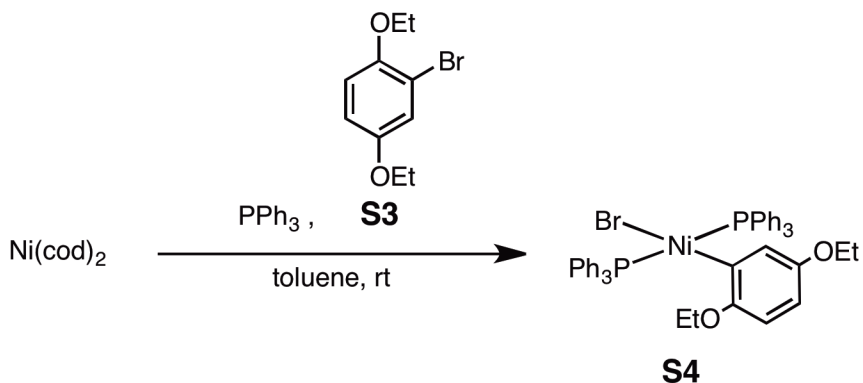
S4. A 20 mL vial was equipped with a stir bar in the glovebox. Sequentially, Ni(cod)$_2$ (550.6 mg, 2.002 mmol, 1.0 equiv), PPh$_3$ (1.050 g, 4.003 mmol, 2.0 equiv), **S3** (735.0 mg, 2.999 mmol, 1.5 equiv), and toluene (15 mL) were added. The solution was stirred at rt for 1 h. The reaction was removed from the glovebox and transferred to a 250 mL round bottom flask. Addition of hexanes (200 mL) led to an yellowish orange precipitate. The solid was filtered and washed with hexanes (20 mL) and cold MeOH (5 mL). The resulting solid was recrystallized in THF/hexanes to give 1.175 g of **S4** as a yellow solid (71% yield). Elemental Analysis: Calcd for $C_{46}H_{43}BrNiO_2P_2$, C, 66.7; H, 5.2; Found C, 66.5; H, 5.3. ^{31}P NMR (202 MHz, CD_2Cl_2) δ 22.55.
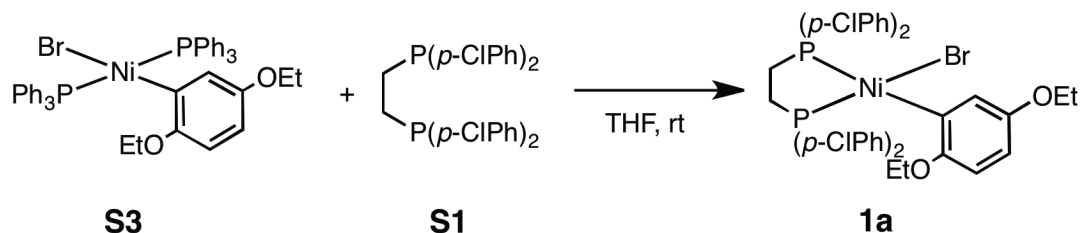
1a. A 20 mL vial was equipped with a stir bar in the glovebox. Sequentially, **S3** (415.1 mg, 0.5011 mmol, 1.0 equiv), **S1** (294.2 mg, 0.5510 mmol, 1.1 equiv), and THF (10 mL) were added. The solution was stirred at rt for 1.5 h. The deep red soln was concentrated in vacuo until ~2 mL of soln was left. Addition of hexanes (18 mL) led to a yellowish orange precipitate. The solid was filtered and washed with hexanes (20 mL). The resulting solid was recrystallized in THF/hexanes to give an orange solid. The solids were then redissolved in THF (~50 mL), passed through a 0.2 µm PTFE filter to remove any undissolved solids, and concentrated in vacuo to give 323.7 mg of **1a** as an orange solid (77% yield). Elemental Analysis: Calcd for $C_{36}H_{33}BrCl_4NiO_2P_2$, C, 51.5; H, 4.0; Cl, 16.9; Found C, 51.6; H, 4.0; Cl, 16.6. ^{31}P NMR (202 MHz, acetone-d_6) δ 57.31 (d, J = 24.6 Hz), 39.23 (d, J = 24.6 Hz).
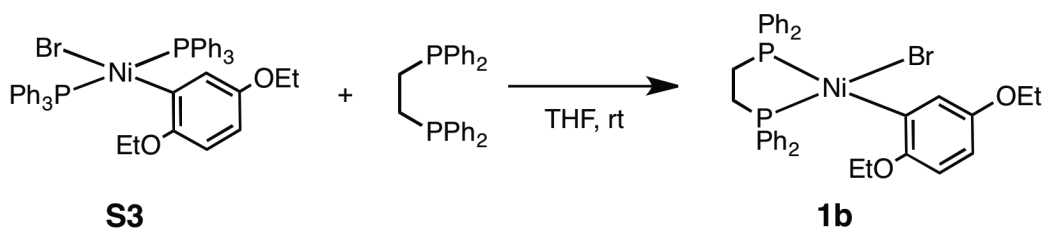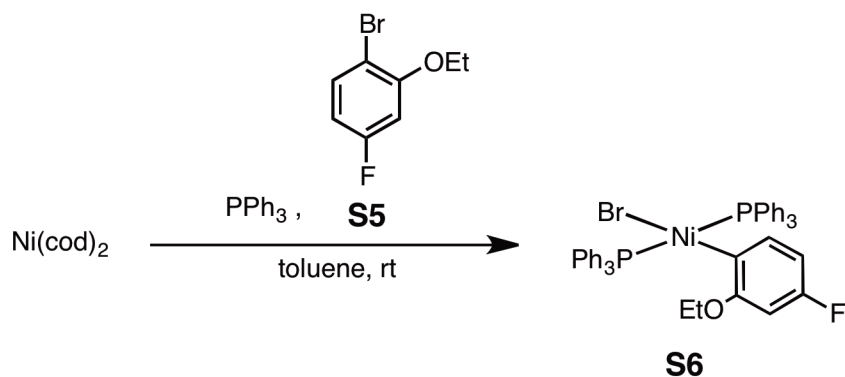

1b. A 20 mL vial was equipped with a stir bar in the glovebox. Sequentially, **S3** (414.2 mg, 0.5000 mmol, 1.0 equiv), 1,2-bis(diphenylphosphino)ethane (dppe) (219.1 mg, 0.5500 mmol, 1.1 equiv), and THF (10 mL) were added. The solution was stirred at rt for 1 h. The deep red soln was concentrated in vacuo until ~2 mL of soln was left. Addition of hexanes (18 mL) led to a yellowish orange precipitate. The solid was filtered and washed with hexanes (20 mL). The resulting solid was recrystallized in THF/hexanes to give an orange solid. The solids were then redissolved in THF (~50 mL), passed through a 0.2 µm PTFE filter to remove any undissolved solids, and concentrated in vacuo to give 281.1 mg of **1b** as an orange solid (80% yield). Elemental Analysis: Calcd for $C_{36}H_{37}BrNiO_2P_2$, C, 61.6; H, 5.3; Found C, 61.5; H, 5.4. ^{31}P NMR (202 MHz, acetone-d_6) δ 57.12 (d, J = 26.4 Hz), 39.69 (d, J = 26.4 Hz).
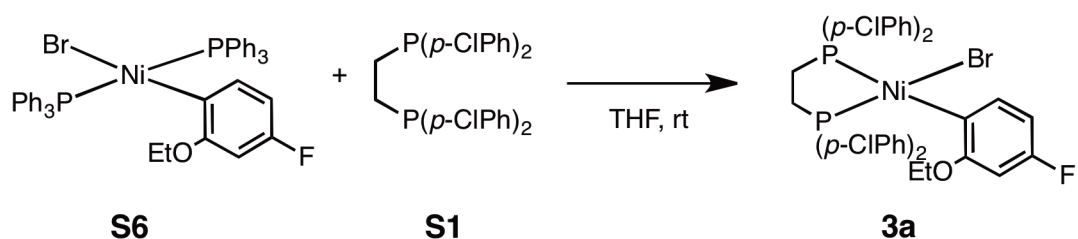
S3   **S2**   **1c**
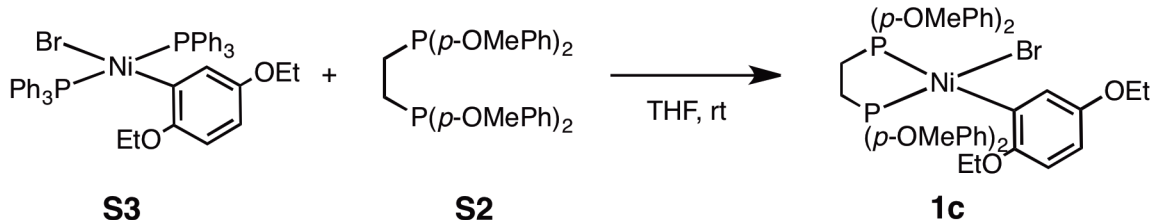
1c. A 20 mL vial was equipped with a stir bar in the glovebox. Sequentially, **S3** (414.2 mg, 0.5000 mmol, 1.0 equiv), **S2** (285.1 mg, 0.5502 mmol, 1.1 equiv), and THF (10 mL) were added. The solution was stirred at rt for 1.5 h. The deep red soln was concentrated in vacuo until ~2 mL of soln was left. Addition of hexanes (18 mL) led to a yellowish orange precipitate. The solid was filtered and washed with hexanes (20 mL) and Et_2O (10 mL). The resulting solid was recrystallized in THF/hexanes to give an orange solid. The solids were then redissolved in THF (~40 mL), passed through a 0.2 μm PTFE filter to remove any undissolved solids, and concentrated in vacuo to give 261.9 mg of **1c** as an orange solid (64% yield). Elemental Analysis: Calcd for $C_{40}H_{45}BrNiO_6P_2$, C, 58.4; H, 5.5; Found C, 58.6; H, 5.8. ^{31}P NMR (160 MHz, acetone-d_6) δ 54.79 (d, J = 29.2 Hz), 37.17 (d, J = 29.2 Hz).


S5
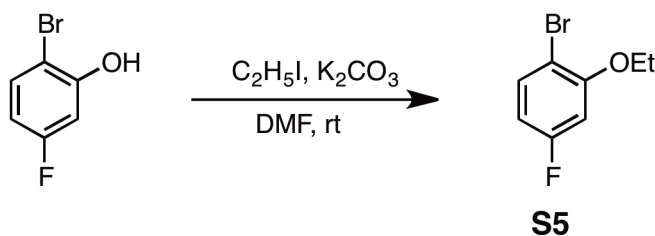
S5. A 100 mL round bottom flask was equipped with a stir bar. Sequentially, 2-bromo-5-fluorophenol (2.580 g, 13.51 mmol, 1.0 equiv), anhydrous DMF (30 mL), iodoethane (8.410 g, 53.92 mmol, 4.0 equiv), and K_2CO_3 (4.660 g, 33.72 mmol, 2.5 equiv) were added. The solution was stirred at rt under N_2. After 2 h, the reaction mixture was filtered and the solid was washed with hexanes (60 mL). The filtrate was poured into water (90 mL) and extracted with hexanes (3 x 50 mL). The combined organic layers were washed with water (2 x 50 mL) and brine (50 mL), dried over $MgSO_4$, filtered, and concentrated in vacuo. The resulting oil was purified with silica gel chromatography, using hexanes as the eluent to give 2.762 g of **S5** as a clear colorless oil (93% yield). HRMS (EI): [M+] Calcd. for C_8H_8BrFO, 217.9743; found, 217.9753. ^{19}F NMR (376 MHz, $CDCl_3$) δ -112.10 (m).

S6. A 100 mL oven-dried round bottom flask was equipped with a stir bar in the glovebox. Sequentially, Ni(cod)$_2$ (275.4 mg, 1.001 mmol, 1.0 equiv), PPh$_3$ (525.5 mg, 2.004 mmol, 2.0 equiv), **S5** (299.2 mg, 1.501 mmol, 1.5 equiv), and toluene (10 mL) were added. The solution was stirred at rt for 1 h. The reaction was removed from the glovebox. Addition of hexanes (80 mL) led to a yellow precipitate. The solid was filtered and washed with hexanes (20 mL) and cold MeOH (10 mL). The resulting solid was recrystallized in THF/hexanes to give 647.4 mg of **S6** as a yellow solid (81% yield). Elemental Analysis: Calcd for C$_{44}$H$_{38}$BrFNiOP$_2$, C, 65.9; H, 4.8; F, 2.4; Found C, 65.9; H, 4.8; F, 2.3. ^{19}F NMR (376 MHz, CDCl$_3$) δ -124.65. ^{31}P NMR (202 MHz, CD$_2$Cl$_2$) δ 22.06.

3a. A 20 mL vial was equipped with a stir bar in the glovebox. Sequentially, **S6** (320.9 mg, 0.4000 mmol, 1.0 equiv), **S1** (235.0 mg, 0.4400 mmol, 1.1 equiv), and THF (8 mL) were added. The solution was stirred at rt for 1 h. The deep red soln was concentrated in vacuo until ~2 mL of soln was left. Addition of hexanes (18 mL) led to a yellowish orange precipitate. The solid was filtered and washed with hexanes (20 mL). The resulting solid was recrystallized in THF/hexanes to give an orange solid. The solids were then redissolved in THF (~40 mL), passed through a 0.2 μm PTFE filter to remove any undissolved solids, and concentrated in vacuo to give 259.4 mg of **3a** as an orange solid (80% yield). Elemental Analysis: Calcd for C$_{34}$H$_{28}$BrCl$_4$FNiOP$_2$, C, 50.2; H, 3.5; Cl, 17.4; Found C, 50.4; H, 3.4; Cl, 17.1. ^{19}F NMR (470 MHz, acetone-d_6) δ -123.22 (m). ^{31}P NMR (200 MHz, acetone-d_6) δ 57.95 (d, J = 26.4 Hz), 40.28 (d, J = 26.4 Hz).

S6 + (dppe) → **3b**   THF, rt
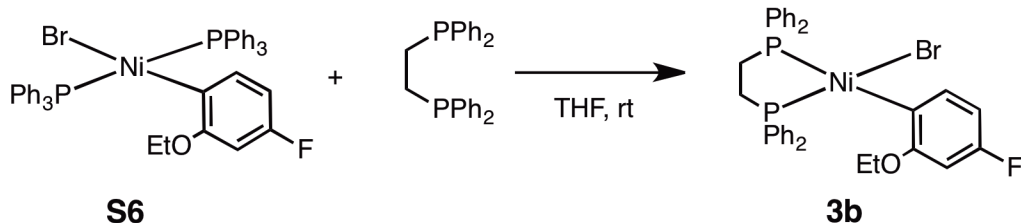
3b. A 20 mL vial was equipped with a stir bar in the glovebox. Sequentially, **S6** (324.0 mg, 0.4000 mmol, 1.0 equiv), 1,2-bis(diphenylphosphino)ethane (dppe) (175.3 mg, 0.4400 mmol, 1.1 equiv), and THF (8 mL) were added. The solution was stirred at rt for 1 h. The deep red soln was concentrated in vacuo until ~2 mL of soln was left. Addition of hexanes (18 mL) led to a yellow precipitate. The solid was filtered and washed with hexanes (20 mL). The resulting solid was recrystallized in THF/hexanes to give an orange solid. The solids were then redissolved in THF (~40 mL), passed through a 0.2 µm PTFE filter to remove any undissolved solids, and concentrated in vacuo to give 208.5 mg of **3b** as an orange solid (77% yield). Elemental Analysis: Calcd for $C_{34}H_{32}BrFNiOP_2$, C, 60.4; H, 4.8; F, 2.8; Found C, 60.3; H, 5.1; F, 2.4. ^{19}F NMR (470 MHz, acetone-d_6) δ -124.05 (m). ^{31}P NMR (202 MHz, acetone-d_6) δ 57.82 (d, J = 28.5 Hz), 40.61 (d, J = 28.5 Hz).

S6 + **S2** → **3c**   THF, rt
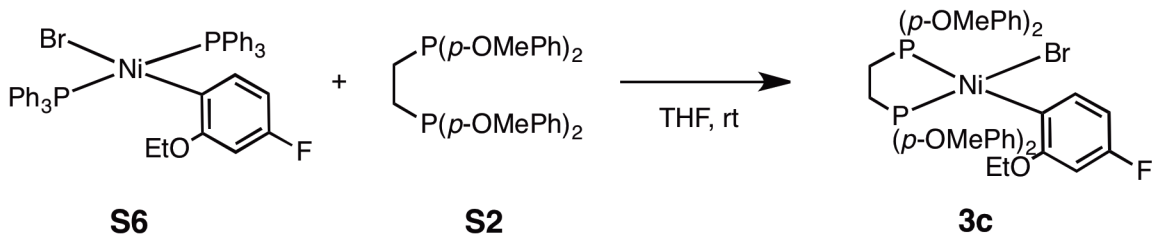
3c. A 20 mL vial was equipped with a stir bar in the glovebox. Sequentially, **S6** (321.0 mg, 0.4000 mmol, 1.0 equiv), **S2** (228.3 mg, 0.4400 mmol, 1.1 equiv), and THF (8 mL) were added. The solution was stirred at rt for 1 h. The deep red soln was concentrated in vacuo until ~2 mL of soln was left. Addition of hexanes (18 mL) led to a yellowish orange precipitate. The solid was filtered and washed with hexanes (20 mL) and cold MeOH (5 mL). The resulting solid was recrystallized in THF/hexanes to give an orange solid. The solids were then redissolved in THF (~50 mL), passed through a 0.2 µm PTFE filter to remove any undissolved solids, and concentrated in vacuo to give 102.9 mg of **3c** as an orange solid (32% yield). Elemental Analysis: Calcd for $C_{39}H_{40}BrFNiO_5P_2$, C, 57.3; H, 5.1; F, 2.4; Found C, 57.7; H, 5.3; F, 2.1. ^{19}F NMR (660 MHz, CDCl$_3$) δ -124.15 (m). ^{31}P NMR (283 MHz, CDCl$_3$) 55.21 (d, J = 30.7 Hz), 38.75 (d, J = 30.7 Hz).
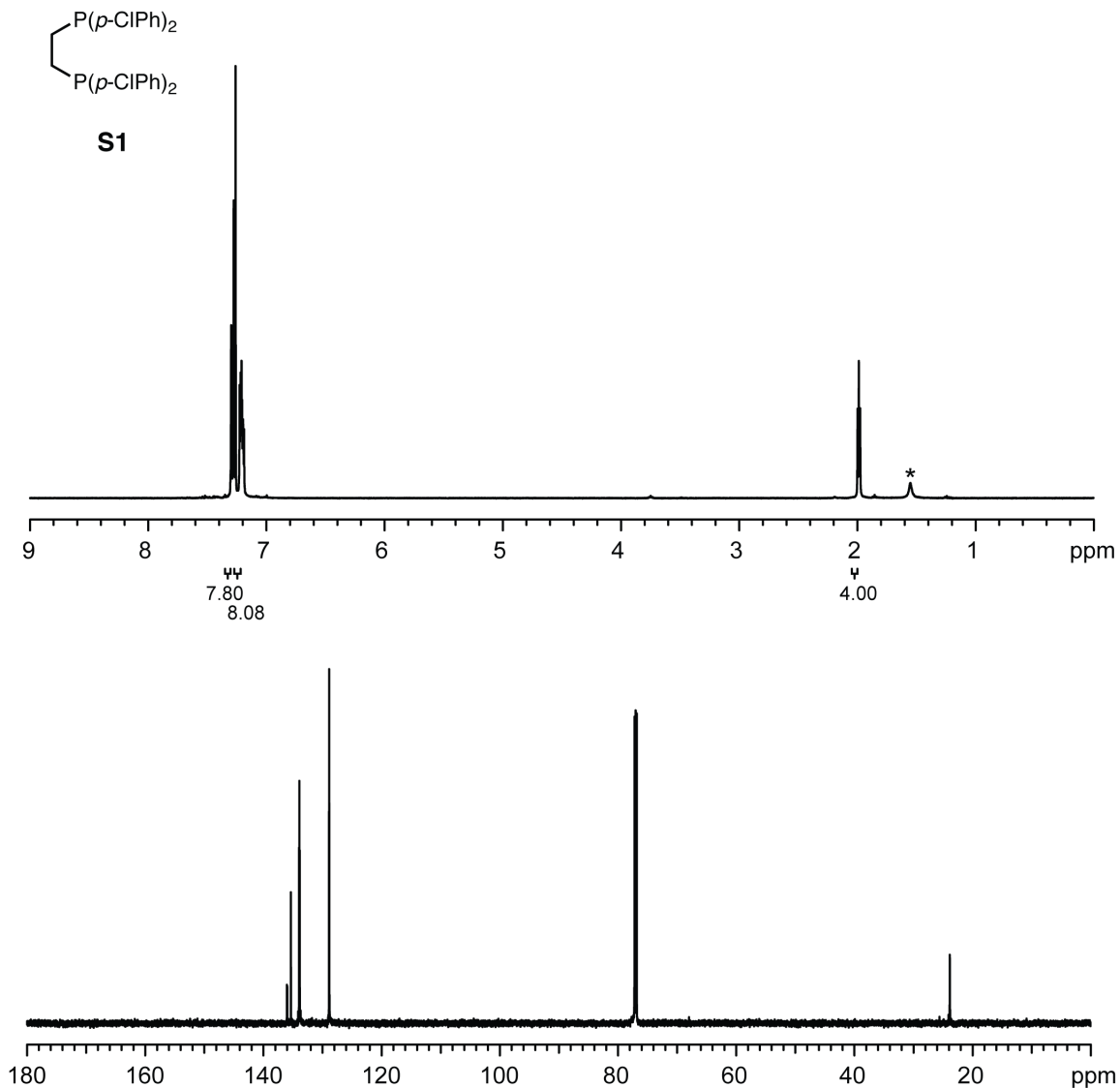
IV. NMR Spectra

Figure S1-1. ^{1}H and ^{13}C NMR spectra of **S1**.
^{1}H NMR (400 MHz, CDCl$_3$) δ 7.30-7.28 (m, 8H), 7.23-7.19 (m, 8H), 1.99 (dd, J = 4.4, 4.2 Hz, 4H). *residual H$_2$O. ^{13}C NMR (176 MHz, CDCl$_3$) δ 135.98 (dd, J = 8.8, 6.2 Hz), 135.34, 133.90 (at, J = 9.9 Hz), 128.87 (at, J = 3.4 Hz), 23.85 (d, J = 2.5 Hz).
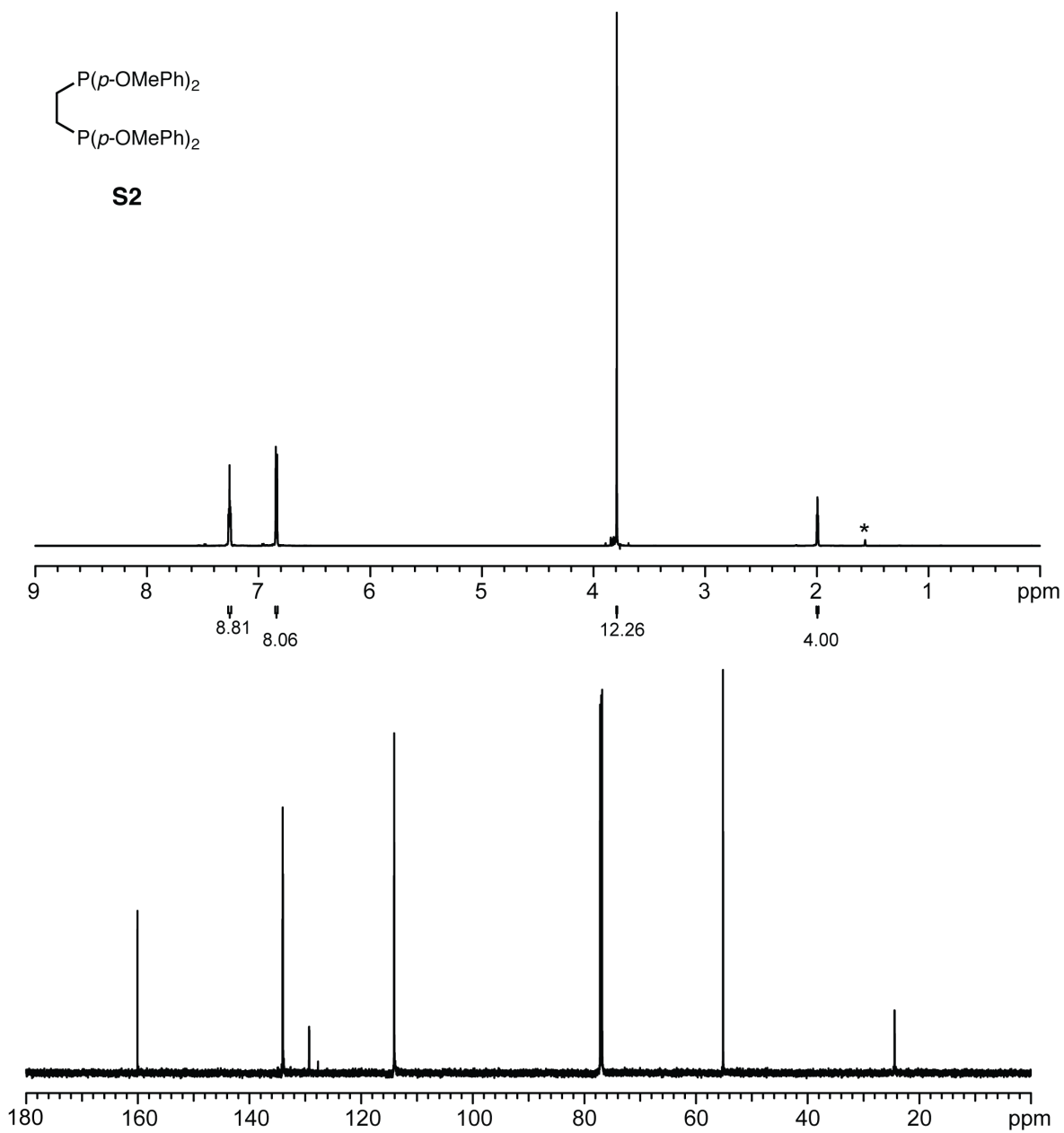
Figure S1-2. ^{1}H and ^{13}C NMR spectra of **S2**.
^{1}H NMR (700 MHz, CDCl$_3$) δ 7.27-7.25 (m, 8H), 6.84 (d, J = 8.6 Hz, 8H), 3.79 (s, 12H), 1.99 (dd, J = 4.2, 3.5 Hz, 4H). *residual H$_2$O. ^{13}C NMR (176 MHz, CDCl$_3$) δ 160.06, 134.04 (at, J = 9.9 Hz), 129.30 (at, J = 5.5 Hz), 114.07 (at, J = 3.7 Hz), 55.15, 24.41 (d, J = 3.3 Hz).
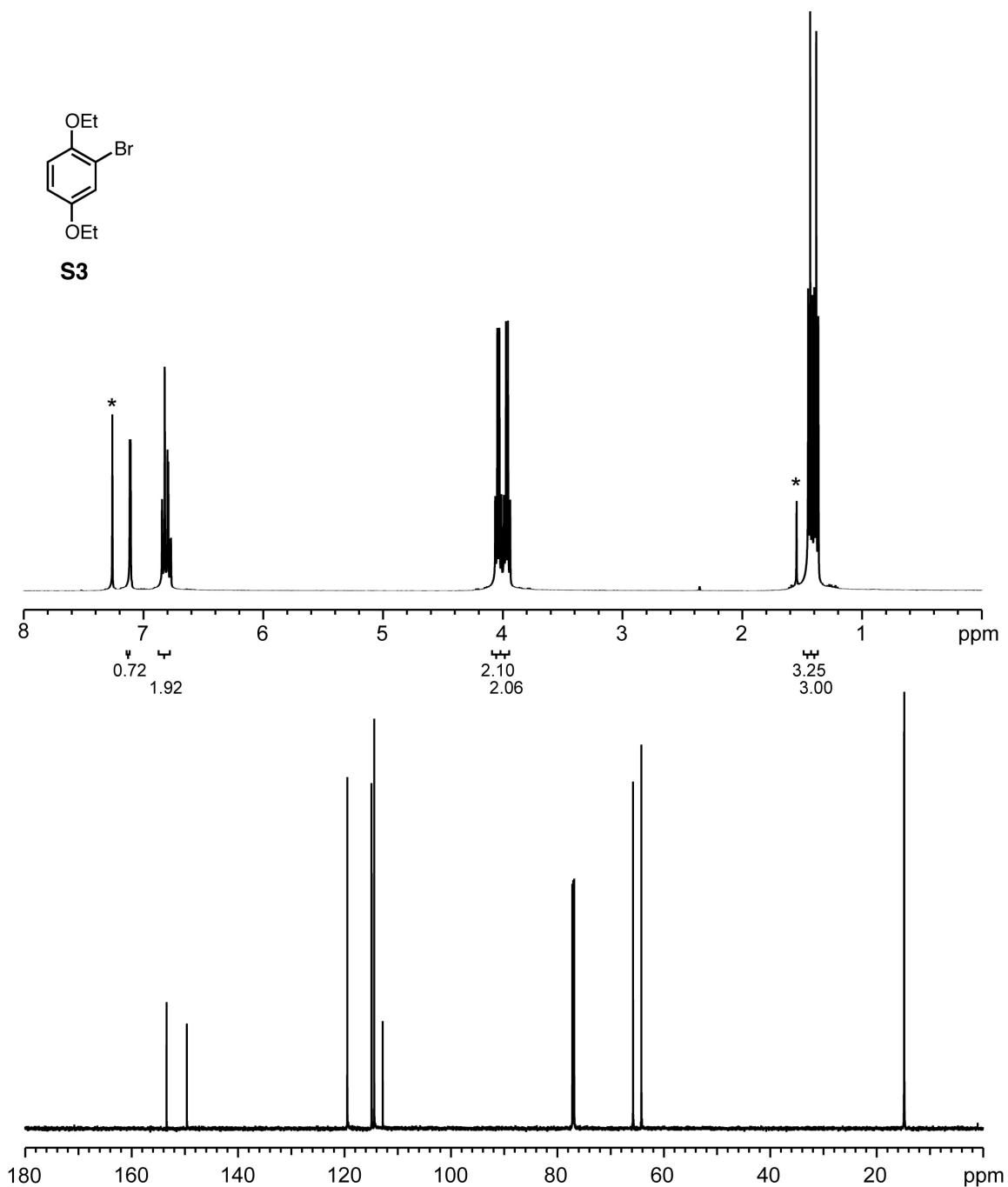
Figure S1-3. ^{1}H and ^{13}C NMR spectra of **S3**.
^{1}H NMR (400 MHz, CDCl$_3$) δ 7.11 (d, J = 2.8 Hz, 1H), 6.85-6.77 (m, 2H), 4.03 (q, J = 7.0 Hz, 2H), 3.96 (q, J = 7.0 Hz, 2H), 1.43 (t, J = 7.0 Hz, 3H), 1.38 (t, J = 7.0 Hz, 3H). *residual H$_2$O. ^{13}C NMR (176 MHz, CDCl$_3$) δ 153.43, 149.62, 119.48, 114.91, 114.41, 112.82, 65.78, 64.21, 14.86, 14.80.
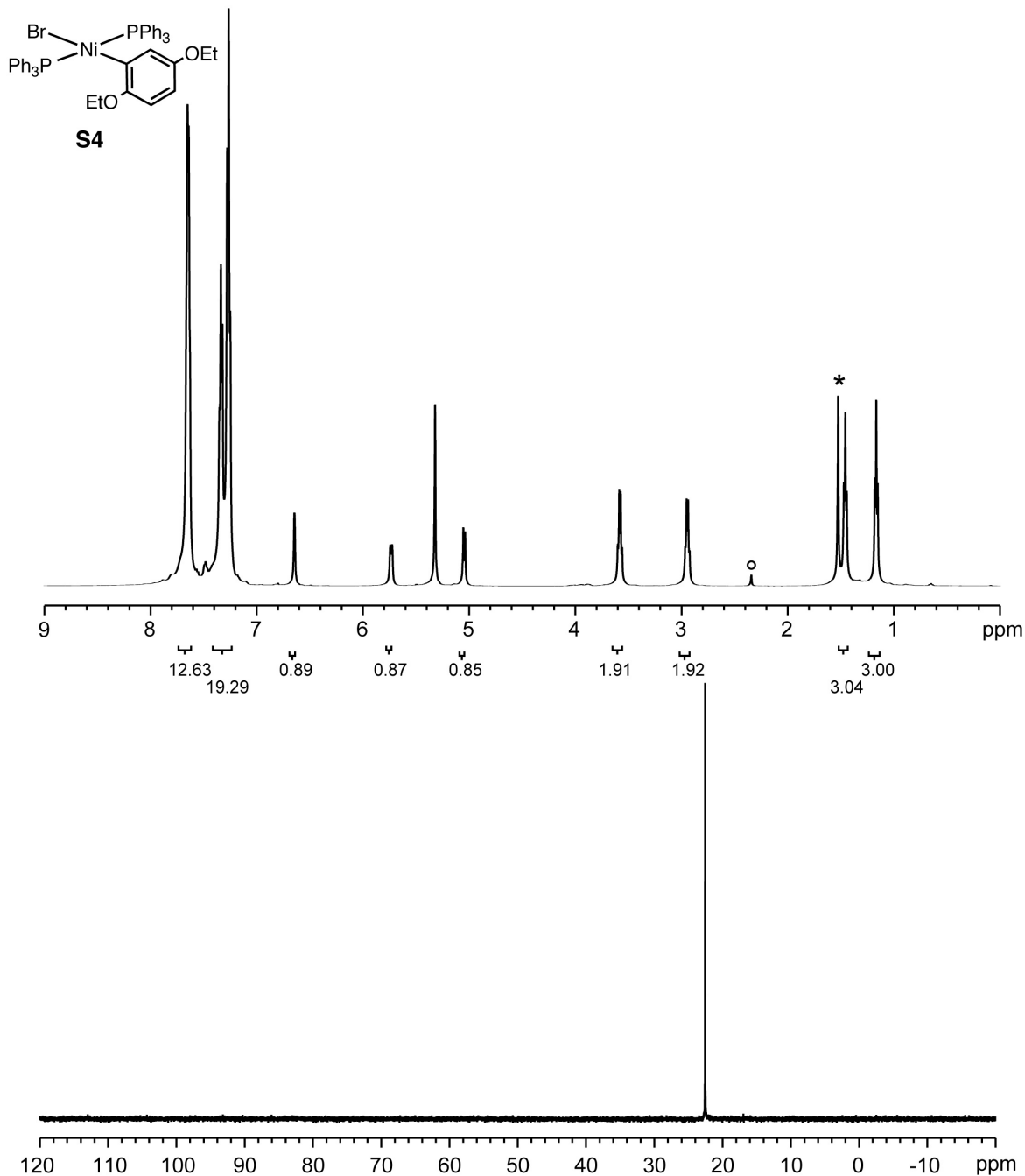
Figure S1-4. ^{1}H and ^{31}P NMR spectra of **S4**.
^{1}H NMR (500 MHz, CD$_2$Cl$_2$) δ 7.64 (bs, 12H), 7.35-7.25 (m, 18H), 6.65 (s, 1H), 5.73 (t, J = 7.8 Hz, 1H), 5.05 (d, J = 8.8 Hz, 1H) 3.58 (q, J = 6.9 Hz, 2H), 2.94 (q, J = 6.9 Hz, 2H), 1.46 (t, J = 6.8 Hz, 3H), 1.17 (t, J = 6.8 Hz, 3H). residual *H$_2$O and °toluene. ^{31}P NMR (202 MHz, CD$_2$Cl$_2$) δ 22.55.
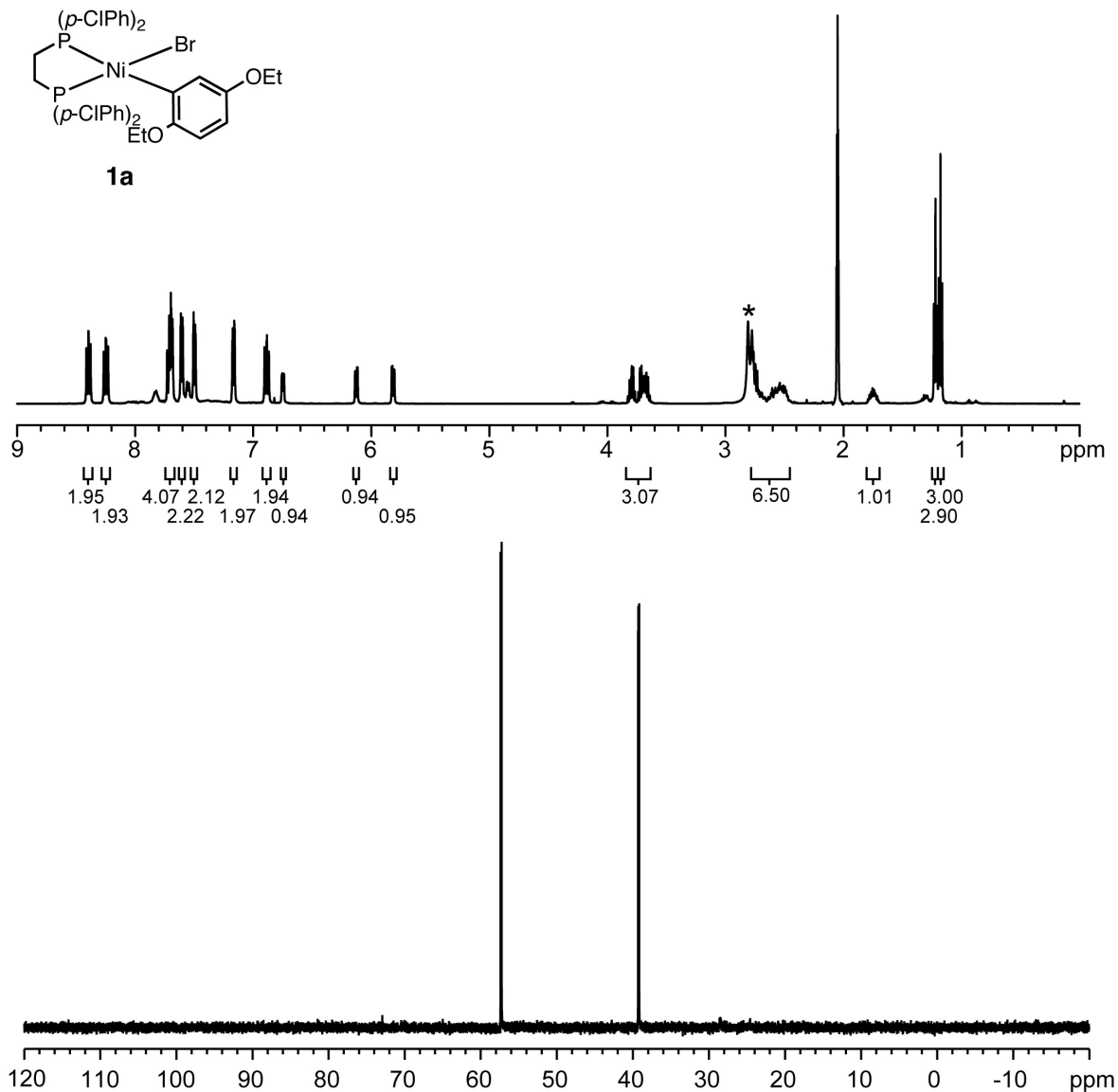
Figure S1-5. ^{1}H and ^{31}P NMR spectra of **1a**.

^{1}H NMR (500 MHz, acetone-d_6) δ 8.41-8.38 (m, 2H), 8.27-8.23 (m, 2H), 7.73-7.68 (m, 4H), 7.61 (dd, J = 8.0, 1.5 Hz, 2H), 7.50 (dd, J = 8.5, 1.5 Hz, 2H), 7.18 (dd, J = 8.5, 1.9 Hz, 2H), 6.90-6.87 (m, 2H), 6.75 (dd, J = 7.1, 1.9 Hz, 1H), 6.13 (dd, J = 8.6, 2.8 Hz, 1H), 5.82 (dd, J = 8.6, 3.4 Hz, 1H), 3.83-3.64 (m, 3H), 2.80-2.47 (m, 4H), 1.79-1.70 (m, 1H), 1.22 (t, J = 7.0 Hz, 3H), 1.18 (t, J = 7.0 Hz, 3H). *residual H$_2$O. ^{31}P NMR (202 MHz, acetone-d_6) δ 57.31 (d, J = 24.6 Hz), 39.23 (d, J = 24.6 Hz).
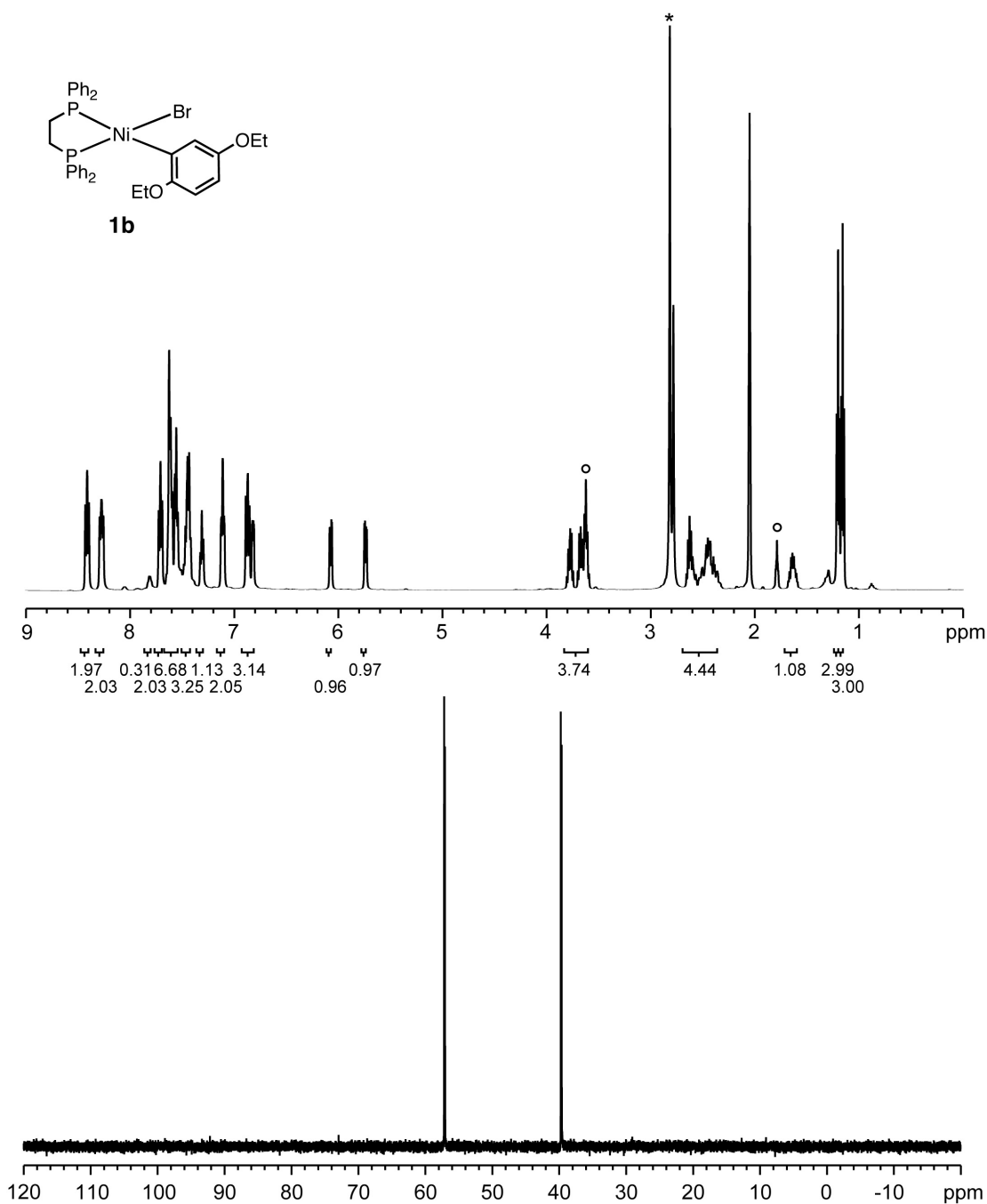
73

Figure S1-6. ^{1}H and ^{31}P NMR spectra of **1b**.
^{1}H NMR (500 MHz, acetone-d_6) δ 8.41 (t, J = 8.5 Hz, 2H), 8.27 (t, J = 8.5 Hz, 2H), 7.71 (t, J = 8.5 Hz, 2H), 7.62-7.54 (m, 6H), 7.47-7.42 (m, 3H), 7.31 (t, J = 7.2 Hz, 1H), 7.11 (t, J = 6.8 Hz, 2H), 6.89-6.81 (m, 3H), 6.07 (dd, J = 8.5, 2.5 Hz, 1H), 5.74 (dd, J = 8.5, 3.2 Hz, 1H), 3.81-3.59 (m, 4H), 2.66-2.33 (m, 3H), 1.68-1.59 (m, 1H), 1.20 (t, J = 6.9 Hz, 3H), 1.16 (t, J = 6.9 Hz, 3H). residual *H_2O and °THF. ^{31}P NMR (202 MHz, acetone-d_6) δ 57.12 (d, J = 26.4 Hz), 39.69 (d, J = 26.4 Hz).
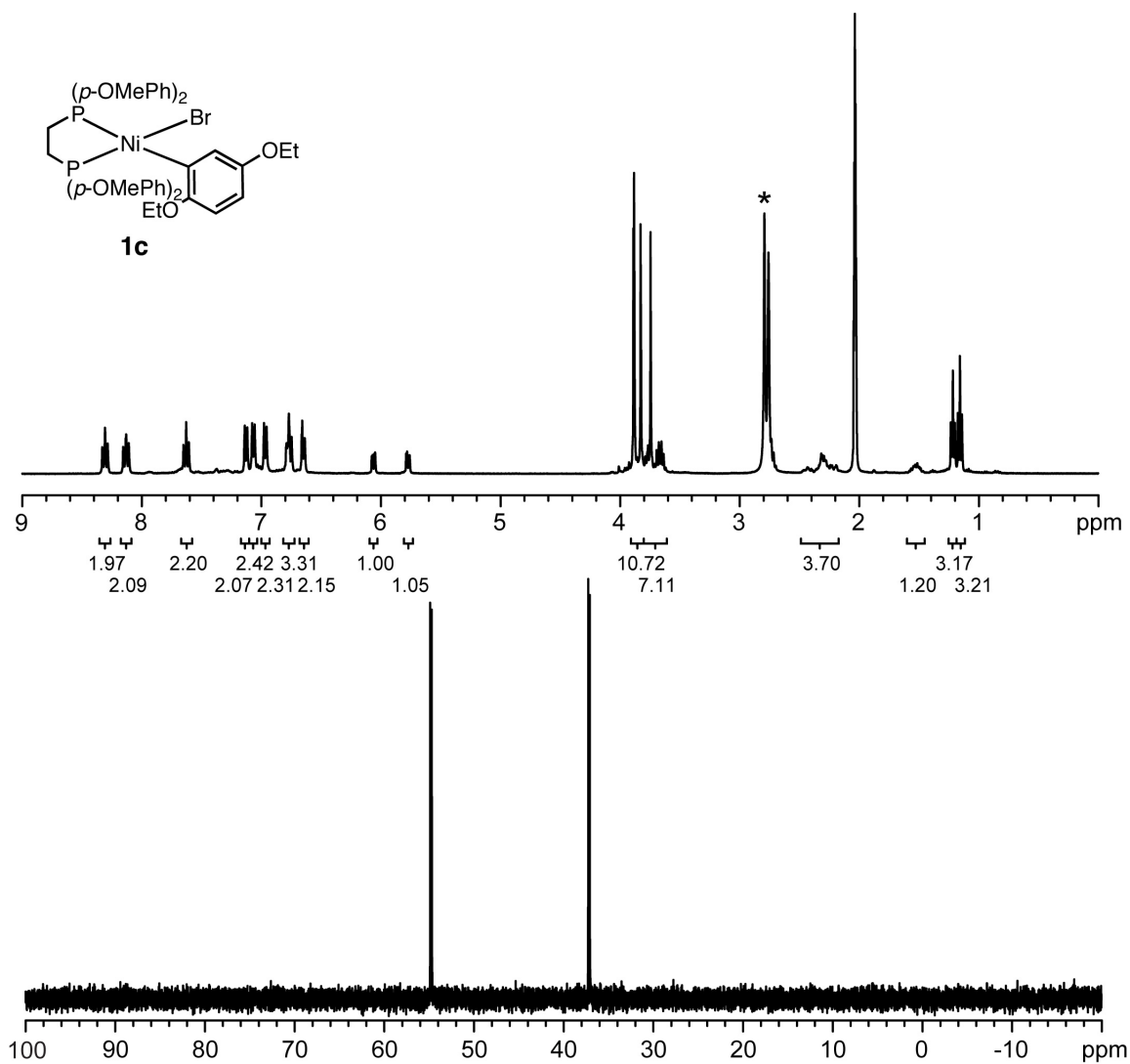
Figure S1-7. ^{1}H and ^{31}P NMR spectra of **1c**.

^{1}H NMR (400 MHz, acetone-d_6) δ 8.32 (t, J = 8.7 Hz, 2H), 8.15 (t, J = 9.3 Hz, 2H), 7.64 (t, J = 9.1 Hz, 2H), 7.14 (d, J = 8.7 Hz, 2H), 7.08 (d, J = 8.6 Hz, 2H), 6.98 (d, J = 8.2 Hz, 2H), 6.80-6.76 (m, 3H), 6.66 (dd, J = 8.7, 1.7 Hz, 2H), 6.08 (dd, J = 8.3, 2.7 Hz, 1H), 5.79 (dd, J = 8.5, 3.2 Hz, 1H), 3.90 (s, 3H), 3.89 (s, 3H), 3.81 (s, 3H), 3.79-3.77 (m, 2H), 3.76 (s, 3H), 3.71-3.65 (m, 2H), 2.47-2.19 (m, 3H), 1.59-1.44 (m, 1H), 1.23 (t, J = 7.0 Hz, 3H), 1.17 (t, J = 7.0 Hz, 3H).*residual H$_2$O. ^{31}P NMR (160 MHz, acetone-d_6) δ 54.79 (d, J = 29.2 Hz), 37.17 (d, J = 29.2 Hz).
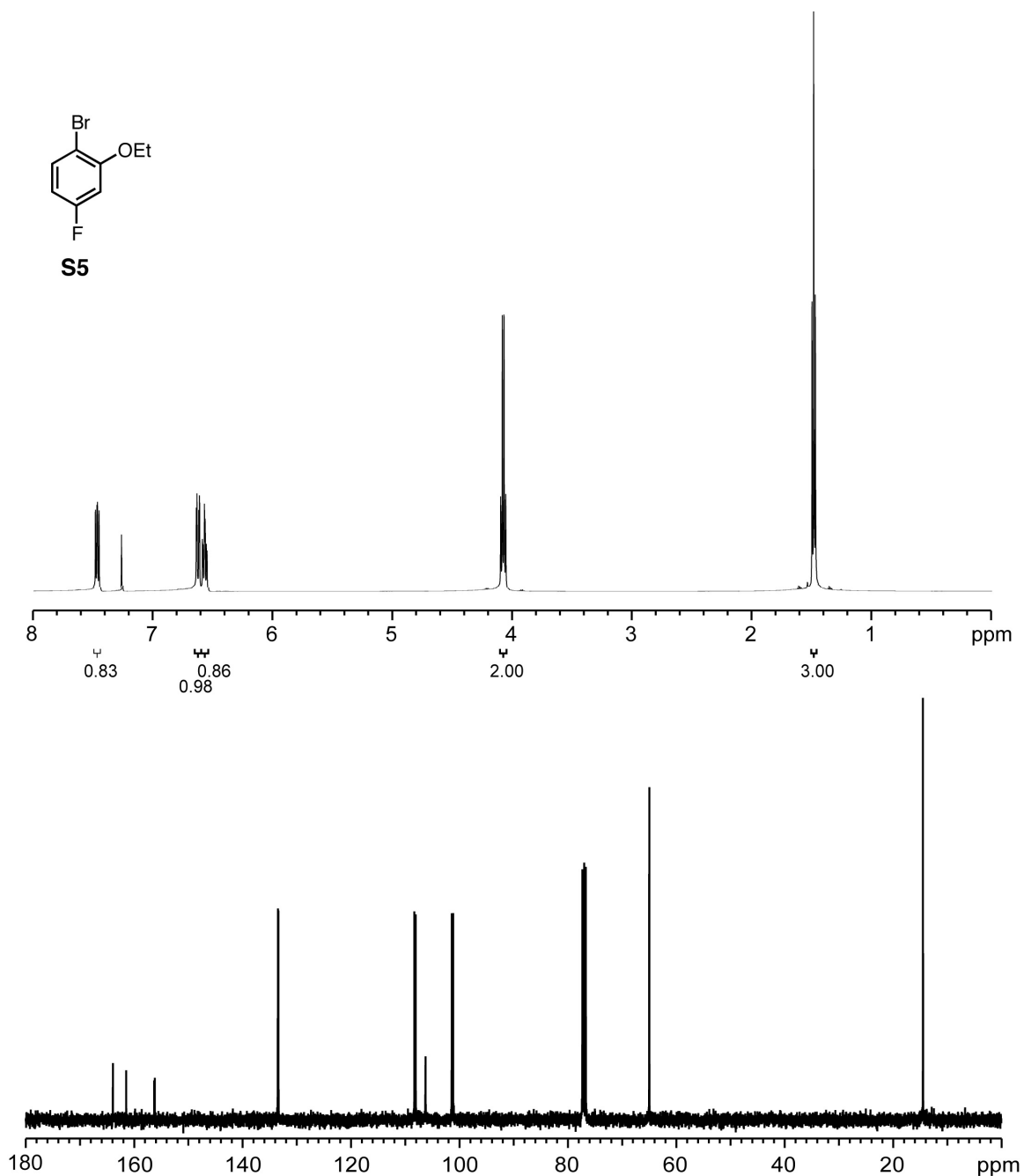
Figure S1-8. ^{1}H and ^{13}C NMR spectra of **S5**.
^{1}H NMR (500 MHz, CDCl$_3$) δ 7.46-7.43 (m, 1H), 6.60 (dd, J = 10.6, 2.8 Hz, 1H), 6.55 (dt, J = 8.2, 2.8 Hz, 1H), 4.05 (q, J = 7.0 Hz, 2H), 1.46 (t, J = 6.7 Hz, 3H). ^{13}C NMR (100 MHz, CDCl$_3$) δ 162.70 (d, J = 245 Hz), 156.25 (d, J = 10.2 Hz), 133.42 (d, J = 9.8 Hz), 108.20 (d, J = 22.5 Hz), 106.25 (d, J = 3.6 Hz), 101.29 (d, J = 26.7 Hz), 64.98, 14.49.
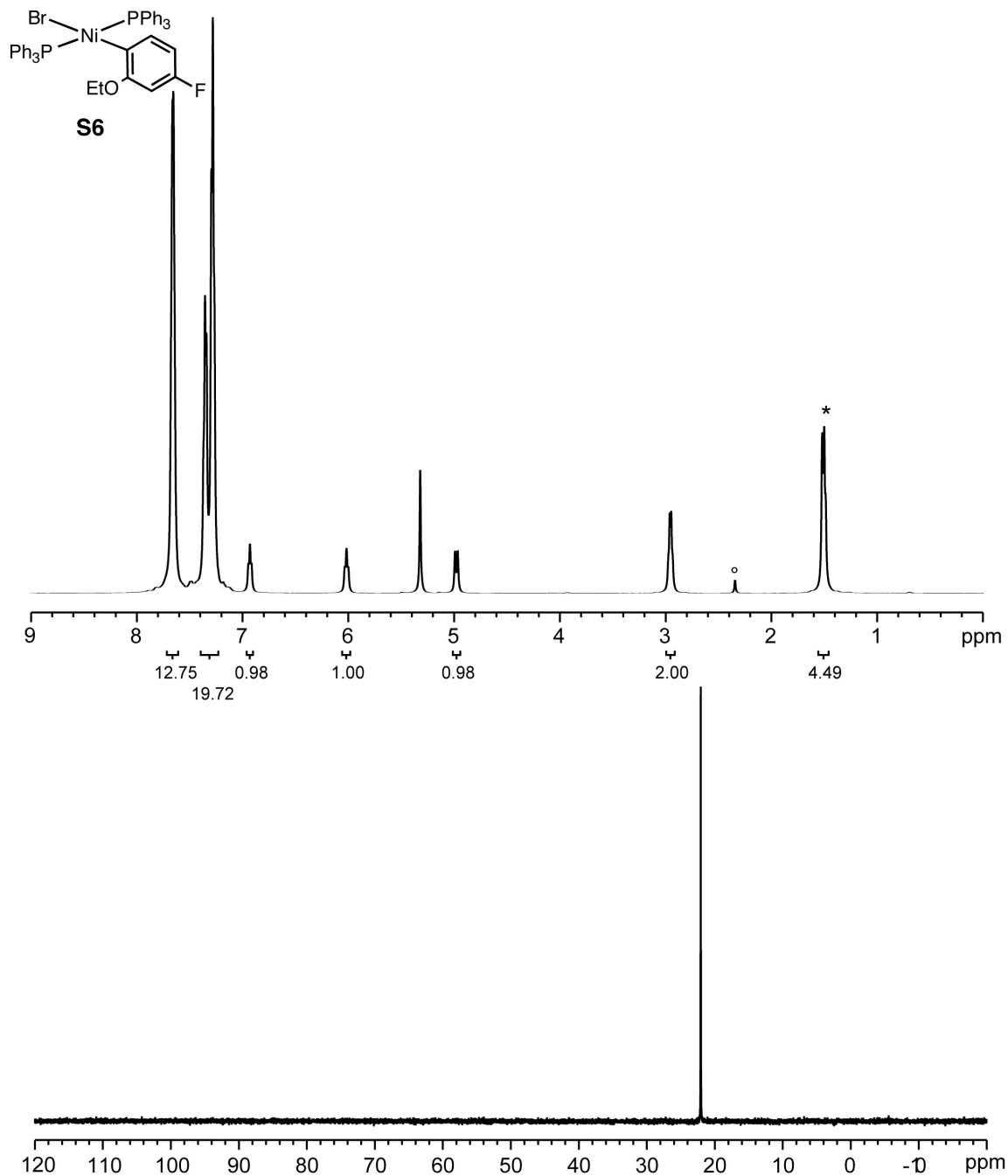
Figure S1-9. ^{1}H and ^{31}P NMR spectra of **S6**.
^{1}H NMR (500 MHz, CD$_2$Cl$_2$) δ 7.66 (bs, 12H), 7.37-7.26 (m, 18H), 6.93 (t, J = 7.0 Hz, 1H), 6.02 (t, J = 8.3 Hz, 1H), 4.98 (d, J = 12.7 Hz, 1H) 2.95 (q, J = 6.6 Hz, 2H), 1.50 (t, J = 5.9 Hz, 3H). residual *H$_2$O and °Toluene. ^{31}P NMR (202 MHz, CD$_2$Cl$_2$) δ 22.06.
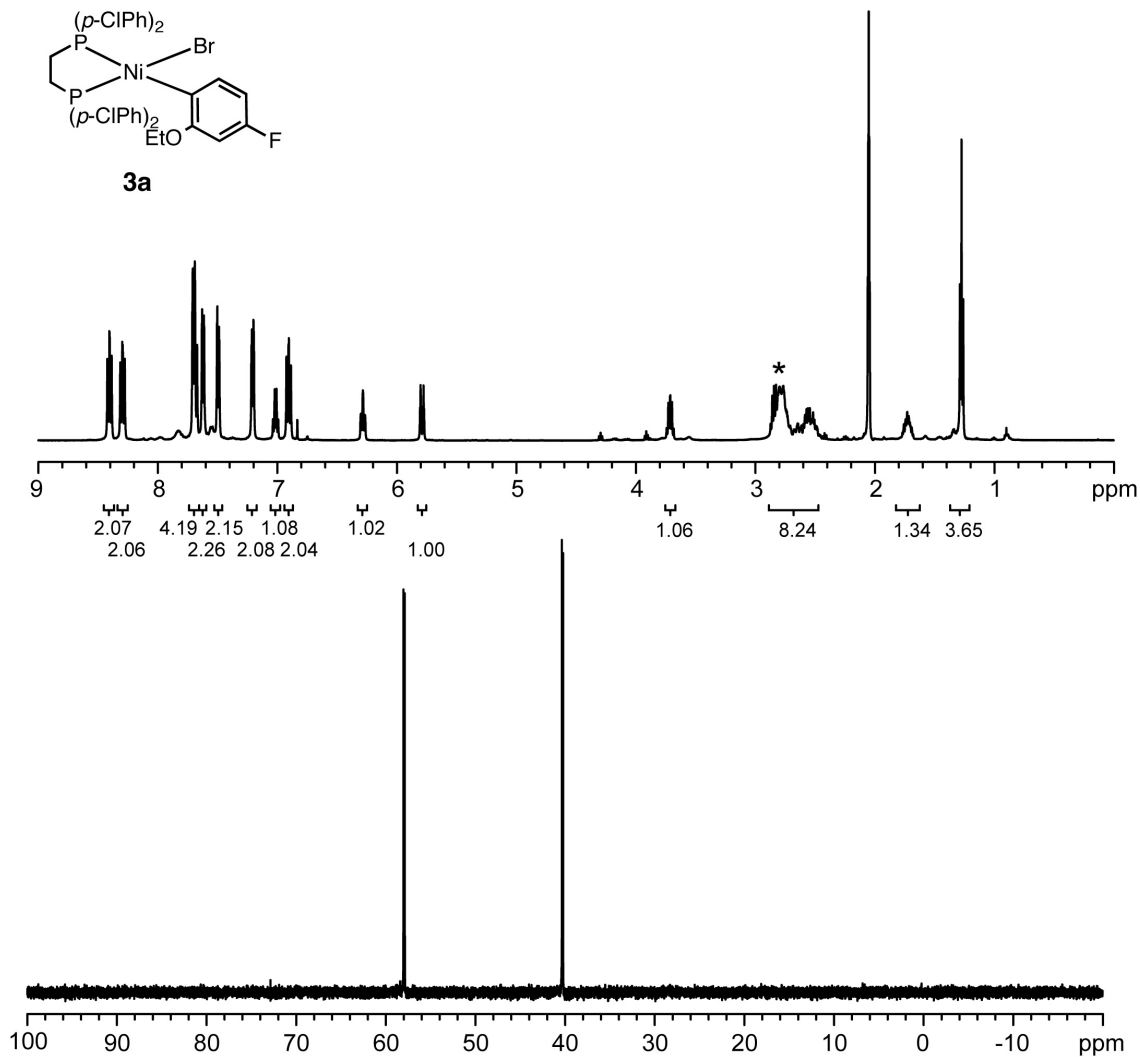
Figure S1-10. ^{1}H and ^{31}P NMR spectra of **3a**.
^{1}H NMR (500 MHz, acetone-d_6) δ 8.43-8.39 (m, 2H), 8.32-8.28 (m, 2H), 7.71-7.67 (m, 4H), 7.63-7.62 (m, 2H), 7.51-7.49 (m, 2H), 7.22-7.20 (m, 2H), 7.04-7.00 (m, 1H), 6.92-6.89 (m, 2H), 6.30-6.27 (m, 1H), 5.81-5.77 (m, 1H), 3.75-3.68 (m, 1H), 2.86-2.46 (m, 4H), 1.80-1.69 (m, 1H), 1.28 (t, J = 7.0 Hz, 3H). *residual H_2O.
^{31}P NMR (200 MHz, acetone-d_6) δ 57.95 (d, J = 26.4 Hz), 40.28 (d, J = 26.4 Hz).
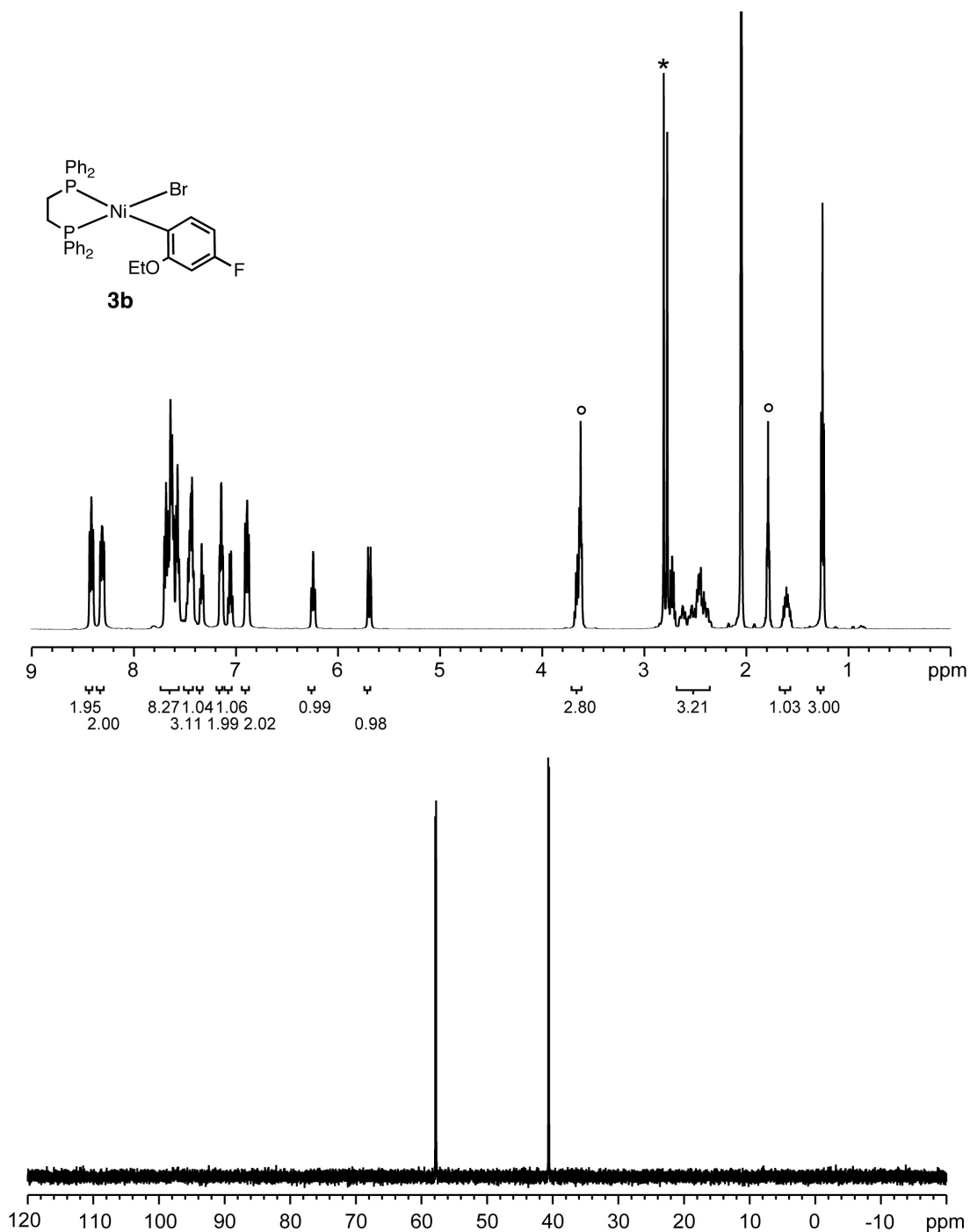
Figure S1-11. ^{1}H and ^{31}P NMR spectra of **3b**.
^{1}H NMR (500 MHz, acetone-d_6) δ 8.42 (t, J = 8.6 Hz, 2H), 8.31 (t, J = 8.6 Hz, 2H), 7.70-7.56 (m, 8H), 7.47-7.41 (m, 3H), 7.34 (t, J = 7.3 Hz, 1H), 7.15 (td, J = 7.7, 2.1 Hz, 2H), 7.05 (q, J = 7.4 Hz, 1H), 6.89 (t, J = 9.0 Hz, 2H), 6.24 (t, J = 8.4 Hz, 1H), 5.69 (dt, J = 12.6, 2.4 Hz, 1H), 3.68-3.61 (m, 2H), 2.76-2.37 (m, 3H), 1.64-1.57 (m, 1H), 1.25 (t, J = 6.9 Hz, 3H). residual *H$_2$O and °THF. ^{31}P NMR (202 MHz, acetone-d_6) δ 57.82 (d, J = 28.5 Hz), 40.61 (d, J = 28.5 Hz).

79
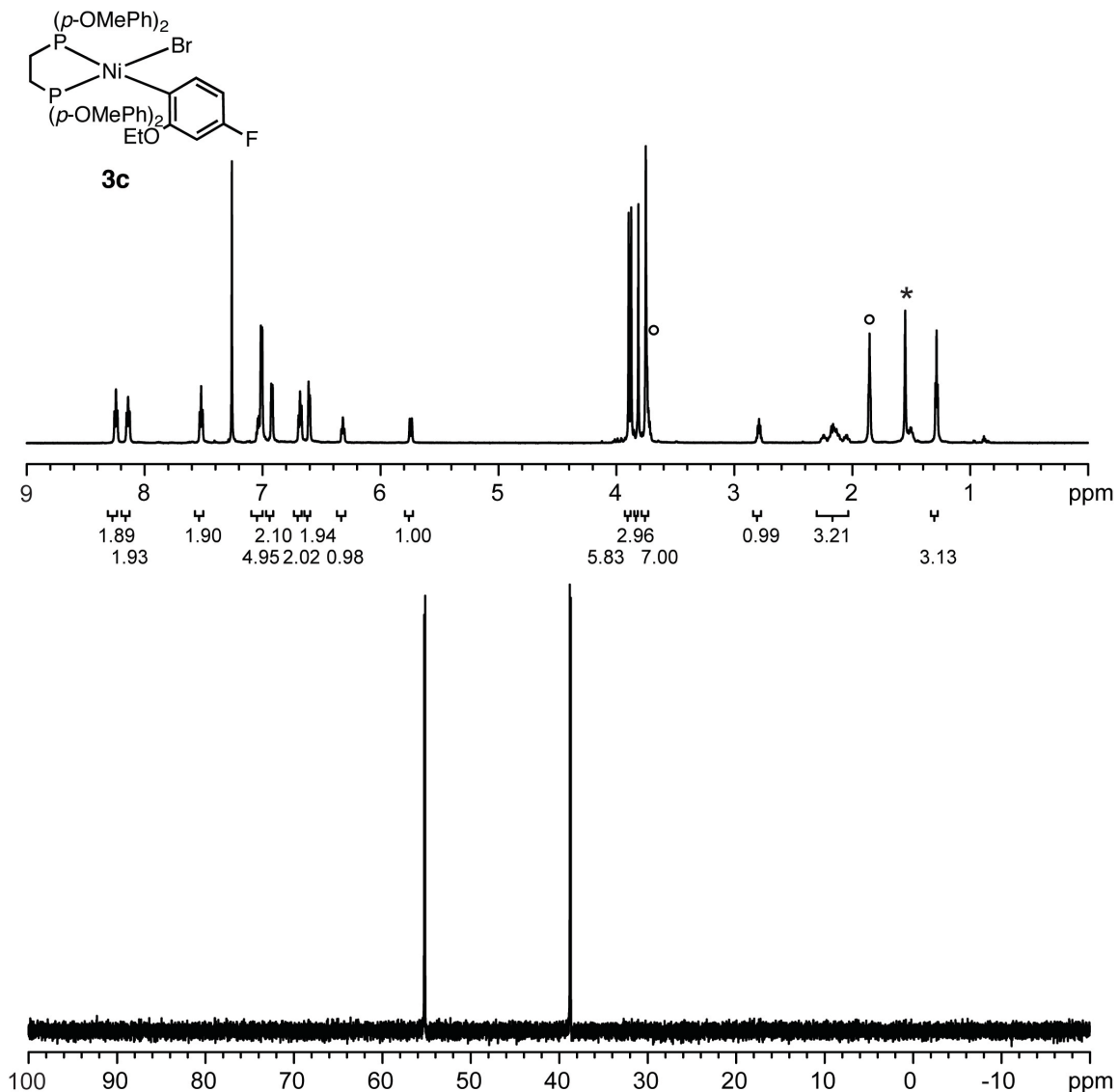
Figure S1-12. ^{1}H and ^{31}P NMR spectra of **3c**.
^{1}H NMR (700 MHz, CDCl$_3$) δ 8.24 (t, J = 9.0 Hz, 2H), 8.14 (t, J = 9.3 Hz, 2H), 7.52 (t, J = 8.9 Hz, 2H), 7.05-7.00 (m, 5H), 6.92 (d, J = 8.4 Hz, 2H), 6.68 (t, J = 9.7 Hz, 2H), 6.60 (d, J = 7.6 Hz, 2H), 6.32 (t, J = 8.5 Hz, 1H), 5.74 (d, J = 12.5 Hz, 1H), 3.90 (s, 3H), 3.87 (s, 3H), 3.81 (s, 3H), 3.75 (s, 3H), 3.74-3.72 (m, 2H), 2.79 (quin, J = 7.9 Hz, 1H), 2.26-2.03 (m, 3H), 1.29 (t, J = 6.8 Hz, 3H). residual *H$_2$O and °THF. ^{31}P NMR (283 MHz, CDCl$_3$) 55.21 (d, J = 30.7 Hz), 38.75 (d, J = 30.7 Hz).

V. Propagation Rate Studies

Representatitve Procedure for Performing Propagation Rate Studies:
The IR probe was inserted through an O-ring sealed 14/20 ground glass adapter (custom made) into an oven-dried 50 mL 2-neck flask containing a Teflon magnetic stir bar. The other neck was equipped with a three-way adapter fitted with a septum for injections and an N_2 line. The flask was cooled under vacuum and then refilled with N_2. Following two more cycles of evacuation and refilling, the flask was charged with THF (4.6 mL) and cooled to 0 °C over ~5 min. After recording a background spectrum, monomer **2** (4.4 mL, 0.46 M in THF) was added by syringe and allowed to equilibrate for at least 5 min at 0 °C. After 5 min, the solution of **1b** (1 mL, 0.015 M in THF) was injected and spectra were recorded every 15 s over the first 15-20% conversion. To account for mixing and temperature equilibration, spectra recorded in the first 60 s of the reaction were discarded. The data for first 10% conversion were converted to concentrations using the appropriate calibration curve prepared as previously reported.[2]
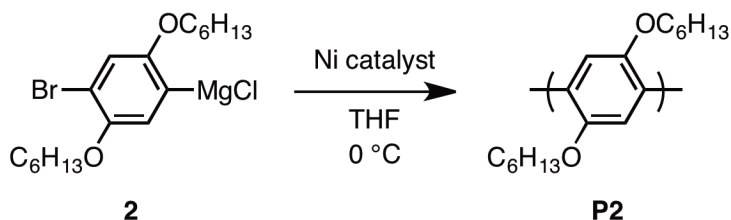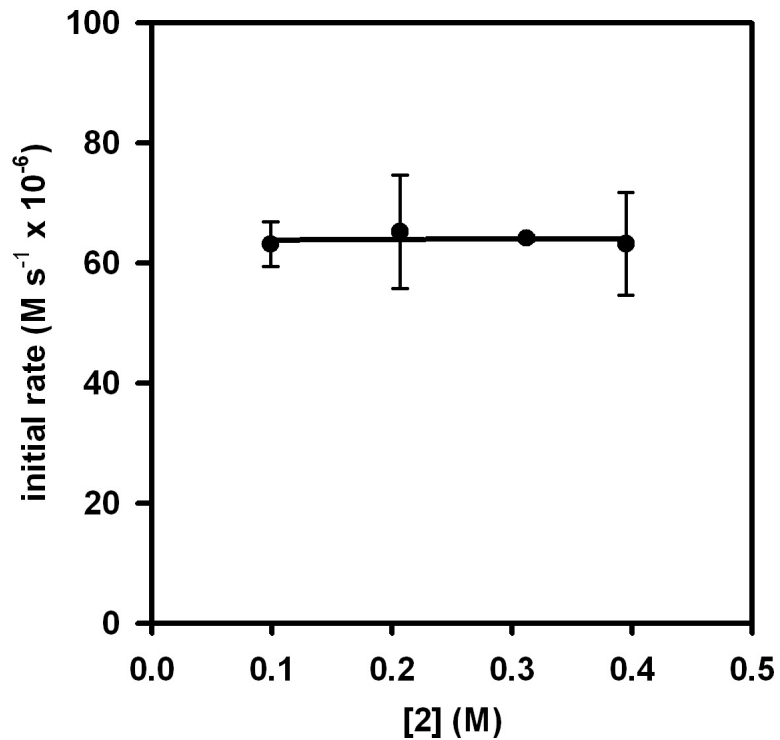
Figure S1-13. Plot of initial rate versus [monomer] for the polymerization of **2** with catalyst **1a**. (temp = 0 °C, [**1a**] = 0.0015 M) fitted to y = a[monomer]^n, where a = 64 ± 2 and n = 0.00 ± 0.02.

Table S1-1. Data for the plot in Figure S1-13.

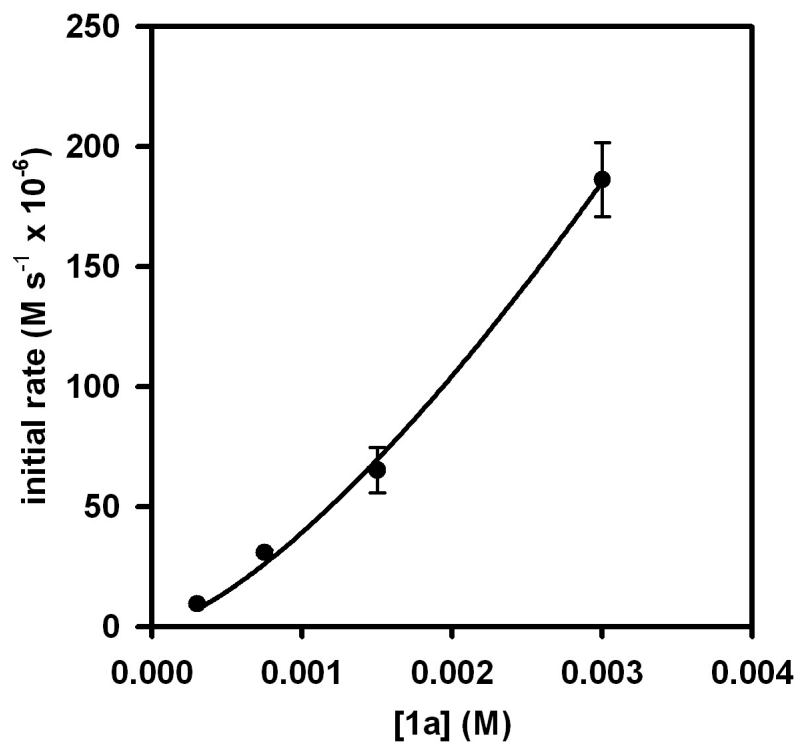| [**2**] (M)	Initial rate (M s^{-1})
0.1	63 ± 4 x 10^{-6}
0.2	65 ± 9 x 10^{-6}
0.3	64.1 ± 0.5 x 10^{-6}
0.4	63 ± 9 x 10^{-6}

Figure S1-14. Plot of initial rate versus [**1a**] for the polymerization of **2** with catalyst **1a**. (temp = 0 °C, [**2**] = 0.02 M) fitted to $y = a[\mathbf{1a}]^n$, where $a = 7 \pm 3 \times 10^5$ and $n = 1.41 \pm 0.08$.

Table S1-2. Data for the plot in Figure S1-14.

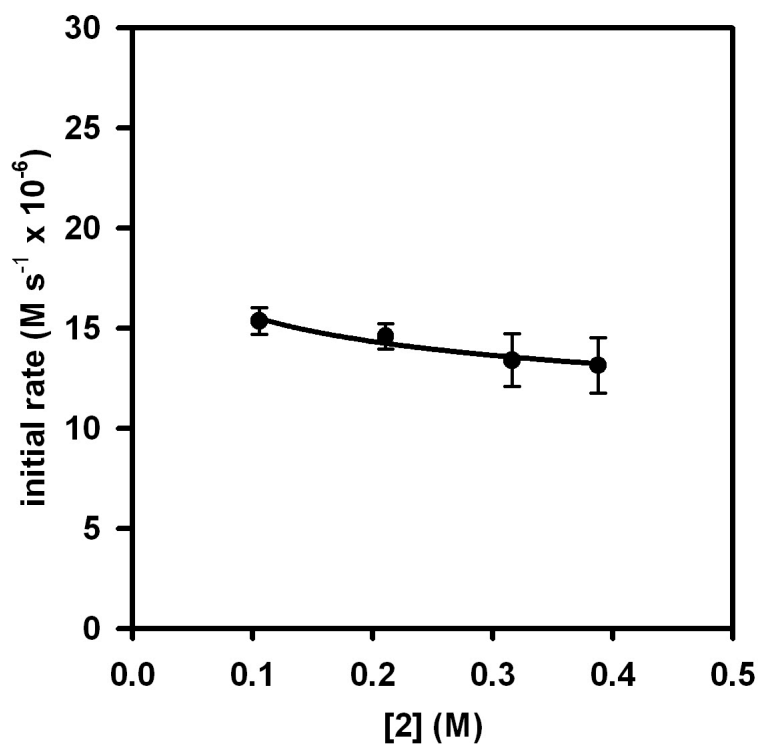| [**1a**] (M)	Initial rate (M s^{-1})
0.00030	$9.5 \pm 0.8 \times 10^{-6}$
0.00075	$30.9 \pm 0.9 \times 10^{-6}$
0.0015	$65 \pm 9 \times 10^{-6}$
0.0030	$190 \pm 20 \times 10^{-6}$

Figure S1-15. Plot of initial rate versus [monomer] for the polymerization of **2** with catalyst **1b**. (temp = 0 °C, [**1b**] = 0.0015 M) fitted to $y = a[monomer]^n$, where $a = 11.8 \pm 0.4$ and $n = -0.12 \pm 0.02$.

Table S1-3. Data for the plot in Figure S1-15.

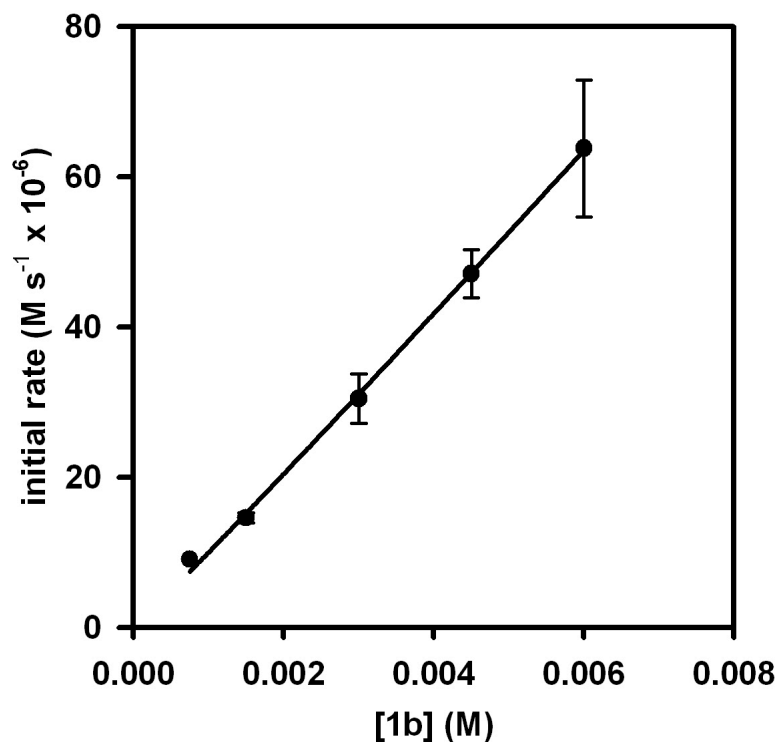| [**2**] (M)	initial rate (M s^{-1})
0.1	$15.4 \pm 0.7 \times 10^{-6}$
0.2	$14.6 \pm 0.6 \times 10^{-6}$
0.3	$13 \pm 1 \times 10^{-6}$
0.4	$13 \pm 1 \times 10^{-6}$

Figure S1-16. Plot of initial rate versus [**1b**] for the polymerization of **2** with catalyst **1b**. (temp = 0 °C, [**2**] = 0.02 M) fitted to y = a[**1b**]^n, where a = 1.3 ± 0.2 x 10^4 and n = 1.03 ± 0.04.

Table S1-4. Data for the plot in Figure S1-16.

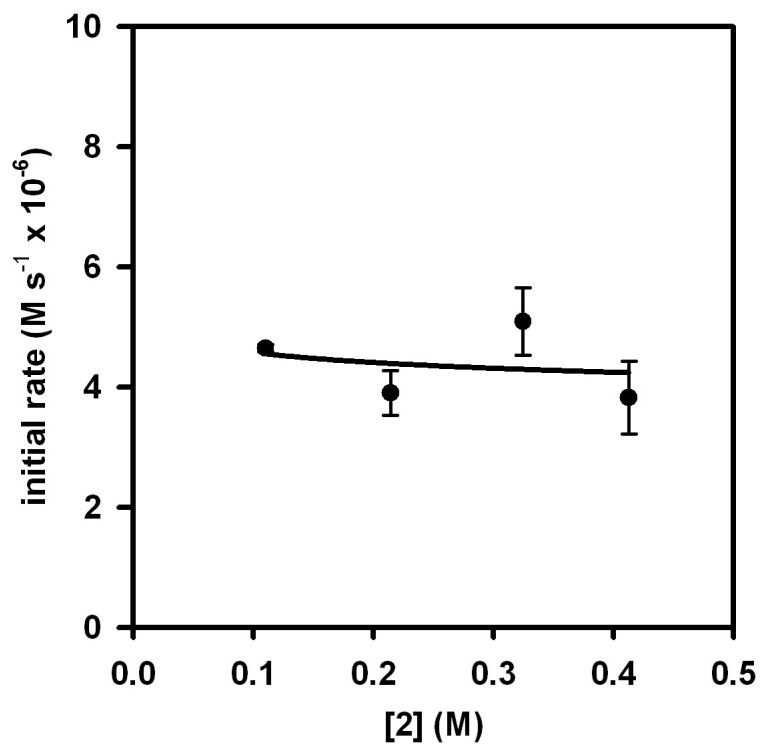| [**1b**] (M)	Initial rate (M s^{-1})
0.00075	9.1 x 10^{-6}
0.0015	14.6 ± 0.6 x 10^{-6}
0.0030	30 ± 3 x 10^{-6}
0.0045	47 ± 3 x 10^{-6}
0.0060	64 ± 9 x 10^{-6}

Figure S1-17. Plot of initial rate versus [monomer] for the polymerization of **2** with catalyst **1c**. (temp = 0 °C, [**1c**] = 0.0015 M) fitted to $y = a[\text{monomer}]^n$, where $a = 4 \pm 1$ and $n = -0.1 \pm 0.2$.

Table S1-5. Data for the plot in Figure S1-17.

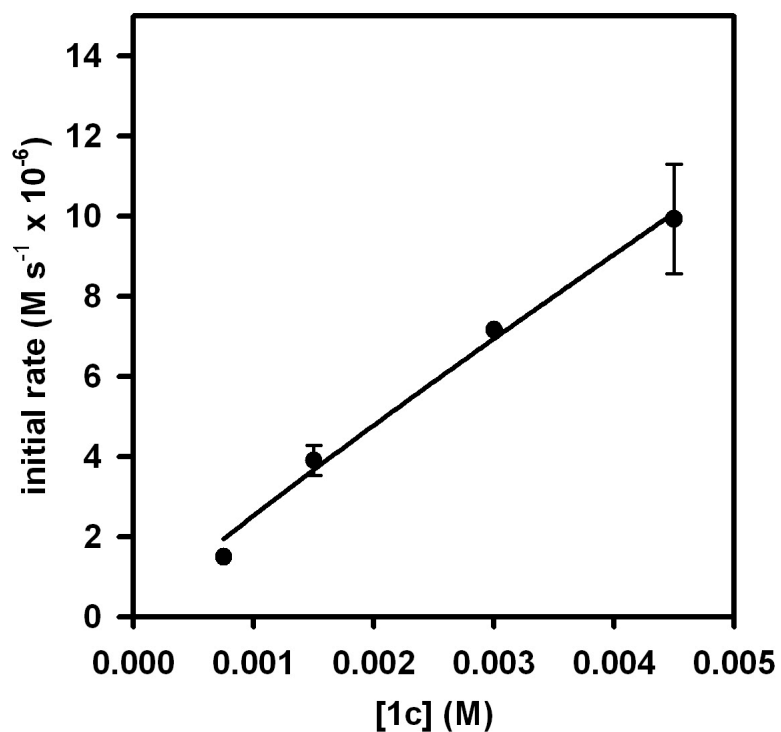| [**2**] (M)	Initial rate (M s^{-1})
0.1	$4.65 \pm 0.06 \times 10^{-6}$
0.2	$3.9 \pm 0.4 \times 10^{-6}$
0.3	$5.1 \pm 0.6 \times 10^{-6}$
0.4	$3.8 \pm 0.6 \times 10^{-6}$

Figure S1-18. Plot of initial rate versus [**1c**] for the polymerization of **2** with catalyst **1c**. (temp = 0 °C, [**2**] = 0.02 M) fitted to $y = a[\mathbf{1c}]^n$, where $a = 9.1 \pm 0.7 \times 10^2$ and $n = 0.92 \pm 0.08$.

Table S1-6. Data for the plot in Figure S1-18.

[**1c**] (M)	Initial rate (M s^{-1})
0.00075	1.5×10^{-6}
0.0015	$3.9 \pm 0.4 \times 10^{-6}$
0.0030	$7.16 \pm 0.03 \times 10^{-6}$
0.0045	$10 \pm 1 \times 10^{-6}$

VI. Spectroscopic Studies for Catalyst Resting States

Representative Procedure for Performing NMR Spectroscopic Studies on the Catalyst Resting States:

Initiation Studies:
In the glovebox, catalyst **1a** (16.8 mg, 0.0200 mmol, 1.0 equiv) was dissolved in THF (0.5 mL) and loaded into a J. Young NMR tube equipped with a rubber septum. Separately, 1.5 mL of **2** (0.40 M in THF) was placed in a 1.5 mL vial equipped with a septum. Once removed from the glovebox, these samples were immediately sealed with parafilm, and the solution of **2** was placed on dry ice.

The NMR tube was cooled to -20 °C in the NMR spectrometer, and both ^{1}H and ^{31}P NMR spectra were recorded. Then, 0.25 mL of **2** (0.40 M, 0.10 mmol, 5.0 equiv) was injected into the NMR tube, and spectra were recorded for both nuclei (Figure S19A). The sample was then removed from the spectrometer and allowed to warm to rt. After 30 min, a second set of ^{31}P and ^{1}H NMR spectra were collected at rt.

Propagation Studies:
In the glovebox, catalyst **1a** (16.8 mg, 0.0200 mmol, 1.0 equiv) was partially dissolved in THF (0.3 mL) followed by 0.75 mL of **2** (0.40 M, 0.30 mmol, 15 equiv) with vigorous mixing. After 30 min at rt, this solution was loaded into a J. Young NMR tube equipped with a septum. Separately, 1.5 mL of **2** (0.40 M in THF) was placed in a 1.5 mL vial equipped with a septum. Once removed from the glovebox, these samples were immediately sealed with parafilm, and the solution of **2** was placed on dry ice.

The NMR tube was cooled to -20 °C in the NMR spectrometer, and both ^{1}H and ^{31}P NMR spectra were recorded. Then, 0.50 mL of **2** (0.40 M, 0.20 mmol, 10 equiv) was injected into the NMR tube, and spectra were recorded for both nuclei (Figure S19B). The sample was then removed from the spectrometer and allowed to warm to rt. After 30 min, a second set of ^{31}P and ^{1}H NMR spectra were collected at rt (Figure S19C).
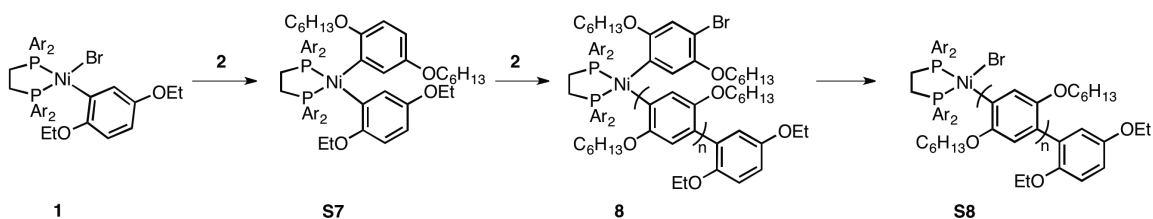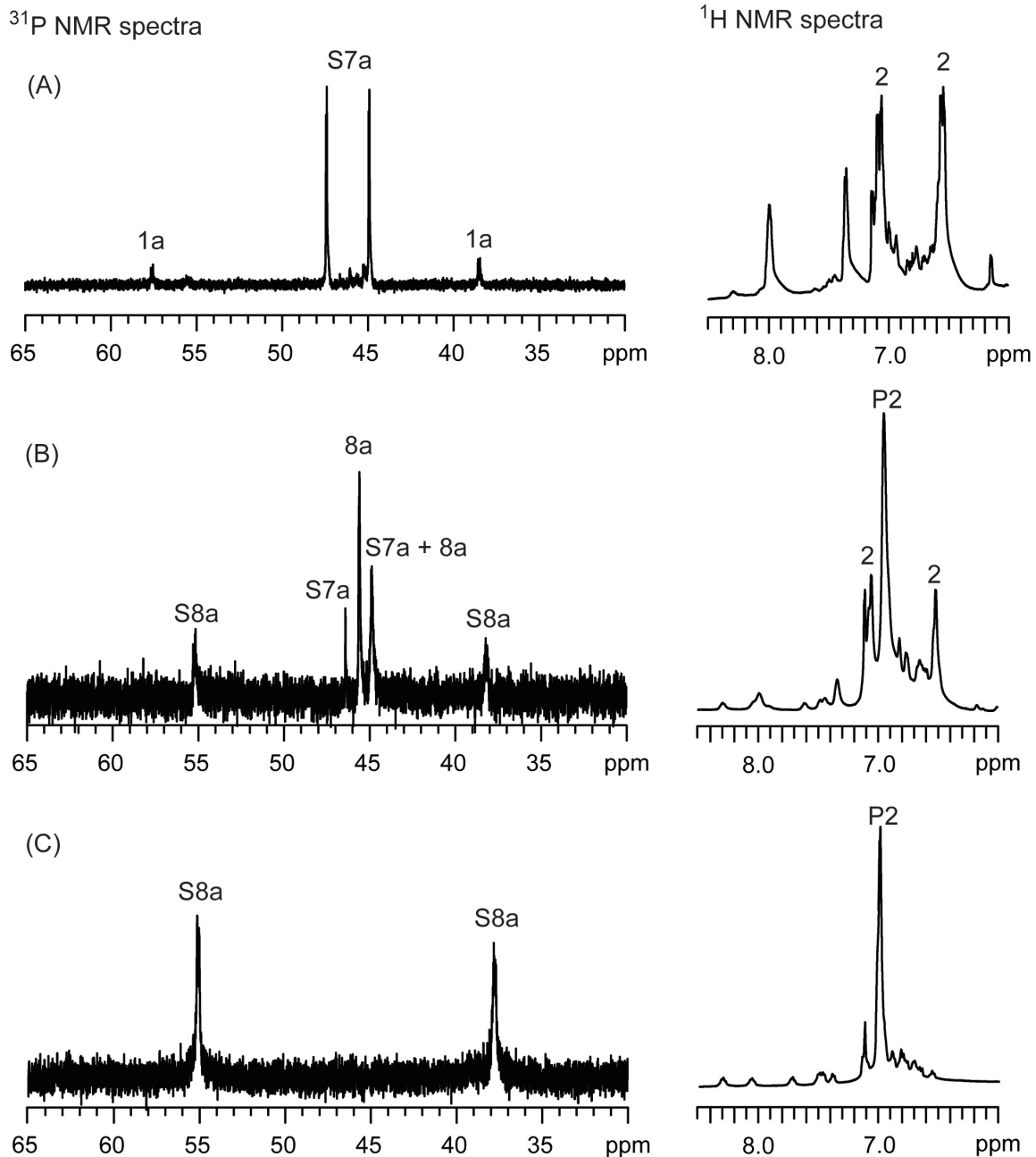
Figure S1-19. ^{31}P NMR spectra (162 MHz, THF, -20 °C) of (A) complex **S7a** δ 47.42 (d, *J* = 9.1 Hz), 44.93 (d, *J* = 9.0 Hz), (B) complex **8a** δ 45.59 (d, *J* = 7.5 Hz), 44.91 (br), (C) complex **S8a** δ 55.08 (d, *J* = 21.9 Hz), 37.82 (d, *J* = 20.9 Hz) in the presence or absence of monomer as confirmed by the aromatic region of the ^{1}H NMR spectra (500 MHz, THF, -20 °C).
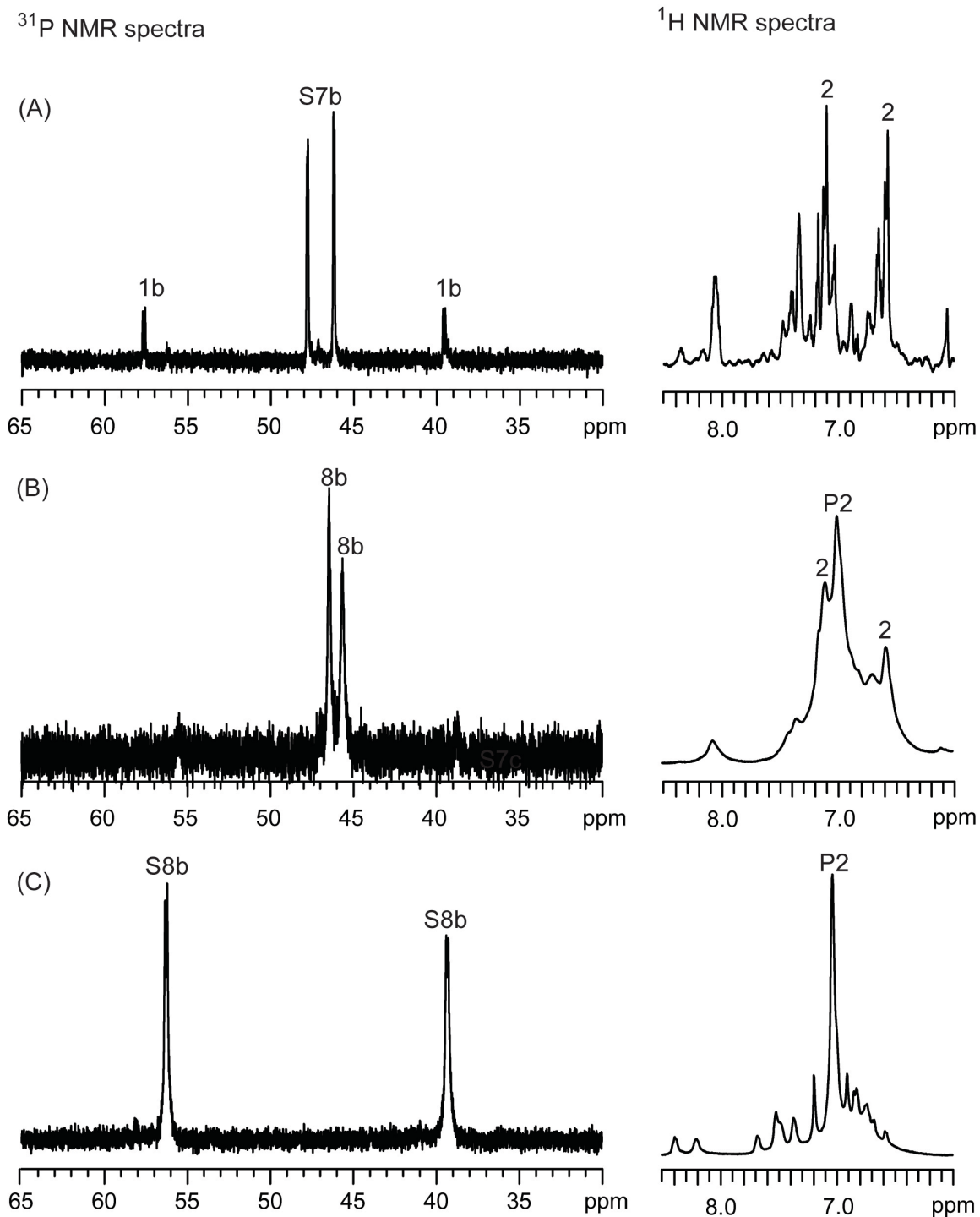
Figure S1-20. ^{31}P NMR spectra (162 MHz, THF, -20 °C) of (A) complex **S7b** δ 47.74 (d, J = 9.9 Hz), 46.18 (d, J = 10.9 Hz), (B) complex **8b** δ 46.46 (br), 45.66 (br), (C) complex **S8b** δ 56.27 (d, J = 26.0 Hz), 39.34 (d, J = 23.4 Hz) in the presence or absence of monomer as confirmed by the aromatic region of the ^{1}H NMR spectra (500 MHz, THF, -20 °C).
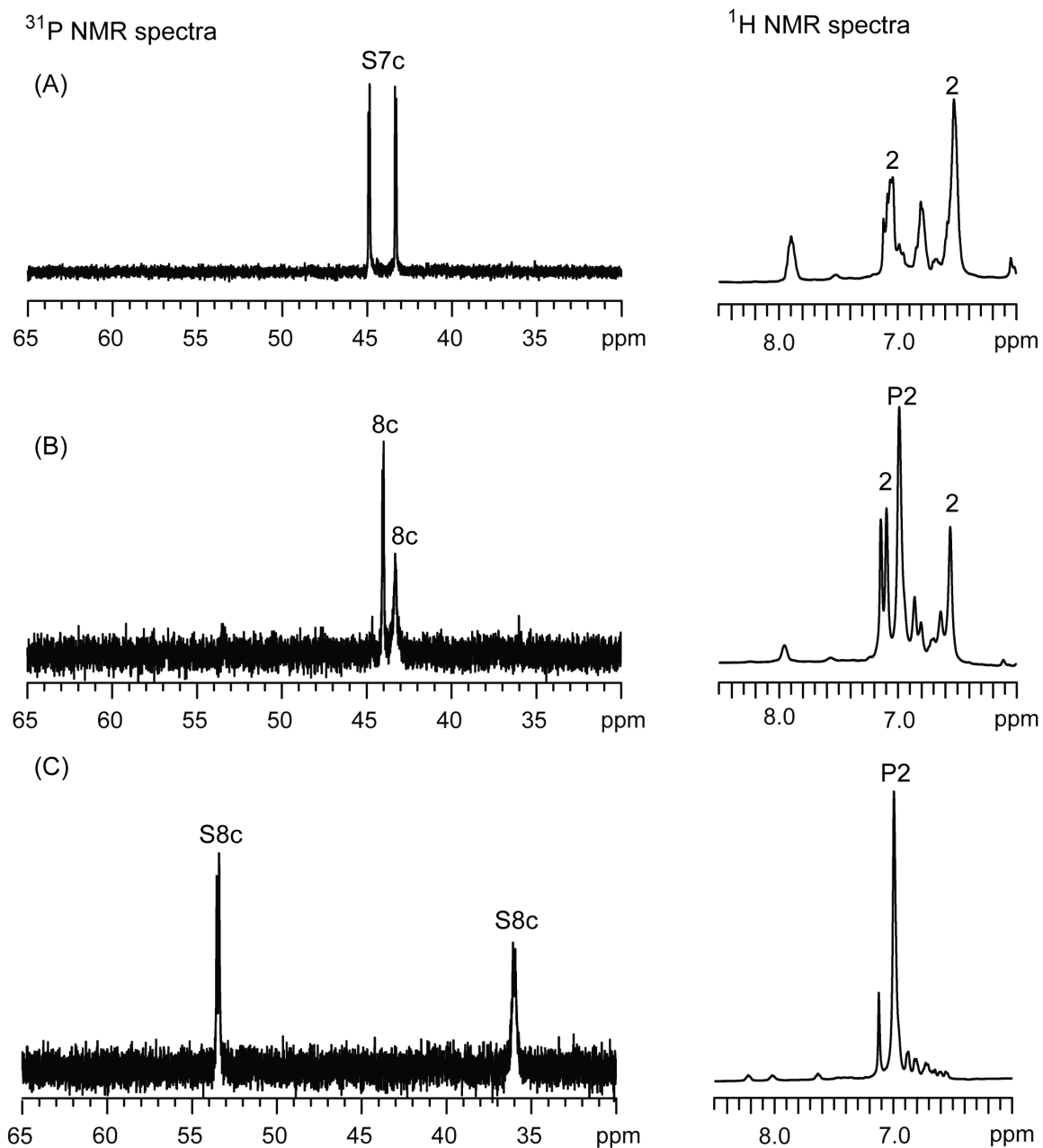
Figure S1-21. ^{31}P NMR spectra (162 MHz, THF, -10 °C) of (A) complex **S7c** δ 44.89 (d, *J* = 13.8 Hz), 43.32 (d, *J* = 14.3 Hz), (B) complex **8c** δ 44.03 (d, *J* = 12.7 Hz), 43.32 (br), (C) complex **S8c** δ 53.47 (d, *J* = 27.7 Hz), 36.07 (d, *J* = 22.2 Hz) in the presence or absence of monomer as confirmed by the aromatic region of the ^{1}H NMR spectra (500 MHz, THF, -10 °C).
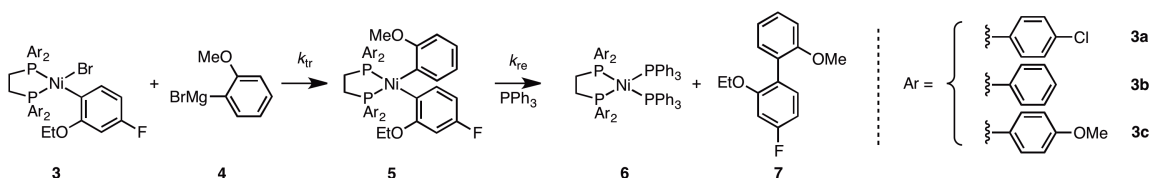
VII. Initiation Rate Studies

Representative Procedure for Performing NMR Spectroscopic Initiation Rate Studies:
All actions were performed in a glovebox under N_2 atmosphere. In 4 mL vial, nickel stock solution was prepared by dissolving **3b** (15.3 mg, 0.0226 mmol, 1.0 equiv) and PPh₃ (11.9 mg, 0.0454 mmol, 2.0 equiv) in THF (0.88 mL). Then, trifluoromethyl benzene (22 μL, 0.34 M in THF, 0.33 equiv) was added as an internal standard. An NMR tube was charged with this solution (0.8 mL), sealed with a septum, and removed from the glovebox. The tube was cooled to -5 °C in the NMR spectrometer for ~40 min. Immediately prior to acquiring kinetic data, **4** (0.2 mL, 0.2 M in THF, 2.0 equiv, kept at 0 °C) was injected into the tube. The tube was rapidly inverted once and then inserted into the spectrometer at -5 °C. Each spectrum was taken with the following parameters using Varian vnmr 500; acquisition time = 1.5 s, relaxation time = 3.0 s, scan size = 4, and pre-acquisition delay = 120 s.

Representative Procedure for Performing Igor Pro Analysis:
The integrated peak values of **3**, **5**, and **7** were converted to concentration using internal standard. The concentration was fitted to equations below using Igor Pro v6.22A. 'CollumKinetic 5000' was used as the master procedure file and the analysis was performed using same procedure reported in 'Fitting to Differential equations in Igor Pro' provided by the Collum group.[5]

$$\frac{d\,[\mathbf{3}]}{dt} = -\,k_{tr}\,[\mathbf{3}]\,[\mathbf{4}]$$

$$\frac{d\,[\mathbf{5}]}{dt} = k_{tr}\,[\mathbf{3}]\,[\mathbf{4}] - k_{re}\,[\mathbf{5}]$$

$$\frac{d\,[\mathbf{7}]}{dt} = k_{re}\,[\mathbf{5}]$$

The precatalyst initiation was observed using ^{19}F and ^{31}P NMR spectroscopy to support the peak assignments.
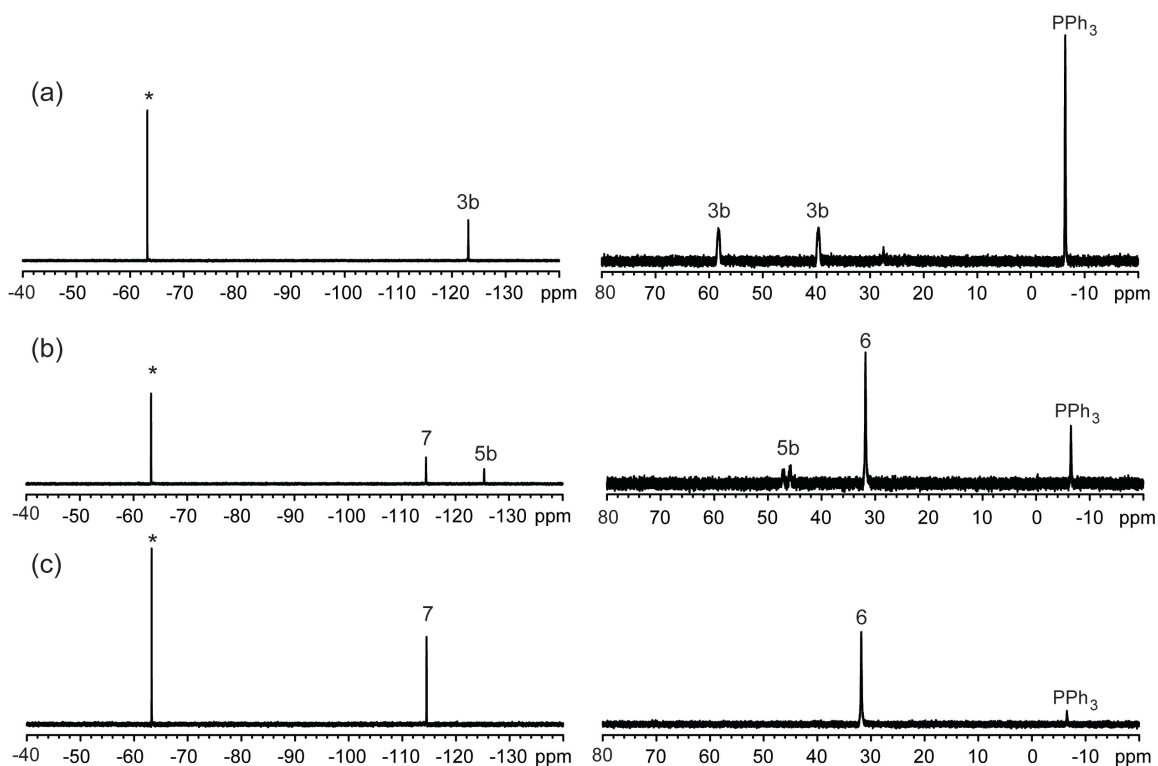

Figure S1-22. Representative ^{19}F and ^{31}P NMR spectra of initiation rate study for catalyst **3b** at the (a) beginning, (b) middle, and (c) end of the reaction.
* represents the internal standard, trifluoromethyl benzene.

Control experiment

Initiation rate studies were performed with varying [PPh$_3$] to determine its effect on the rates of transmetalation and reductive elimination. (temp = -5 °C, [**3b**] = 0.02 M, and [monomer] = 0.04 M)

Table S1-7. Rate data for catalyst **3b** with varying [PPh$_3$].

[PPh$_3$] (M)	k_{tr} (M^{-1} s^{-1} x 10^{-3})	k_{re} (s^{-1} x 10^{-3})
0.04	26 ± 3	0.43 ± 0.07
0.08	16.0 ± 0.6	0.46 ± 0.01
0.16	22.4 ± 0.6	0.57 ± 0.02
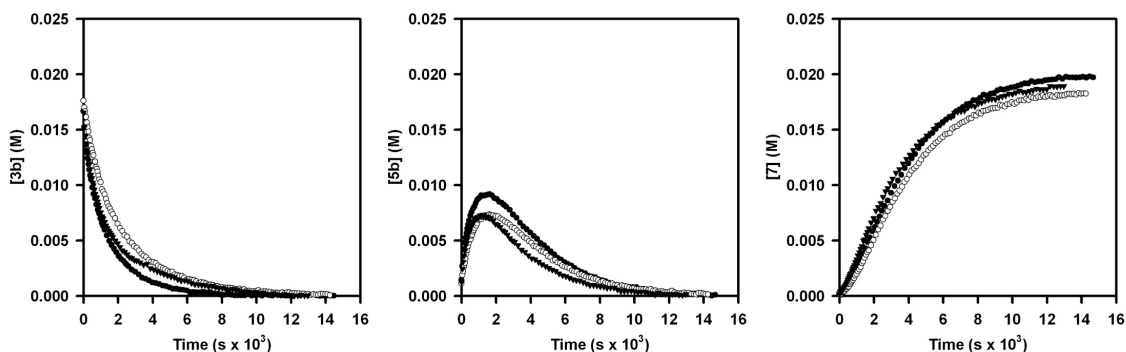
Figure S1-23. Plot of concentration versus time for catalyst **3b** with varying [PPh$_3$], (●= 0.04 M, ○= 0.08 M, ▼= 0.16 M)

Initiation rate studies were performed with varying [**4**] to determine its effect on the rates of transmetalation and reductive elimination. (temp = -5 °C, [**3b**] = 0.02 M, and [PPh_3] = 0.04 M)

Table S1-8. Rate data for catalyst **3b** with varying [**4**].

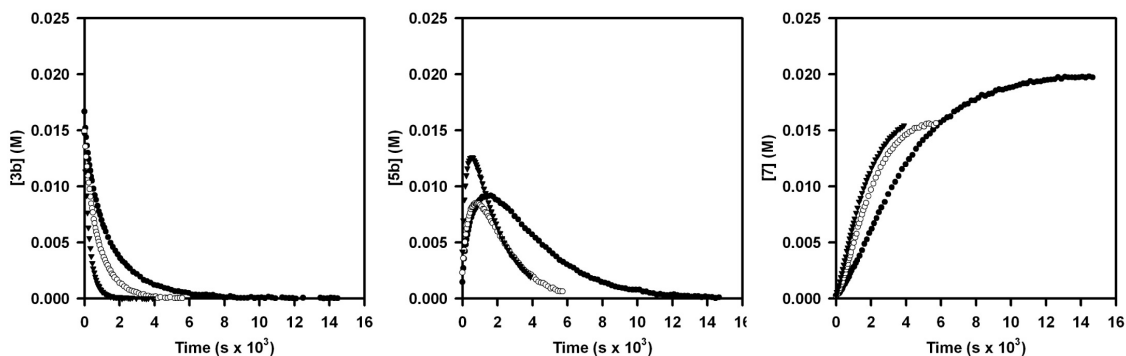| [**4**] (M)	k_{tr} (M^{-1} s^{-1} x 10^{-3})	k_{re} (s^{-1} x 10^{-3})
0.04	26 ± 3	0.43 ± 0.07
0.08	18.3 ± 0.7	0.457 ± 0.006
0.16	22.5 ± 0.6	0.575 ± 0.006

Figure S1-24. Plot of concentration versus time for catalyst **3b** with varying [**4**], (●= 0.04 M, ○= 0.08 M, ▼= 0.16 M)
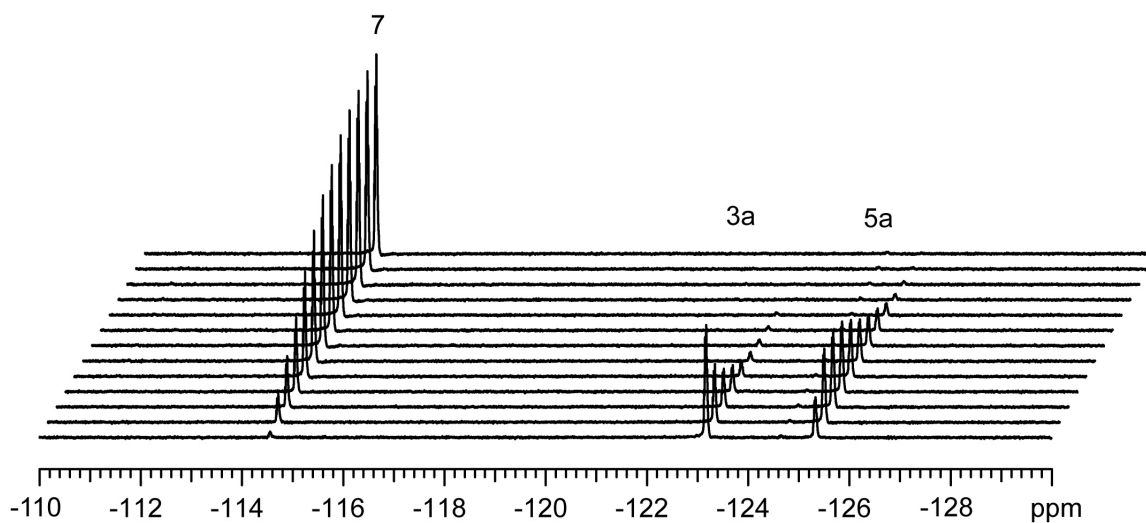
Figure S1-25. Representative ^{19}F NMR spectral array for catalyst **3a**. The internal standard, trifluoromethyl benzene, was observed at -63.33 ppm and is not shown.
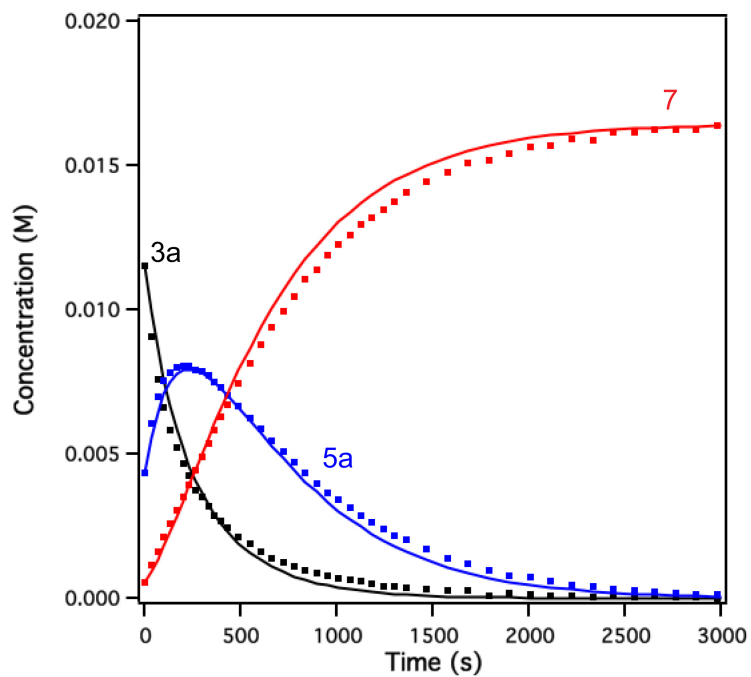

Figure S1-26. Plot of concentration versus time for data in Figure S1-25.

Table S1-9. Rate data for catalyst **3a**.

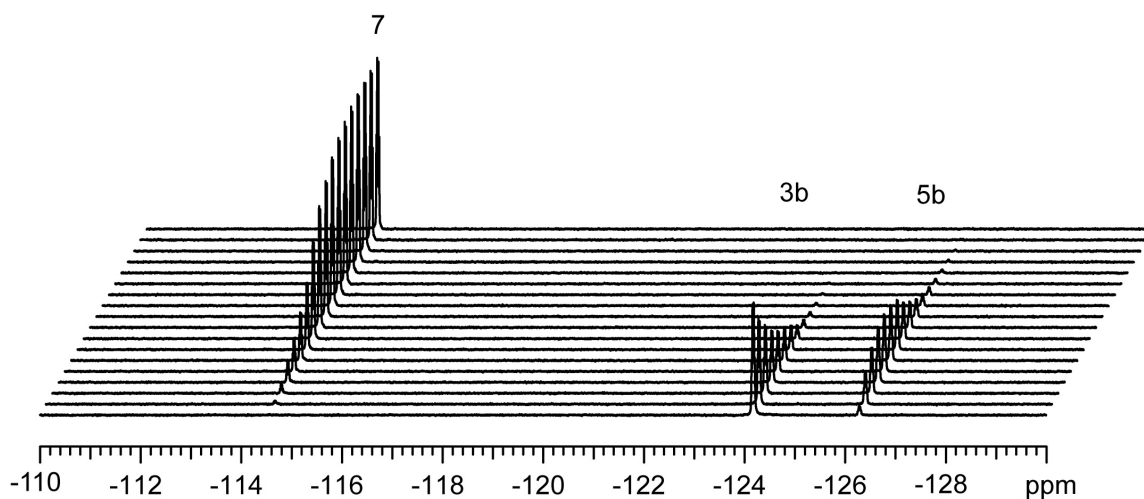| Trial	k_{tr} (M^{-1} s^{-1} x 10^{-3})	k_{re} (s^{-1} x 10^{-3})
1	127	1.66
2	173	1.94
3	128	1.90
Average	140 ± 30	1.8 ± 0.2

Figure S1-27. Representative ^{19}F NMR spectral array for catalyst **3b**. The internal standard, trifluoromethyl benzene, was observed at -63.33 ppm and is not shown.
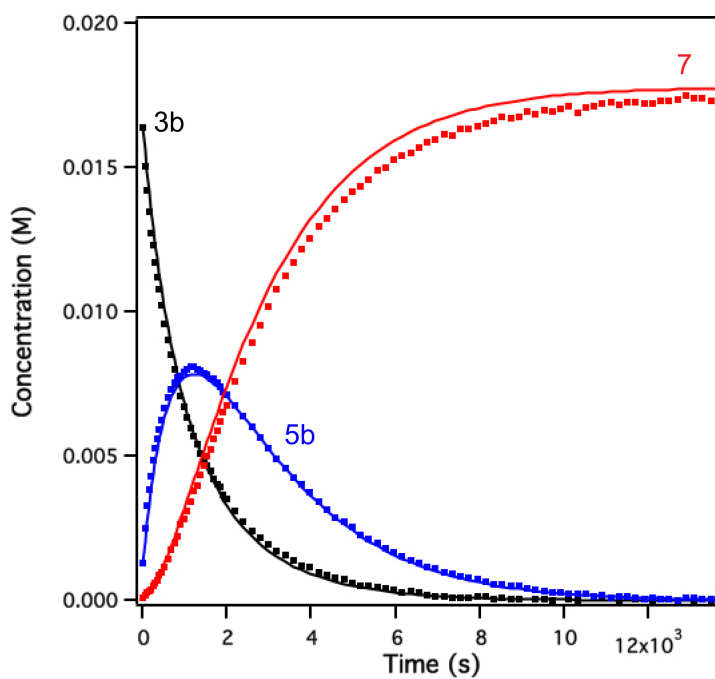

Figure S1-28. Plot of concentration versus time for Figure S1-27.

Table S1-10. Rate data for catalyst **3b**.

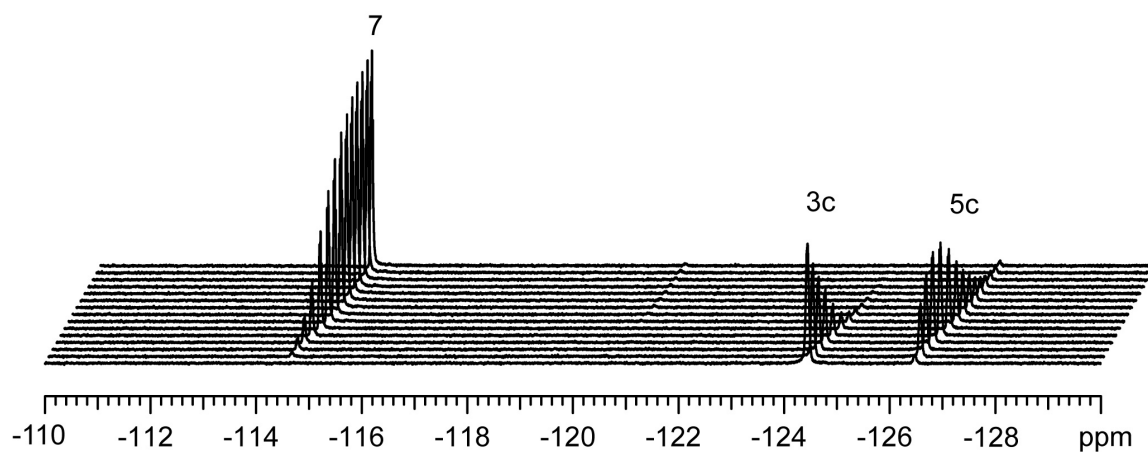| Trial	k_{tr} (M^{-1} s^{-1} x 10^{-3})	k_{re} (s^{-1} x 10^{-3})
1	26.8	0.504
2	28.0	0.406
3	21.9	0.374
Average	26 ± 3	0.43 ± 0.07

Figure S1-29. Representative ^{19}F NMR spectral array for catalyst **3c**. The internal standard, trifluoromethyl benzene, was observed at -63.36 ppm and is not shown.
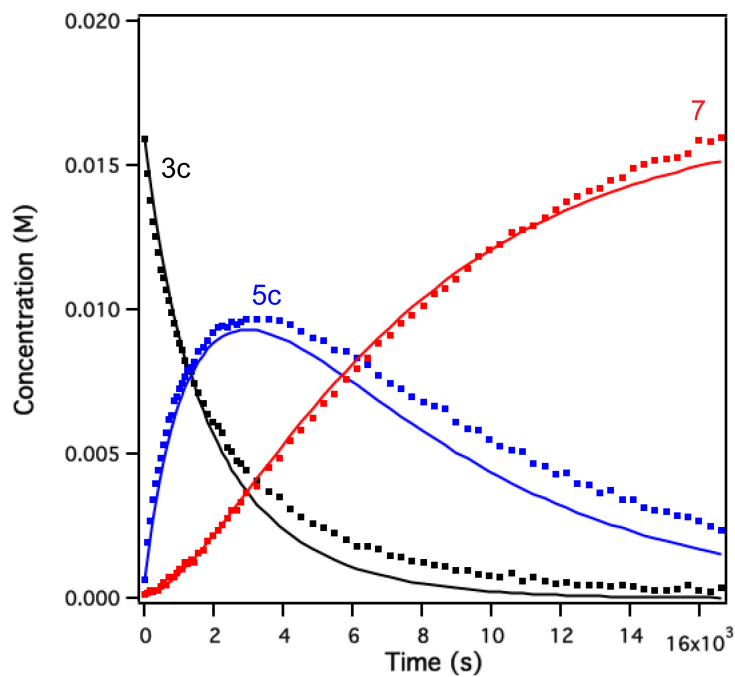

Figure S1-30. Plot of concentration versus time for Figure S1-29.

Table S1-11. Rate data for catalyst **3c**.

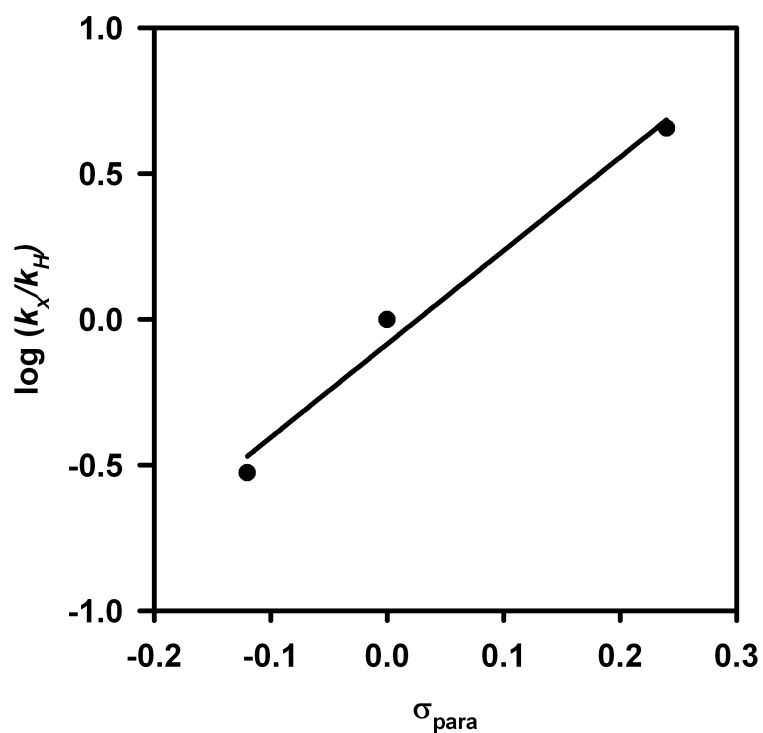| Trial	k_{tr} (M^{-1} s^{-1} x 10^{-3})	k_{re} (s^{-1} x 10^{-3})
1	10.9	0.183
2	10.5	0.195
3	15.8	0.162
4	11.3	0.190
Average	12 ± 2	0.18 ± 0.01

VIII. Hammett Plots

Figure S1-31. Plot of $\log(k_X/k_H)$ versus σ_{para} for reductive elimination during propagation. Fitted to $\log(k_X/k_H) = \rho \times \sigma_{para}$, where $\rho = 3.2 \pm 0.4$.

Table S1-12. Data for the plot in Figure S1-31.

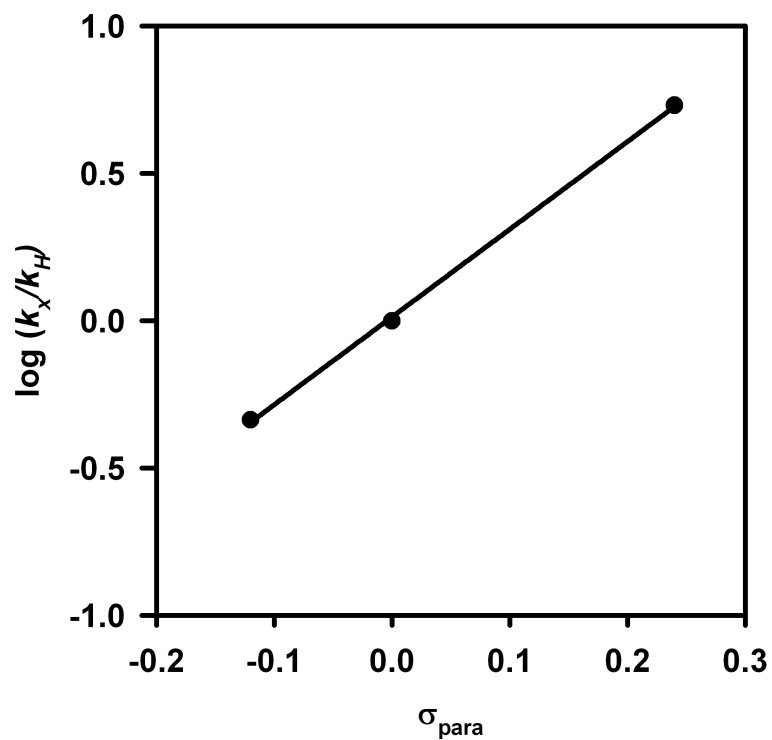| Catalyst	σ_{para}	$\log(k_X/k_H)$
1a	0.24	0.66
1b	0	0
1c	-0.12	-0.53

Figure S1-32. Plot of log(k_X/k_H) versus σ_{para} for transmetalation during precatalyst initiation. Fitted to log(k_X/k_H) = ρ x σ_{para}, where ρ = 2.98 ± 0.06.

Table S1-13. Data for the plot in Figure S1-32.

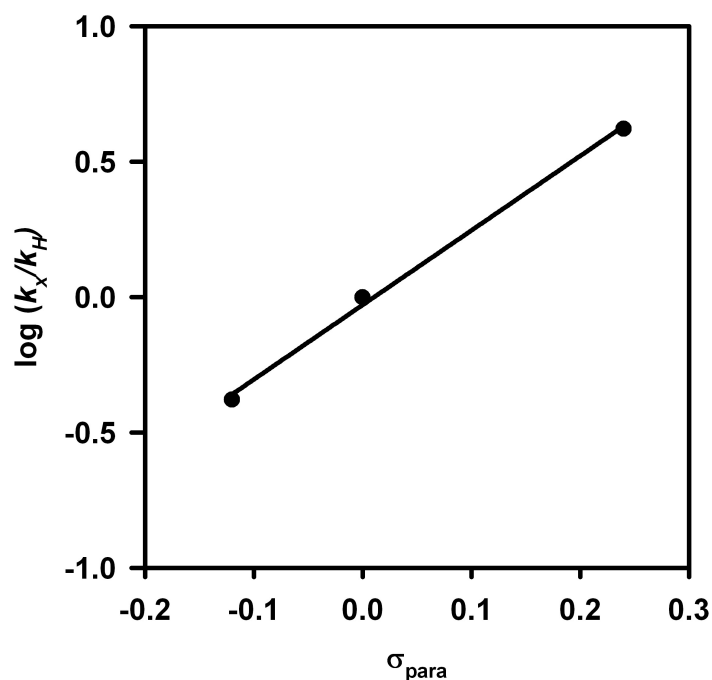| Catalyst	σ_{para}	log (k_X/k_H)
3a	0.24	0.73
3b	0	0
3c	-0.12	-0.34

Figure S1-33. Plot of $\log(k_X/k_H)$ versus σ_{para} for reductive elimination during precatalyst initiation. Fitted to $\log(k_X/k_H) = \rho \times \sigma_{para}$, where $\rho = 2.8 \pm 0.1$.

Table S1-14. Data for the plot in Figure S1-33.

Catalyst	σ_{para}	$\log(k_X/k_H)$
3a	0.24	0.62
3b	0	0
3c	-0.12	-0.38

IX. Chain-growth Polymerization Data

Representative Procedure for M_n and Đ versus Conversion Studies utilizing React IR:

The IR probe was inserted through an O-ring sealed 14/20 ground glass adapter (custom-made) into an oven-dried 50 mL 2-neck flask equipped with a stir bar. The other neck was fitted with a three-way adapter fitted with a septum for injections/aliquot sampling and an N_2 line. The oven-dried flask was cooled under vacuum. The flask was then filled with N_2 and evacuated again for a total of three cycles. The flask was charged with THF (6.5 mL) and cooled to 0 °C over 15 min. After recording a background spectrum, monomer **2** (2.5 mL, 0.41 M, 1.0 equiv) was added by syringe and allowed to equilibrate for at least 10 min at 0 °C before proceeding. The catalyst solution (1.0 mL, 0.015 M, 0.015 equiv) was then injected and spectra were recorded every 30 s over the entire reaction. To account for mixing and temperature equilibration, spectra recorded in the first 60 s of the reaction were discarded. Aliquots (~0.5 mL) were taken through the three way adapter via syringe and immediately quenched with 12 M HCl (~1 mL). Each aliquot was then extracted with CH_2Cl_2 (2 x 1.5 mL) (with mild heating if polymer had precipitated), dried over $MgSO_4$, filtered, and then concentrated. The samples were dissolved in THF (with heating), and passed through a 0.2 μm PTFE filter for GPC analysis.
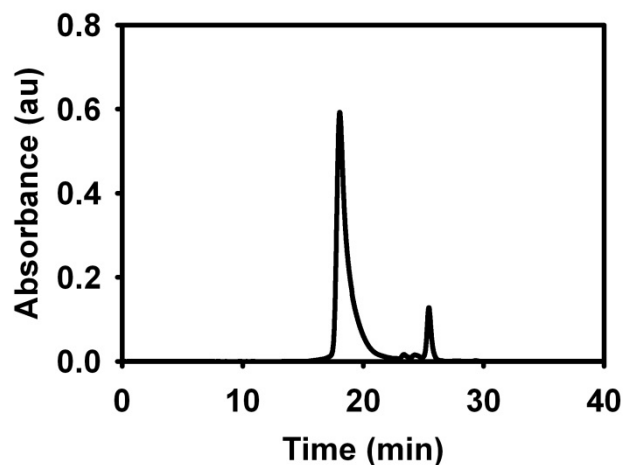
Figure S1-34. Representative GPC trace of **P2** at 60% conversion with catalyst **1a** (M_n: 20.7 kDa, Đ: 1.63).
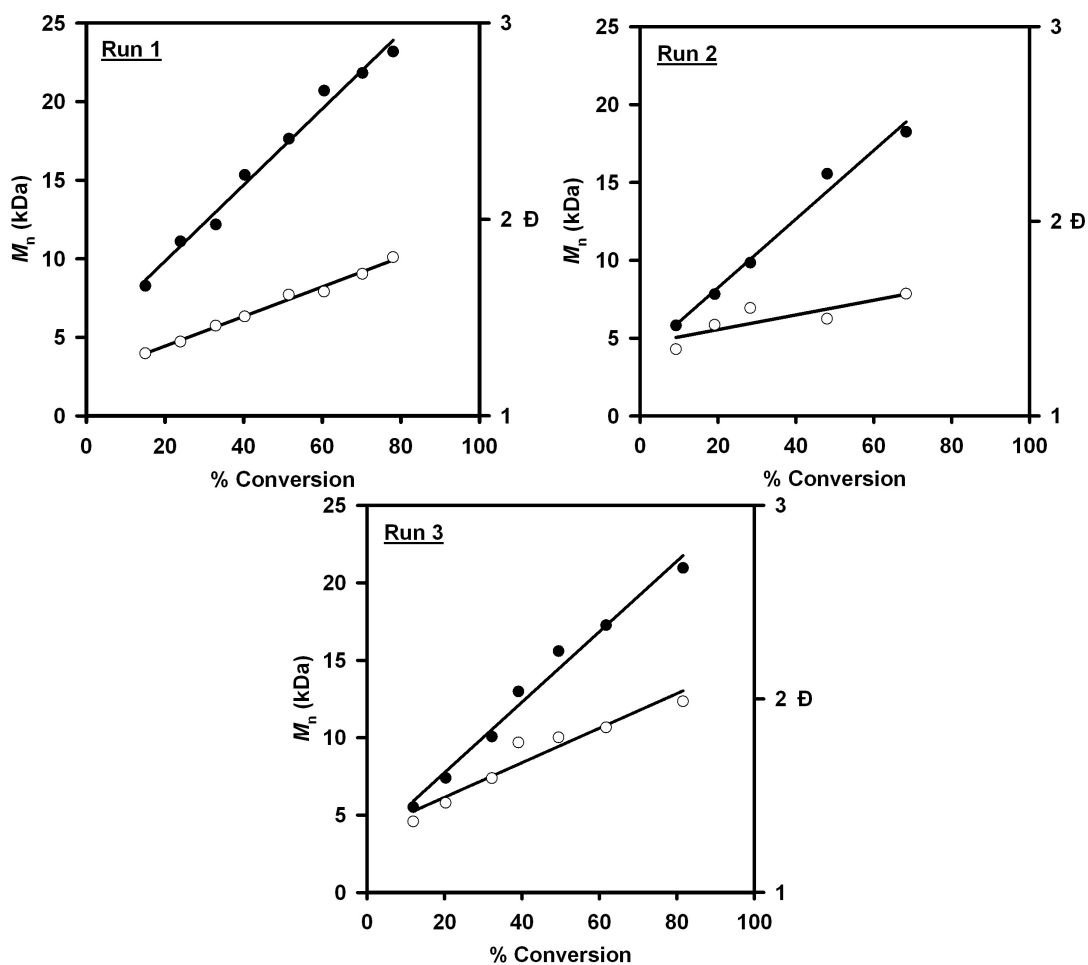

Figure S1-35. Plot of M_n (●) and Đ (o) versus conversion for **2** (temp = 0 °C, [**1a**] = 0.0015 M, [**2**] = 0.10 M (run 1), 0.10 M (run 2), 0.10 M (run 3)).

Table S1-15. Data for the plot in Figure S1-35, run 1.

% Conversion	M_n (kDa)	Đ
15	8.3	1.32
24	11.1	1.38
33	12.2	1.46
40	15.3	1.51
52	17.6	1.62
60	20.7	1.63
70	21.8	1.72
78	23.2	1.81

Table S1-16. Data for the plot in Figure S1-35, run 2.

% Conversion	M_n (kDa)	Đ
9	5.8	1.34
19	7.8	1.47
28	9.8	1.55
48	15.6	1.50
68	18.3	1.63

Table S1-17. Data for the plot in Figure S1-35, run 3.

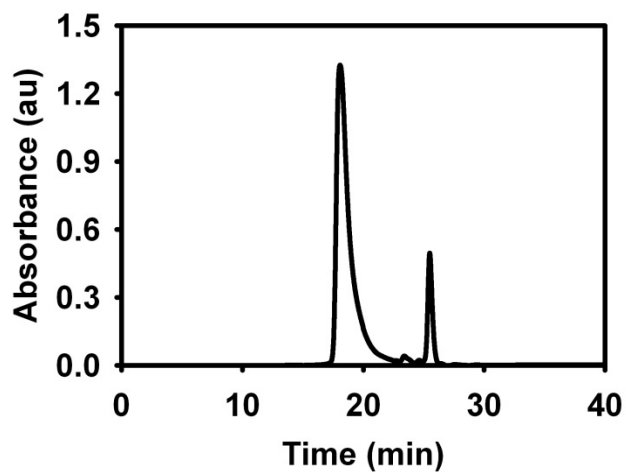| % Conversion	M_n (kDa)	Đ
12	5.5	1.37
20	7.4	1.46
32	10.1	1.59
39	13.0	1.77
49	15.6	1.80
62	17.3	1.85
82	21.0	1.99

Figure S1-36. Representative GPC trace of **P2** at 60% conversion with catalyst **1b** (M_n: 19.1 kDa, Đ: 1.67).
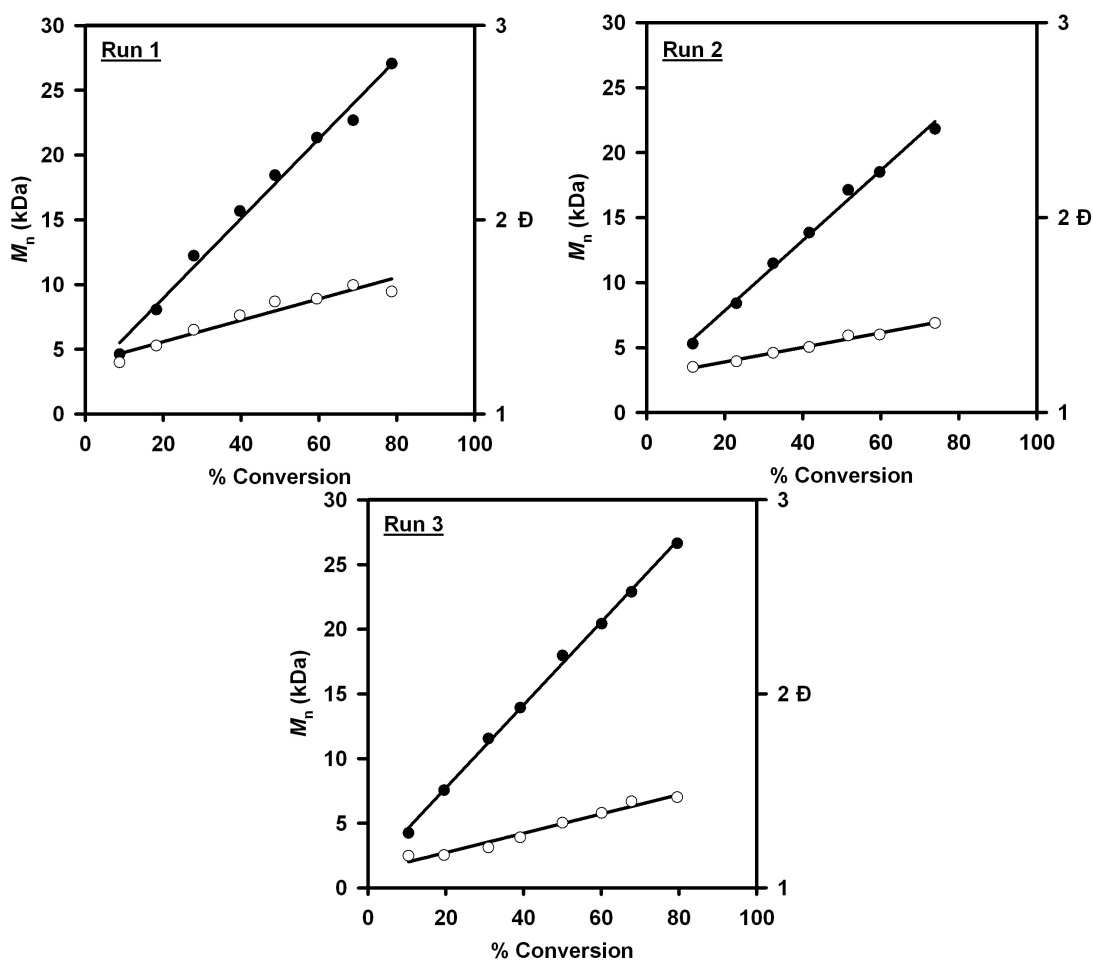

Figure S1-37. Plot of M_n (●) and Đ (o) versus conversion for **2** (temp = 0 °C, [**1b**] = 0.0015 M, [**2**] = 0.11 M (run 1), 0.11 M (run 2), 0.10 M (run 3)).

Table S1-18. Data for the plot in Figure S1-37, run 1.

% Conversion	M_n (kDa)	Đ
9	4.6	1.27
18	8.1	1.35
28	12.2	1.43
40	15.7	1.51
49	18.4	1.58
59	21.3	1.59
69	22.7	1.66
79	27.1	1.63

Table S1-19. Data for the plot in Figure S1-37, run 2.

% Conversion	M_n (kDa)	Đ
12	5.3	1.23
23	8.4	1.26
32	11.5	1.31
42	13.8	1.34
52	17.1	1.39
60	18.5	1.40
74	21.8	1.46

Table S1-20. Data for the plot in Figure S1-37, run 3.

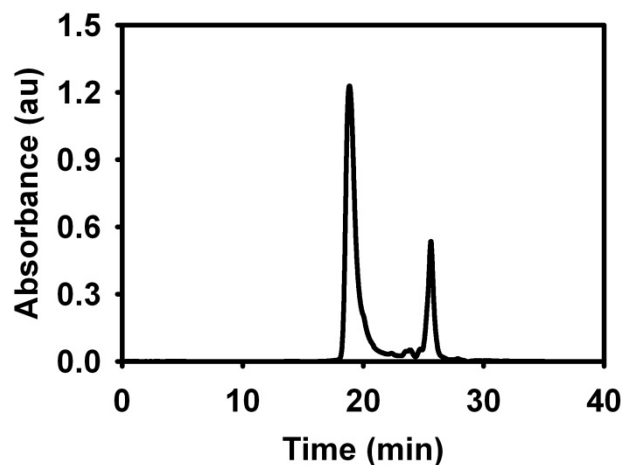| % Conversion	M_n (kDa)	Đ
10	4.3	1.17
20	7.6	1.17
31	11.6	1.21
39	13.9	1.26
50	18.0	1.34
60	20.4	1.39
68	22.9	1.45
80	26.6	1.47

Figure S1-38. Representative GPC trace of **P2** at 60% conversion with catalyst **1c** (M_n: 14.0 kDa, Đ: 1.28).
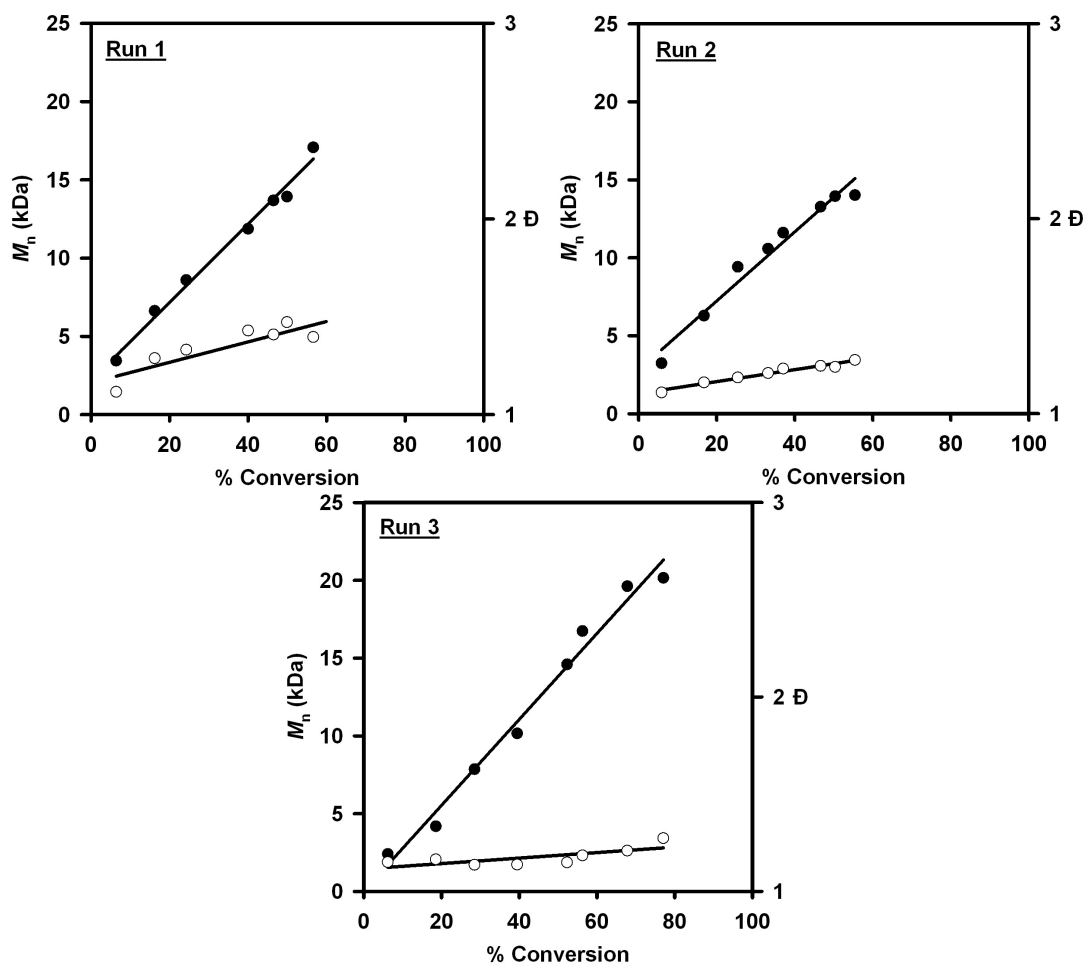

Figure S1-39. Plot of M_n (●) and Đ (o) versus conversion for **2** (temp = 0 °C, [**1c**] = 0.0015 M, [**2**] = 0.095 M (run 1), 0.099 M (run 2), 0.10 M (run 3)).

Table S1-21. Data for the plot in Figure S1-39, run 1.

% Conversion	M_n (kDa)	Đ
6	3.5	1.12
16	6.6	1.29
24	8.6	1.33
40	11.9	1.43
46	13.7	1.41
50	13.9	1.47
57	17.1	1.40

Table S1-22. Data for the plot in Figure S1-39, run 2.

% Conversion	M_n (kDa)	Đ
6	3.2	1.11
17	6.3	1.16
25	9.4	1.19
33	10.6	1.21
37	11.6	1.23
47	13.3	1.24
50	13.9	1.24
55	14.0	1.28

Table S1-23. Data for the plot in Figure S1-39, run 3.

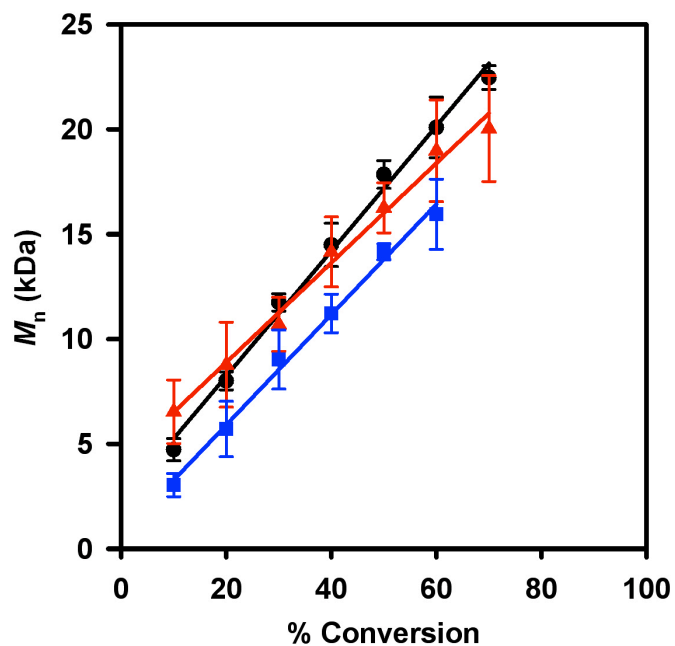| % Conversion	M_n (kDa)	Đ
6	2.4	1.15
19	4.2	1.16
28	7.9	1.14
39	10.2	1.14
52	14.6	1.15
56	16.7	1.18
68	19.6	1.21
77	20.2	1.27

Figure S1-40. Plot of average M_n *versus* conversion for all three catalysts with error bars. Samples within ±4% of target conversion were included (▲ = **1a**, ● = **1b**, ■ = **1c**).
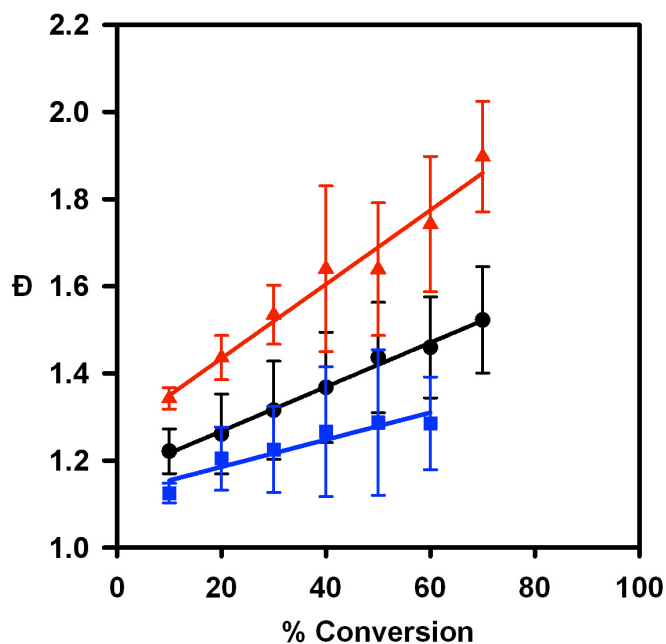

Figure S1-41. Plot of average Đ *versus* conversion for all three catalysts with error bars. Samples within ±4% of target conversion were included (▲ = **1a**, ● = **1b**, ■ = **1c**).

Representative Procedure for Preparation of Oligomers for MALDI-TOF MS Studies:

All actions were performed in a glovebox under N_2 atmosphere. A 20 mL vial was equipped with a stir bar. Sequentially, **1b** (11.0 mg, 0.015 mmol, 1.0 equiv), THF (4.75 mL), and **2** (0.25 mL, 0.44 M, 7 equiv) were added to the flask. After 1 h, the reaction was removed from the glovebox and poured into HCl (aq., 5 mL, 5 M) and then extracted with CH_2Cl_2 (3 x 5 mL). The combined organic layers were concentrated in vacuo. The resulting solid was washed with MeOH (50 mL) to give **P2** as an off-white solid: M_n: 1.76 kDa, Đ: 1.15 (GPC). For MS sample a small amount of polymer dissolved in $CHCl_3$ was first filtered through a pipet column of basic, acidic, and neutral alumina to remove Ni and the solution was concentrated in vacuo. The general procedure was followed for MALDI-TOF MS sample preparation (see General Experimental pS2). For **P2**: M_n: 1.84 kDa, Đ: 1.03 (MALDI-TOF MS)
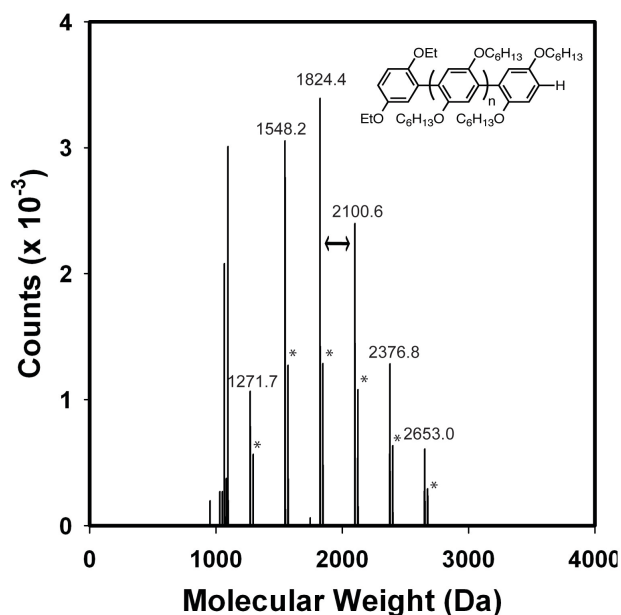

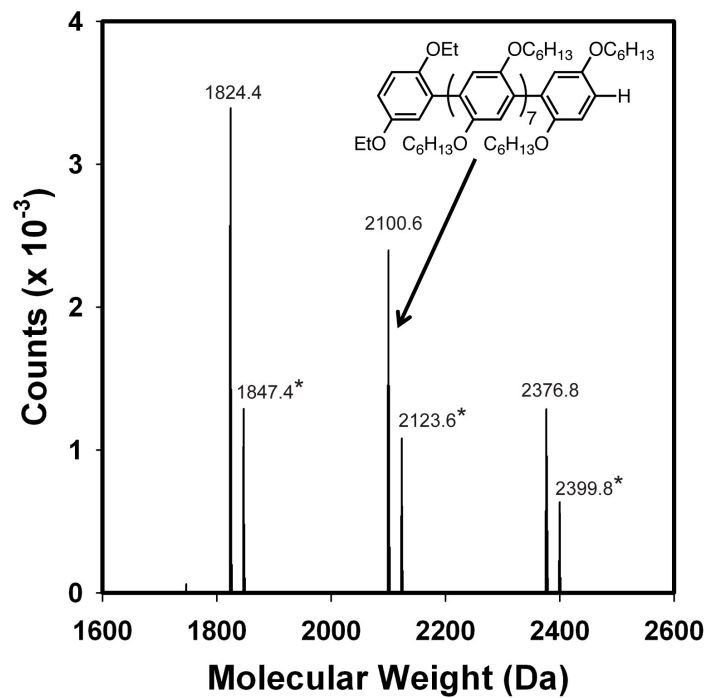**Figure S1-42**. MALDI-TOF MS spectrum of **P2** initiated with **1a**.
* represents $[M + Na]^+$.

Figure S1-43. Expanded view of Figure S1-42.
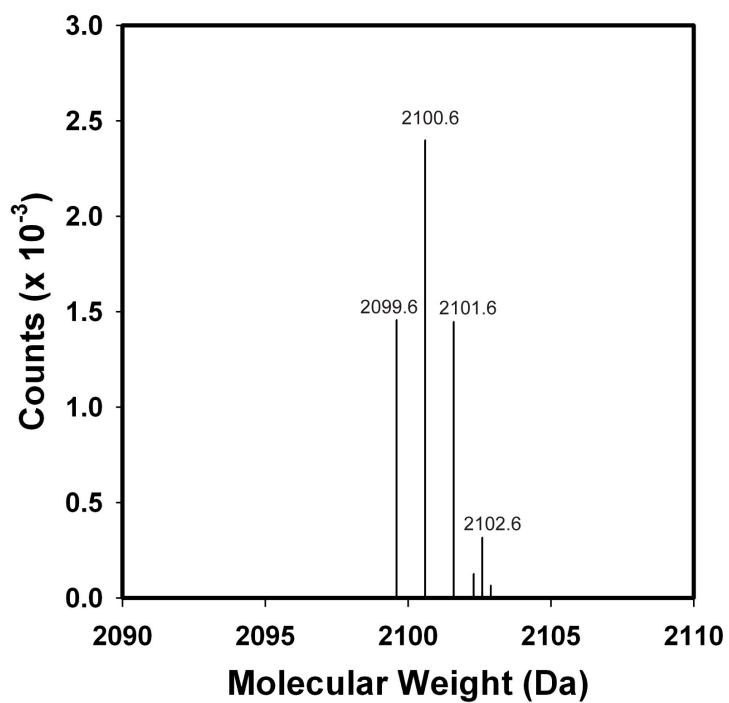* represents [M + Na]$^+$.
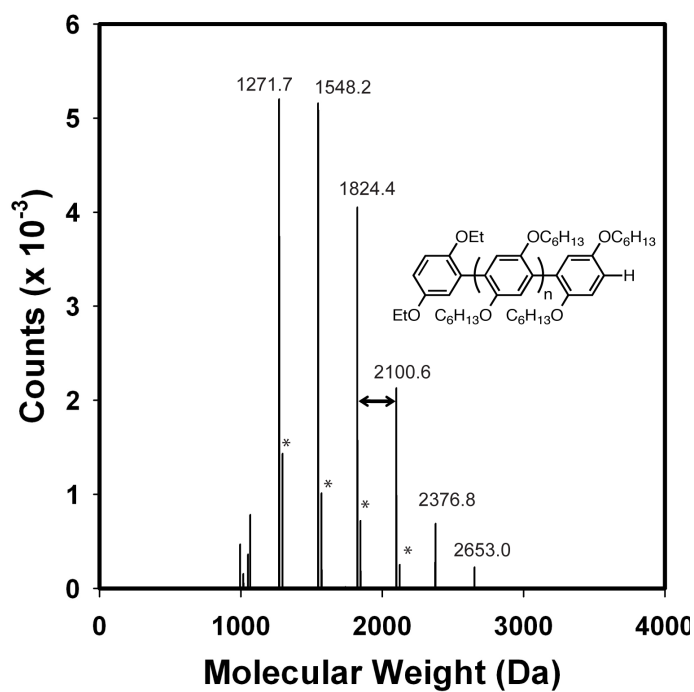

Figure S1-44. Expanded view of Figure S1-43.

114

Figure S1-45. MALDI-TOF MS spectrum of **P2** initiated with **1b**.
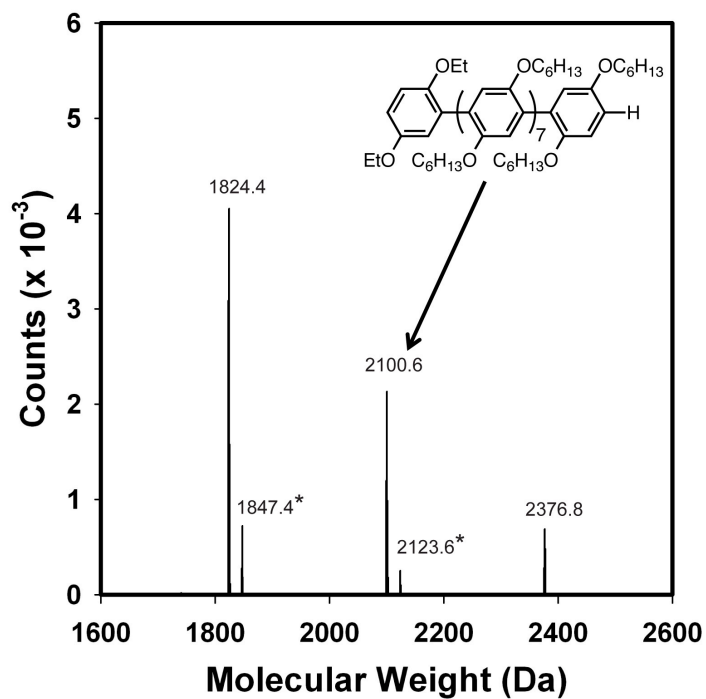* represents [M + Na]$^+$.

Figure S1-46. Expanded view of Figure S1-45.
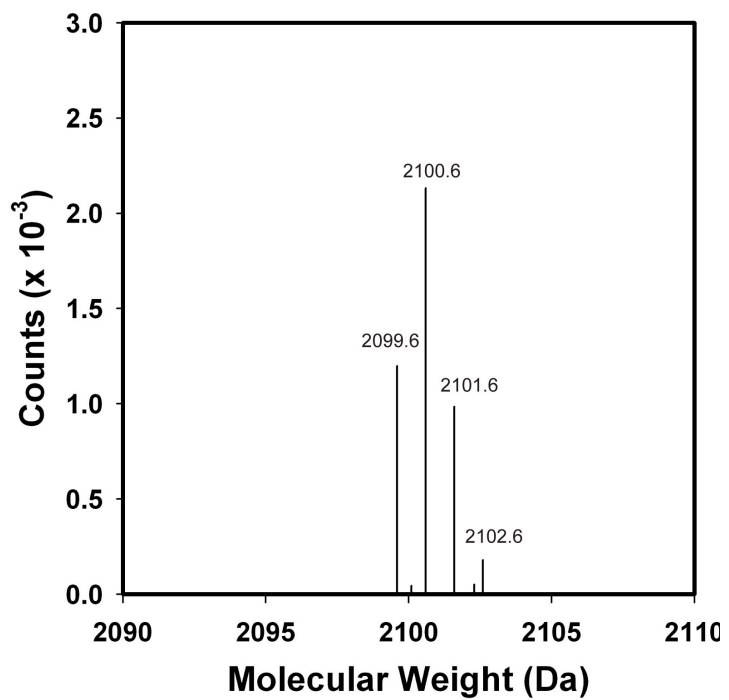* represents [M + Na]$^+$.

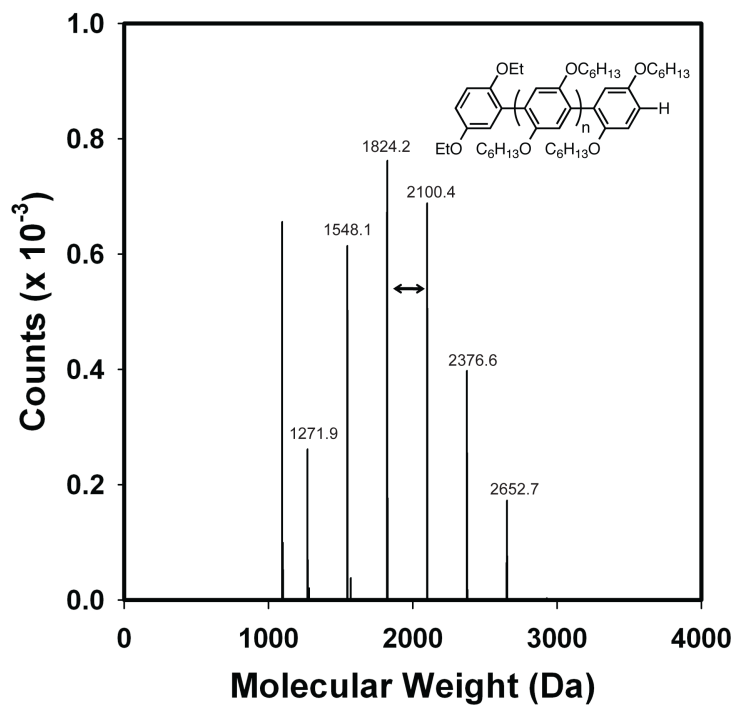**Figure S1-47**. Expanded view of Figure S1-46.

Figure S1-48. MALDI-TOF MS spectrum of **P2** initiated with **1c**.
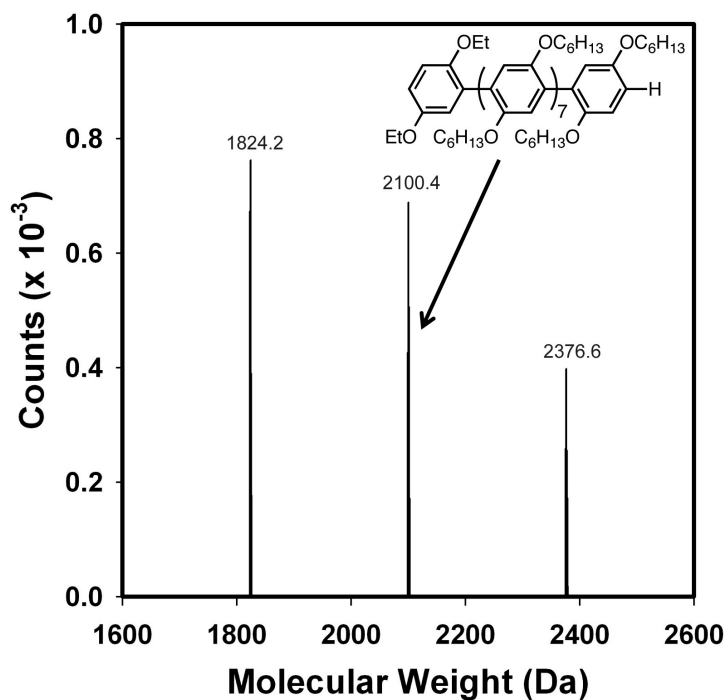

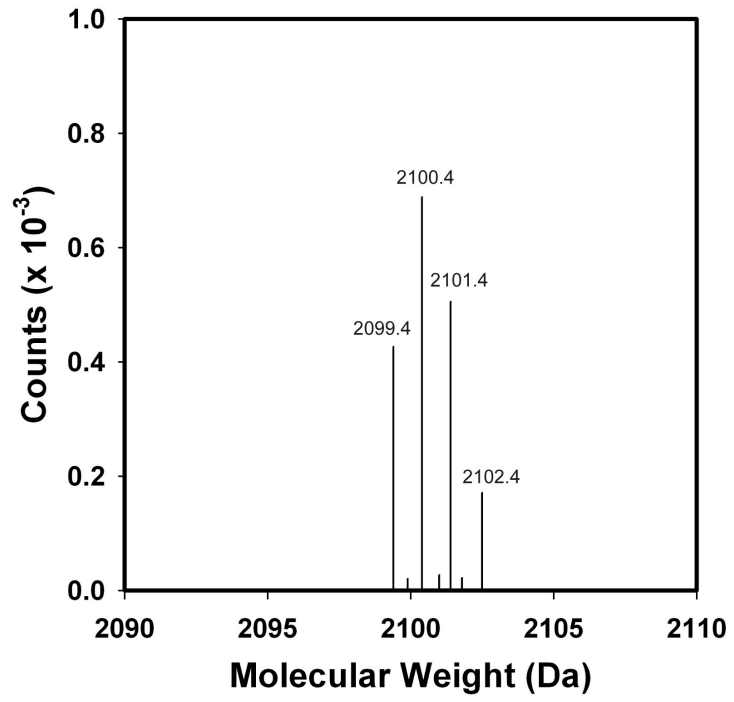**Figure S1-49**. Expanded view of Figure S1-48.

Figure S1-50. Expanded view of Figure S1-49.

Representative Procedure for Obtaining High Molecular Weight Polymer Samples:

An oven-dried 50 mL Schlenk flask was charged with the solution of **1b** (6.8 mL, 0.022 M in THF) and a stir bar in a glovebox. The flask was equipped with a two-way adapter fitted with a septum for injection and brought out of the glovebox. After introducing N_2 through the two-way adaptor and the side-arm of the flask (2 lines), the solution was cooled to 0 °C over 15 min. Then, monomer **2** (3.2 mL, 0.46 M in THF), with docosane added as an internal standard, was added by syringe. After 8 h, an aliquot (~0.5 mL) was taken through the two-way adaptor via syringe and immediately quenched with 12 M HCl (~1 mL). It was then extracted with CH_2Cl_2 (2 x 1.5 mL) with mild heating, dried over $MgSO_4$, filtered, and then concentrated. The sample was then dissolved in THF (with heating), and passed through a 0.2 μm PTFE filter for GPC analysis. The remainder of reaction was quenched with 12 M HCl (~10 mL) followed by the same work-up procedure. The resulting polymer was washed with MeOH (~200 mL) and dried in vacuo. Conversion was determined relative to the initial concentration, using the internal standard as a reference by GC analysis.

Table S1-24. Polymerization data for catalysts **1a-c**.

Catalyst	Reaction Time (h)	M_n (kDa)	Đ	Monomer Conversion (%)	Isolated Yield (%)
1a	4	29.1	2.36	93	67
1b	8	40.0	1.71	90	48
1c	11	41.3	1.56	71	54

X. References Cited

(1)   Chatt, J.; Hussain, W.; Leigh, G. J.; Ali, H. M.; Pickett, C. J.; Rankin, D. A. *J. Chem. Soc., Dalton Trans.* **1985**, 1131–1136.

(2)   (a) Lanni, E. L.; McNeil, A. J. *Macromolecules* **2010**, *43*, 8039–8044. (b) Lanni, E. L.; McNeil, A. J. *J. Am. Chem. Soc.* **2009**, *131*, 16573–16579.

(3)   Locke, J. R.; McNeil, A. J. *Macromolecules* **2010**, *43*, 8709-9710.

(4)   Love, B. E.; Jones, E. G. *J. Org Chem.* **1999**, *64*, 3755–3756.

(5)   For the numerical integration procedure, see:
 http://www.chem.cornell.edu/dbc6/Site_2/Group_Resources.html. For leading references on this procedure, see: (a) Hoepker, A. C.; Gupta, L.; Ma, Y.; Faggin, M. F.; Collum, D. B. *J. Am. Chem. Soc.* **2011**, *133*, 7135–7151. (b) Ma, Y.; Hoepker, A. C.; Gupta, L.; Faggin, M. F.; Collum, D. B. *J. Am. Chem. Soc.* **2010**, *132*, 15610–15623.